UC Merced
UC Merced Electronic Theses and Dissertations

Title
The Chronicles of Transition Metal Chemistry: The Theory, The Computation and The Catalyst

Permalink
https://escholarship.org/uc/item/8bg9w60c

Author
Bidwell, Samantha Lynn

Publication Date
2021

Peer reviewed|Thesis/dissertation

eScholarship.org Powered by the California Digital Library
University of California

UNIVERSITY OF CALIFORNIA, MERCED

The Chronicles of Transition Metal Chemistry:
The Theory, The Computation and The Catalyst

by

Samantha L. Bidwell

A dissertation submitted in partial satisfaction of the
requirements for the degree of
Doctor of Philosophy

in

Chemistry

Committee in charge:
Professor Christine M. Isborn, Chair
Professor Hrant P. Hratchian, Advisor
Professor Ryan D. Baxter
Professor Ashlie Martini

Summer 2021

Chapter 3 © ACS Publications

All other chapters © 2021 Samantha L. Bidwell

All rights are reserved.

The dissertation of Samantha L. Bidwell is approved:

Christine M. Isborn, Chair	Date
Hrant P. Hratchian, Advisor	Date
Ryan D. Baxter	Date
Ashlie Martini	Date

University of California, Merced

©Summer 2021

To My Copper Dog

& Baby Ky

Acknowledgments

The amount of gratitude I have for my family, friends and colleges is immeasurable. I would like this time to thank each person who has helped me work towards my academic goals. I would like to thank my committee for taking their time to mentor and push me along in this process and the agencies that provided all funding that made this process possible. If I could thank each and every person I've encountered along the way I would, but for now I would like to say something to some of the most important individuals in my life.

To my mother,
The amount of strength and perseverance you have combined with your absolute zest for life is what has inspired me to always push the limits and reach for my dreams. You are absolutely inspirational and will always be my reason for trying my hardest in everything I do. Your endless support in all of my academic aspirations is one of the main pillars that has supported me throughout my entire entire academic career.

To my father,
I admire the dedication and hard work you put into anything and everything you face, and one day I hope to be able to do the same. I've learned from you that good things come with time and a little patience. If you have to force it, something isn't right. Thank you for continuously supporting me in everything I do, and always being there.

To my sister,
You are and always will be my favorite person on this planet. Thank you so much for being there any time I need, and for always being able to make me laugh. I am so proud of the amazing person you are turning into, and will support you in anything you want to do.

To my grandparents,
You are the most caring, giving and hard working people I have ever known. Thank you for the endless amounts of support you've given me my entire life. I will always look up to the both of you, and am so grateful for everything you've done. You've shown me what hard work and compassion can get you, and I hope to be as happy and successful as the two of you one day.

To my love,
You will never know how much I appreciate the endless support and care you've provided me through this entire process. You've been understanding when I'm frustrated, supportive when I'm down and always there to show me that I can do this. Without you cheering me on every step of the way there is no way I could've done this. Thank you for everything. The best is yet to come. Forever and for always.

To my best friend,
Many, many hours spent at most two meters from each other could've led to two possibilities... (1.) You could've gotten sick of me after 10 minutes of hearing me whine and attempted to ignore me

the remainder of grad school or (2.) You could've gotten sick of me after 10 minutes and failed at ignoring me the remainder of grad school. Lucky for me option 2 is the way things went. I'm beyond grateful for the friendship and support you've provided me. I expected to experience a lot of things in grad school (stress, anxiety, freak outs, etc.), but the one thing I didn't expect was to find a lifelong friend in the process. Thank you for everything.

To my advisor,
You've not only taught me more about science than I ever dreamed I could learn, you taught me how to be a mentor and what it looks like to truly give your all to the field. Thank you for your patience and persistence this entire process.

To many many more,
I thank you for allowing me to lean on you when I needed, for encouraging me any time my steps wavered and for helping me to create an academic family that I will keep for life.

Curriculum Vitae

Education

Ph.D. in Chemistry & Chemical Biology *August 2015 - June 2021*
University of California, Merced
Merced, CA
Advisor: Hrant P. Hratchian

B.S. in Chemistry (ACS Certified) *August 2011 - May 2015*
Grand Valley State University
Grand Rapids, Michigan
Research Advisor: Richard L. Lord

Awards

- UC Merced Faculty Mentor Fellowship *2017 - 2018*
- UC Merced Chemistry Travel Grant Award *2016 - 2019*
- UC Merced Chemistry Recruitment Fellowship *2015 - 2016*

Publications

3. **Samantha L. Bidwell**, Hrant P. Hratchian. "*Towards a Complete Mechanistic Description of the Molecular Copper-Catalyzed Azide-Alkyne (CuAAC) Reaction*", Submitted.

2. Reimer, Lynn; Leslie, J. Michelle; **Bidwell, Samantha**; Isborn, Christine; Lair, Deborah; Menke, Erik; Stokes, Benjamin; Hratchian, Hrant. "*Aiming Toward an Effective Hispanic Serving Chemistry Curriculum.*" In ACS Symposium Series. Growing Diverse STEM Communities: Methodology, Impact and Evidence. edited by L. L. Winfield, G. Thomas, L. M. Watkins, and Z. S. Wilson-Kennedy (American Chemical Society, Washington D.C.). 29-66 (2019)

1. Alyssa M. Hua†, **Samantha L. Bidwell**†, Sarah I. Baker, Hrant P. Hratchian, Ryan D. Baxter "*Theoretical and Experimental Evidence for Nitrogen-Fluorine Halogen Bonding in Silver-Initiated Radical Fluorination*", ACS Catalysis, 9, 3322-3326. (2019) [† denotes co-first authors]

Mentoring & Teaching Experience

- **Instructor of Record for Introductory Chemistry** ***Summer 2019***
  - Develop course materials (notes, exams, homework, quizzes, syllabus).
  - Implement active learning activities into the lecture and discussion sections.
  - Plan semester schedule and implement course work.
  - Administer lectures at all scheduled course times.

- **Learning Director for UC Merced Chem Center** ***2018 - 2019***
    - Manage and schedule undergraduate tutors and graduate student TA's.
    - Tutor UCM undergraduate chemistry students.
    - Develop and lead workshops offered to undergraduate students.
- **Research Mentor for ACS SEED Students & Undergraduates** ***2016 - 2019***
    - Teach & Introduce students to computational chemistry and quantum mechanics.
    - Design research project steps and goals.
    - Supervise & Mentor visiting student progress.
- **UC Merced Teaching Assistant for General Chemistry I & II** ***2015 - 2017***
    - Supervise and administer laboratory sessions.
    - Prepare and administer discussion sessions.
    - Attend and participate in weekly meetings.
- **UC Merced Teaching Assistant for Quantum Chemistry** ***2015 - 2017***
    - Prepare and administer discussion sessions.
    - Attend and participate in weekly meetings.
    - Hold review sessions and office hours.

Presentations

11. **Samantha L. Bidwell**, Alyssa M. Hua, Sarah I. Baker, Ryan D. Baxter, Hrant P. Hratchian, "*Theoretical and Experimental Evidence for Nitrogen-Fluorine Halogen Bonding in Silver-Initiated Radical Fluorination*", Poster at 258th Meeting of the ACS, August 2019.

10. **Samantha L. Bidwell**, Hassan Harb, Sarah I. Baker, J. Michelle Leslie, Hrant P. Hratchian, "*Near-Peer Tutoring: Chemistry Center Designed to Increase Success of a Diverse Student Body*", Poster at 258th Meeting of the ACS, August 2019.

9. **Samantha L. Bidwell**, Hrant P. Hratchian, "*A Cu(I) Catalyzed Azide Alkyne Synthesis: The Importance of a 3-Center 2-Electron Bond*", Poster at Canadian Symposium of Theoretical and Computational Chemistry, July 2018.

8. **Samantha L. Bidwell**, Hassan Harb, Hrant P. Hratchian, Michael Colvin, Erik J. Menke, Paul Gibbons, Anne Zanzucchi, and J. Michelle Leslie. "*Integrating Writing and Computing in the General Chemistry Curriculum*", Poster at 255th Meeting of ACS, March 2018.

7. **Samantha L. Bidwell**, Hrant P. Hratchian. "*Investigation of Copper Catalyzed Triazole Synthesis: A Computational Exploration*", Presentation at 253rd Meeting of the ACS, April 2017.

6. **Samantha L. Bidwell**, Hrant P. Hratchian. "*Investigation of Copper Catalyzed Triazole Synthesis: A Computational Exploration*", Poster at 251st Meeting of the ACS, April 2016.

5. **Samantha L. Bidwell**, Hrant P. Hratchian. "*Investigation of Copper Catalyzed Triazole Synthesis: A Computational Exploration*", Poster at GVSU Student Scholars Day, April 2015.

4. **Samantha L. Bidwell**, Hrant P. Hratchian. "*Investigation of Copper Catalyzed Triazole Synthesis: A Computational Exploration*", Seminar at GVSU Senior Student Seminar, February 2015.

3. **Samantha L. Bidwell**, Hrant P. Hratchian. "*Investigation of Copper Catalyzed Triazole Synthesis: A Computational Exploration*", Poster at UCM Summer Symposium, July 2014.

2. **Samantha L. Bidwell**, Richard L. Lord. "*Benchmarking a computational protocol for redox-induced electron transfer*", Poster at GVSU Student Scholars Day, April 2014.

1. **Samantha L. Bidwell**, Richard L. Lord. "*Benchmarking a computational protocol for redox-induced electron transfer*", Poster at 248th Meeting of the ACS, March 2014.

Contents

List of Figures

List of Tables

Abstract

The Chronicles of Transition Metal Chemistry:

The Theory, The Computation and The Catalyst

by

Samantha Bidwell

Doctor of Philosophy

in

Chemistry

University of California, Merced

Professor Christine M. Isborn, Chair

Understanding the fundamental mechanistic steps of transition metal catalyzed reactions is crucial for the advancement of organometallic chemistry. Theoretical chemistry techniques are central to the investigations of the electronic structure of these complexes where experimental abilities are limited. Theoretical explorations of a copper catalyzed azide alkyne, a silver initiated fluorination and an electrophilic bromination allowed for the realization that a tool to quantitatively analyze the bonding present in many transition metal complexes did not exist. A tool to analyze multi-center bonding interactions was developed using perturbational molecular orbital theory, and will be applied to the systems studied.

Professor Christine M. Isborn
Dissertation Committee Chair

Chapter 1

Introduction

It is overwhelmingly evident that scientific research is central to the progress of society. Science is everywhere. The ability to discover novel scientific findings is at the core of this progress. This can only be accomplished with years of training combined with the innate curiosity that naturally exists amongst most scientists. The collaborations and interconnections between different fields of science (biology, chemistry, physics, etc.) is what leads to success.

Chemistry is defined as the science that studies the matter of the universe and the changes that this matter undergoes. With a definition like that, it is no surprise that chemistry is often referred to the *central science*. Most phenomena that occur in our world involve chemical changes, and there are vast areas of chemistry with numerous unanswered questions. Many open questions are on foundational observations that range from enzyme kinetics in biochemistry [1], the abiologic origin of chirality in organic compounds [2], and how one can efficiently turn photons into chemical energy in physical chemistry [3, 4]. A scientific are that is full of these unanswered questions also includes quantum chemistry. Quantum chemistry applies the theories of quantum mechanics to chemical problems in order to calculate thermodynamic properties, interpret spectral observations, explore molecular geometries, and understand fundamental intermolecular bonding present in. The rapid increase in computer speed combined with continual developments of new quantum chemical methods has made quantum chemistry applicable in nearly all areas of science. [5, 6]

1.1 Quantum Mechanics

1.1.1 Timeline of Quantum Mechanics

The discovery of the wave-like nature of light in 1801 by Thomas Young serves as one of the foundations of the field now called quantum mechanics. [7] This wave-like nature was discovered using a double-slit experiment which proved that light and matter have classical characteristics of particles and waves. Within a year of this discovery J. J. Thompson's cathode ray tube experiment lead to the discovery of negatively charged particles in all atoms called electrons. [8] Following the discovery of electrons, in 1864 James Clerk Maxwell predicted the speed of light and concluded that light is an electromagnetic wave. [9] Some years later, in 1888 Heinrich Hertz discovered radio waves and concluded that the wavelength of the light multiplied by the frequency is equal to the speed of the light, as shown in Eq. 1.1. [10]

$$c = \lambda\nu \tag{1.1}$$

In the early 1900's the blackbody experiment showed that a blackbody is an object that absorbs all light falling on it. Using data provided by the blackbody experiment, Max Planck determined what is now known as Planck's constant ($h = 6.6x10^{-34} J \cdot s$). [11] With the knowledge that the intensity of this radiation is a measure of the energy per unit area, it was initially assumed the energy should change in a continuous manner with all temperatures. Surprisingly, the energy did change in a continuous manner except those in the ultraviolet region where a sharp downturn in energy is observed. To explain this result, Planck proposed that the energy of an electromagnetic wave is quantized, rather than continuous. During this time, what is now known as the photoelectric effect was also being investigated. With the combined work of multiple scientists, it was determined that when electromagnetic waves (light) strike a metal surface photoelectrons are emitted. Many believed that the energy of a wave was proportional to the intensity, leading to the assumption that a dim light would lead to a delayed emission of photoelectrons. Experimental results disagreed

with this prediction. It was discovered that once light reaches a frequency threshold, photoelectrons would continue to be emitted regardless of intensity or time. With this discovery, Einstein proposed light is not comprised of a continuous wave, but instead is made of small discrete wave clusters. He defined the energy of a photon as,

$$E_{photon} = h\nu. \tag{1.2}$$

Rutherford, Geiger, and Marsden determined in the early 1900's that there is an infinitesimally small positively charged center in each atom that contains most of the atom's mass. [12] The discovery of a positively charged atomic center was done via the Rutherford gold foil experiment. The gold foil experiment was done by bombarding thin gold foil sheets with α-particles and detecting the deflected particles. Rutherford then coined this model as the planetary model of the atom in 1911. The planetary model is the accepted representation that is still taught in classes today.

Using knowledge gained from previous scientists, Niels Bohr proposed that the energy of the electron in the hydrogen atom is quantized. [13] In 1923, Louis de Broglie postulated the motion of electrons may have wave-like aspects to them. [14] Four years later in 1927 Davidson and Germer proved de Broglie's hypothesis by observing diffraction patterns from nickel. [15] Following de Broglie, Stern and Gerlach observed that the wave-like properties of electrons follows the general laws of motion for microscopic particles. [16] Using information gathered from Bohr, de Broglie, Stern and Gerlach the hypothesis of wave-particle duality for electrons was now proven true. This work shows that an electron is neither a wave or particle, but behaves in some respects like both. Heisenberg then investigated the wave-particle duality of electrons, and how it affects the ability to measure position and momentum at the same time. [17] Heisenberg demonstrated that there is an intrinsic error associated with measuring both of these observables at the same time, which is now known as the uncertainty principle, as shown in Eq. 1.3. [18]

$$\Delta x \Delta p \approx h \tag{1.3}$$

In addition to the mentioned breakthroughs, several other experiments, theories and discoveries

happened and serve as foundational findings and inspirations for the field. Blackbody radiation, the gold foil experiment, and the photoelectric effect serve as just a brief overview of the birth of quantum mechanics in which its fundamental theories and equations are used in research today.

1.1.2 The Postulates of Quantum Mechanics

With a wide range of information gathered over the previous 100 years and a multitude of interpretations to be formed from this, the founders of quantum mechanics have developed a set of postulates that serve as the basis that most of the physics to describe and study systems are derived. [19]

1. The state of a system is entirely described by a function of constituent coordinates and time. This functional is required to be single-valued, continuous over all space, quadratically integrable and representable in a vector space.

2. Every observeable property of a system has a corresponding linear hermitian operator.

3. When measuring an observable a, corresponding to operator $\hat{A}$, the only possible measurements will be equal to an eigenvalue of $\hat{A}$. The set of eigenkets of a linear hermitian operator form a complete set.
$$\hat{A}|f_i\rangle = a_i|f_i\rangle \tag{1.4}$$

4. The expectation value of a property corresponding to an operator $\hat{A}$ on a system defined by state function $|\Psi\rangle$ is defined as
$$\langle\hat{A}\rangle = \frac{\langle\Psi|\hat{A}|\Psi\rangle}{\langle\Psi|\Psi\rangle}. \tag{1.5}$$

5. The system evolves according to the time dependent Schrödinger equation (see Eq. 1.6, below).

6. Due to the fact that electrons are fermions, their electronic state functions must obey the anti-symmetry principle.

1.1.3 The Schrodinger Equation

Using the work done by Planck, Einstein, and others, Erwin Schrödinger developed a linear partial differential equation that describes the wave function of a quantum mechanical system that is known as the time-dependent Schrödinger equation. [20]

$$\frac{-\hbar}{i}\frac{\partial\Psi(x,t)}{\partial t} = \frac{-\hbar^2}{2m}\frac{\partial^2\Psi(x,t)}{\partial t^2} + V(x)\Psi(x,t) \tag{1.6}$$

The wave function, Ψ, is defined as

$$\Psi(x,t) = e^{\frac{-iEt}{\hbar}}\Psi(x) = g(t)\Psi(x) \tag{1.7}$$

which can be separated into respective time and position dependent functions. The time-independent Schrödinger equation can be derived from Eq. 1.6, by using Eq. 1.7 to give,

$$\frac{-\hbar}{i}\frac{1}{g(t)}\frac{\partial g(t)}{\partial t} = \frac{-\hbar^2}{2m}\frac{1}{\Psi(x)}\frac{\partial^2\Psi(x)}{\partial x^2} + V(x). \tag{1.8}$$

The left hand side of this equation is exclusively dependent on time and the right hand side is only position dependent. Introducing a separability constant E, we have

$$E\Psi(x) = \left[\frac{-\hbar^2}{2m}\frac{\partial^2}{\partial x^2} + V(x)\right]\Psi(x), \tag{1.9}$$

where the quantity inbrackets is referred to the Hamiltonian operator ($\hat{H}$), leading to,

$$\hat{H}\Psi(x) = E\Psi(x). \tag{1.10}$$

The Hamiltonian operator in atomic units, where the elementary charge (e), electron rest mass (m_e), and reduced Planks constant ($\hbar$) are equal to 1, is defined as

$$\hat{H} = -\sum_{i=1}^{N} \frac{1}{2}\nabla_i^2 - \sum_{A=1}^{M} \frac{1}{2M_A}\nabla_A^2 - \sum_{i=1}^{N}\sum_{A=1}^{M} \frac{Z_A}{r_{iA}} + \sum_{i=1}^{N}\sum_{j>i}^{N} \frac{1}{r_{ij}} + \sum_{A=1}^{M}\sum_{B>A}^{M} \frac{Z_A Z_B}{R_{AB}} \tag{1.11}$$

where ∇_i^2 and ∇_A^2 are the Laplacian operators for the i^{th} electron and A^{th} nucleus, M_A is the mass of nucleus A, Z_A is the atomic number of nucleus A, and r_{iA}, r_{ij} and R_{AB} are the electron-nucleus, electron-electron and nucleus-nucleus distances respectively. The first two terms of Eq. 1.11 are the kinetic energy terms, the third is the Coulombic attraction term between the electron and nucleus and the fourth and fifth terms are the repulsion integrals between like particles.

To simplify Eq. 1.11 one applies the Born-Oppenheimer approximation. [21] This approximation states that the rate of change in the position of the nuclei (R) is much slower than that of the electron (x), making them time-scale separable. This allows for the seperability of the electronic and nuclear parts of the Schrödinger equation. Overall this approximation allows one to use this separability to give an electronic Hamiltonian and a nuclear Hamiltonian. This then reduces the overall Hamiltonian from five terms to three terms and a constant, while allowing the electronic Hamiltonian operator to be explicitly dependent on only the electron coordinates. (Eq. 1.12)

$$\hat{H}_{el} = -\sum_{i=1}^{N} \frac{1}{2}\nabla_i^2 - \sum_{i=1}^{N}\sum_{A=1}^{M} \frac{Z_A}{r_{iA}} + \sum_{i=1}^{N}\sum_{j>i}^{N} \frac{1}{r_{ij}} + \hat{V}_{NN}(R) \tag{1.12}$$

1.1.4 Hartree Fock Theory & Density Functional Theory

To solve the multi-electron Schrödinger equation one needs to apply approximations. The most widely used is Hartree-Fock theory, which seeks to reduce a multi-electron problem into an effective one electron problem. [22–28] This theory begins with the idea that wave functions are made of one electron orbitals. To obey the anti-symmetry principle for an N-electron system a normalized Slater determinant ($|\Psi_0\rangle$) containing N spin orbitals (ψ_i) is used as the wave function.

$$|\Psi_0\rangle = |\psi_1\psi_2...\psi_N|, \tag{1.13}$$

where $|\square|$ denotes a normalized Slater determinant. Via the variational principle, the Slater determinant is optimized to minimize the energy expectation value,

$$E = \langle\Psi_0|\mathbf{H}|\Psi_0\rangle \tag{1.14}$$

where $\mathbf{H}$ is the electronic Hamiltonian. Under the constraint of orthonormality the following one electron eigenvalue equations are generated.

$$\hat{\mathbf{f}}_i\psi_i = \epsilon_i\psi_i \tag{1.15}$$

where $\hat{\mathbf{f}}$ is the Fock operator which is defined as,

$$\hat{\mathbf{f}}_i = \hat{\mathbf{h}}_i + \hat{\mathbf{V}}_i^{HF}. \tag{1.16}$$

In this equation $\mathbf{h}_i$ is the one electron operator that describes the kinetic energy of electron i in the field generated by a nucleus with a charge Z_A and the electrons kinetic energy.

$$\hat{\mathbf{h}}_i = -\frac{1}{2}\nabla_i^2 - \sum_A \frac{Z_a}{r_{iA}} \tag{1.17}$$

The second term of the Fock operator, $\mathbf{V}_i^{HF}$, is defined as,

$$\mathbf{V}_i^{HF} = \sum_j \mathbf{J}_j - \mathbf{K}_j \tag{1.18}$$

$$\mathbf{J}_j|\psi_i(1)\rangle = \langle\psi_j(2)|\frac{1}{r_{12}}|\psi_j(2)|\psi_i(1)\rangle \tag{1.19}$$

$$\mathbf{K}_j|\psi_i(1)\rangle = \langle\psi_j(2)|\frac{1}{r_{12}}|\psi_i(2)|\psi_j(1)\rangle \tag{1.20}$$

Using the above definitions and expanding each of the orbitals as a linear combination of basis functions, χ_ν, the following equation arises,

$$\sum_\nu \hat{\mathbf{f}}_i\,|\chi_i\rangle\,C_{\nu i} = \epsilon_i \sum_\nu |\chi_\nu\rangle\,C_{\nu i} \tag{1.21}$$

Left multiplication of χ_μ and rearrangement of Eq. 1.21 leads to,

$$\mathbf{FC} = \mathbf{SCe} \tag{1.22}$$

where **F** is the Fock matrix, **C** is the MO coefficient matrix, **S** is the overlap matrix and **e** is a diagonal matrix containing the MO energies. This equation is solved in an iterative manner. This starts with a guess for **C**, which is used to build **F** and this process repeats until a predefined numeric threshold is met.

The difference between the Hartree-Fock energy and the exact non-relativistic energy is called *electron correlation*. [29] Hartree-Fock theory accounts for Fermi correlation, but if Löwdins definition of electron correlation is used then there is zero correlation. Unfortunately the remaining missing part of the energy usually plays an important role in studying and explaining most chemical processes. The electron correlation energy is composed of static and dynamic correlation. The poor representation of the static correlation is due to the fact that the wave function is represented by a Slater determinant which may poorly represent many electron systems. The error in the dynamic portion of the correlation energy is because Hartree-Fock theory does not account for the instantaneous interactions of electrons, and instead treats electron-electron interaction by a mean-field approach. Hartree-Fock serves as the foundation or starting point for most higher levels of theory.

In an attempt to advance the calculation of the ground state electronic energy Hohenberg and Kohn hypothesized that the total can be written as a function of the electron density. This result is the model known as density functional theory (DFT). [30–33] The proof of this theory was due to

three arguments presented by E. B. Wilson,

1. An integral over the density will be equal to the number of electrons;

2. The positions of the nuclei are at the cusps in the density; and

3. The nuclear charges correspond to the height of the cusps.

Initially an orbital free DFT was proposed, [34] but later Kohn and Sham (KS) developed an orbital based approach that is a self-consistent method. KS also suggested that an orbital scheme provides a better representation of the kinetic energy. In KS DFT most terms are closely related to those in Hartree-Fock, with the two-electron contributions to the KS Fock-like operator now including exchange correlation terms.

1.2 Computational Chemistry

Theoretical chemistry is a field made up of many different sub-fields including electronic structure theory, quantum nuclear dynamics, quantum chemistry, molecular mechanics and molecular dynamics. Quantum chemists apply the laws of quantum mechanics to fundamental chemical problems, while computational chemists focuses on the application of approximation schemes such as Hartree-Fock and DFT to chemical problems to compliment experimental results. Molecular mechanics focuses on modeling without necessarily including quantum mechanics and molecular dynamics uses classical mechanics to simulate nuclei movement.

The entire field relies on the connections between mathematics, physics, computer science and chemistry. This collaboration of knowledge and expertise opens avenues of research that were once not possible. Using the theories and experiments discovered by the founders of quantum mechanics, Heitler and London performed the first electronic structure theory calculation in 1927. In the years that followed, computer technology rapidly increased and by the 1950's the first sets of semi-empirical and ab initio Hartree-Fock calculations were completed. As time progressed and science advanced, efficient ab initio programs, such as Gaussian [35], Q-Chem [36], NWChem [37],

Terachem [38], Psi4 [39] and many others were developed to efficiently carry out complex quantum chemical calculations. Within the field of computational chemistry there are a three main classes of methods that have been developed: (1) molecular mechanics; (2) semi-empirical; and (3) ab initio.

1.2.1 Molecular Mechanics Methods

When studying large molecular systems such as proteins, one generally attempts to avoid quantum mechanical methods due to cost, and instead attempts to find more cost efficient methods. [40, 41] Molecular mechanical (MM) methods compute the potential energy surface for molecules using potential functions derived from classical models. [42, 43] There are several assumptions applied to a systems when using MM on a system.

- The Born-Oppenheimer approximation is still applied, but the potential energy is usually calculated via force fields that are functions of the nuclear positions.
- The potential energy function is calculated by summing up the individual components of a bond (i.e. stretching, bending, torsions and non-bonding interactions).
- The atoms are modeled as hard spheres with assigned radius, polarizability and charge.
- The bonds of the molecule are treated as springs with an equilibrium distance calculated from experiments.
- The potential functions are formed from experimental data such as force constants an equilibrium values.

The main advantage of these methods is that they requires less computational cost than other quantum mechanical methods making them useful for large systems. The disadvantages of these methods include limited modeling ability due to parameterization, ill defined atom types and an inability to account for possible bond changes. [44, 45]

1.2.2 Semi-Empirical Methods

This method is generally used on large molecular systems when Hartree-Fock like methods are too expensive. A large component of the cost of many methods is due to the calculation of

the two electron integrals. Semi-empirical methods attempt to reduce the number of integrals that need to be calculated In addition to the reduction of the two electron integrals, semi-empirical methods reduce core electrons to a nuclear charge and only consider valence electrons. [46, 47] These methods uses many of the formalism's in Hartree-Fock but approximate many integrals with empirical parameters that can be adjusted to ensure agreement with experimental data. The accuracy of these methods is heavily dependent on the data set used for parameterization.

Most semi-empirical methods exclude some expensive two electron integrals that are part of the Hamiltonian in other methods. Below is an overview of different semi-empirical methods from oldest to newest. [48]

1. The zero differential overlap (ZDO) method neglects all two electron integrals that include orbitals that are not the same.

$$(\mu\nu|\lambda\sigma) = (\mu\mu|\lambda\lambda)\delta_{\mu\nu}\delta_{\lambda\sigma} \tag{1.23}$$

   where $\delta_{\mu\nu} = 1$ if $\mu = \nu$ and $\delta_{\mu\nu} = 0$ if $\mu \neq \nu$. An additional approximation to ZDO is that it uses s orbitals only.

2. The neglect of diatomic differential overlap (NDDO) method developed by John Pople, neglects fewer integrals that ZDO. Instead of neglecting all two electron integrals with different orbitals. This method excludes integrals where orbitals μ and ν are not on the same atom, and where λ and σ are not on the same atom. This methods provides more accurate results and a larger number of adjustable parameters.

3. The intermediate and complete neglect of differential overlap (INDO & CNDO) methods neglects all two-center two-electron integrals that are not Coulombic.

4. The modified neglect of diatomic overlap (MNDO) method is a modified NDDO that differs on in the treatment of the core electrons and how parameters are assigned. Some limitations to this method is that it cannot model high energy changes suck as bond breaking and transition

states. This method also provides results with exaggerated steric crowding and non-reliable hydrogen bonding data. Multiple variations of this method have been developed with the intention of improving some of the disadvantages. This includes the Austin Model 1 (AM1) and the Parametric Method 3 (PM3) methods where the treatment of the core functions and the parametrization is altered. These methods offer a larger amount of atoms that can be used and mild improvements to bonding issues.

Overall, semi-empirical methods neglect all 3 and 4 center integrals and reduce the amounts of 1 and 2 electron integrals that are calculated reducing the cost. These methods preform well for systems where experimental data exists, and are considered mildly robust because they are based on quantum mechanical methods.

1.2.3 Ab Initio Methods

Ab initio methods are used on a variety of problems and their derivations are based on quantum mechanics. [49, 50] The name ab initio translates to "from the beginning", meaning that there is no parametric input into these methods and they only start with physical constants. The goal of these methods is to solve the Schrödinger equation using the positions of the nuclei and electrons. The results obtained from these methods include molecular geometries, electron densities, energies and other properties. This class includes commonly used methods such as Hartree-Fock, post Hartree-Fock and multi-reference techniques. *Hartree-Fock* calculates an upper-bound to the true energy quantum mechanically for many-body systems by approximating the wave function as a single Slater determinant. This method is described in detail in section 1.1.4. *Post Hartree-Fock* methods include Moller-Plesset perturbation theory (MP) [51], couple cluster theory (CC) [52] and configuration interaction theory (CI) [53]. These methods add additional cost to the calculation, but are used to improve upon areas that Hartree-Fock cannot capture. MP is a method that attempts to improve the electron correlation by adding 2nd, 3rd or 4th order correction terms to the Schrödinger equation. CI methods generate wave functions as a linear combination of all configuration state functions. This methods requires a large amount of memory and CPU cost, so this is

limited to relatively small systems. This class includes Full CI, which gives a ”true” solution to the Schrödinger equation within a given basis. CC methods construct multi-electron wave functions similar to CI, but applies an exponential ansatz and basics provided by the Hartree-Fock orbitals. These methods can include contributions from single, double and triple excitations. *Multi-Reference* methods include multi-configurational SCF (MCSCF) [54, 55], complete active space perturbation theory (CASPT) [56, 57] and multi-reference configuration interaction theory (MRCI) [58, 59]. All of these methods are generally used to treat systems with a strong static correlation, but at this time are not usually applicable to large systems.

1.3 Transition Metal Chemistry

Transition metals play an important role in a wide range of chemical processes such as catalysis. [60] These elements generally have multiple electronic configurations of valence d-shell electrons and have the ability to form bonds with both their p and d-shells simultaneously. These properties of transition metals create a variety of possible obstacles when studying them computationally. These obstacles include electron configurations, bonding and degenerate states.The variety of electron configurations leads to a range of oxidation states and electron spin configurations. To address this, initial studies are generally preformed to determine the lowest energy state for the metal involved. Once the ground state oxidation state and electron configuration are determined, this is generally followed by investigations into the chemistry the transition metals are involved in or catalyzing.Transition metals can bond with a variety of ligands in different geometric orientations. Investigations into this bonding must be thoroughly explored to accurately describe chemical processes that involve transition metals. The introduction of d-shell orbitals into the calculations can cause challenges in the initial single-determinant approximation. [61] This is due to the large amount of low-lying near-degenerate states. Many methods have been developed over the years with the intention of fixing this error, but these are usually cost prohibitive for systems of realistic size. Recently, DFT has become the primary method used for these investigations. Over the last

several decades the combination of unprecedented computational speed and new methods allows for the efficient and accurate study of transition metal systems.

1.4 Dissertation Overview

The work in this thesis has been motivated by applying and expanding the computational chemistry models for exploring transition metal catalyzed organic transformations. In particular this thesis focuses on developing a thorough understanding of multiple mechanisms of interest.

Studies of transition metal catalyzed organic transformation and an analysis of the electronic structure of all intermediates involved allows one to thoroughly understand complex chemical bonding. This knowledge permits one to build upon other similar processes and suggest alternate explanations as to why specific chemical processes occur. Below are general descriptions of the projects described in detail in the chapters that follow.

Copper Catalyzed Azide-Alkyne Cycloaddition (CuAAC) to Regio-Selectively form Triazole

A computational investigation into the governing mechanism of an azide-alkyne cycloadditon that is catalyzed by copper(I). This click chemistry reaction is highly versatile and plays an important role in a variety of fields. This exploration was performed to explain interesting published experimental observation .

Experimental and Theoretical Evidence for Nitrogen–Fluorine Halogen Bonding in Silver–Initiated Radical Fluorinations

In collaboration with synthetic organic chemists an investigation of the nitrogen-fluorine bonding motif in the context of silver (I) initiated radical C-H fluorinations was preformed. Halogen bonding has gained attention as a potential surrogate for hydrogen bonding and promoting organic transformations. This theoretical study accurately predicted and explained current counter-intuitive experimental results.

A Novel Approach for Asymmetric Bromination: A Computational Investigation

In collaboration with synthetic organic chemists we explored a new method for aromatic bromina-

tion using lactic acid derivatives as halogen-bond acceptors with N–bromosuccinimide (NBS). With combined effort we investigated a series of additives and looked at their halogen-bonding abilities.

Intermolecular Perturbational Analysis: A Quantitative Non-Traditional Bonding Study

Transition metals contain a multitude of unique properties, including but not limited to their ability to bind in non-traditional ways. Inspired by previous research, a model to quantitatively describe the energy contributions produced by multi-center bonding was developed. The basis of the method relies on equations derived using molecular orbital perturbation theory.

Chapter 2

A Computational Exploration of the Copper Catalyzed Azide-Alkyne Cycloaddition

Transition metal-catalyzed transformations are essential for the development of many compounds that serve as a cornerstone of modern-day organic chemistry. The copper(I) catalyzed azide-alkyne cycloaddition is an extremely versatile reaction with an impressive array of applications across chemistry. Computational investigations provide a thorough understanding of fundamental and open mechanistic questions. Here we present a complete mechanistic picture of this reaction that seek to explain recent intriguing experimental reports for this reaction.

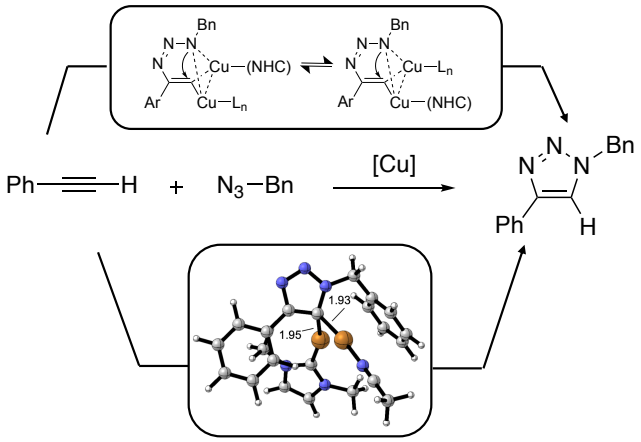

2.1 Introduction

The copper-catalyzed azide-alkyne cycloaddition (CuAAC) reaction provides a highly selective route for the formation of triazoles. [62–99] Indeed, the CuAAC reaction tolerates a wide variety of functional groups and reaction conditions. Due to its experimental simplicity and versatility, the CuAAC reaction has been employed in myriad applications from small molecule synthesis to materials science, polymer chemistry, and medicinal and bio-chemistry. Despite its wide use, questions regarding mechanistic aspects of this reaction remain open. As a result, interest in fundamental reaction scope and mechanism studies remain of paramount and continued interest.

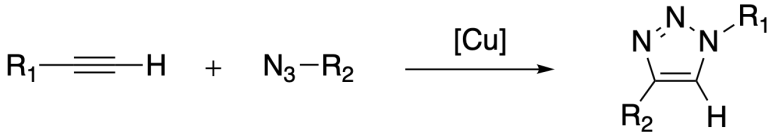

Figure 2.1: The overall reaction of a copper catalyzed azide alkyne cycloaddition to form 3,5-substituted triazole.

Sharpless and co-workers first reported the CuAAC reaction 20 years ago. [100, 101] Regioselectivity was achieved using azides and terminal acetylenes to yield exclusive production of 1,4-disubstituted 1,2,3-triazoles. They further determined reaction conditions using Cu(II) salts for in-situ catalyst preparation provide enhanced performance. The initially proposed reaction mechanism involves a single copper center and invokes a six-member metallacycle intermediate that undergoes rapid conversion to a five-member triazolide.

A computational study by Straub suggested that acetylide oligomers with multiple copper centers may facilitate improved chemical kinetics in the CuAAC reaction. [102] Specifically, it was shown that dinuclear and tetranuclear copper acetylide complexes exhibit a higher stability and reactivity when compared to mononuclear counterparts. Straub hypothesized the improved reactivity and stability is due to reduced ring strain and fragment stabilization of intermediates formed from such multi-copper complexes. Straub's calculations modeled copper acetylides without N-

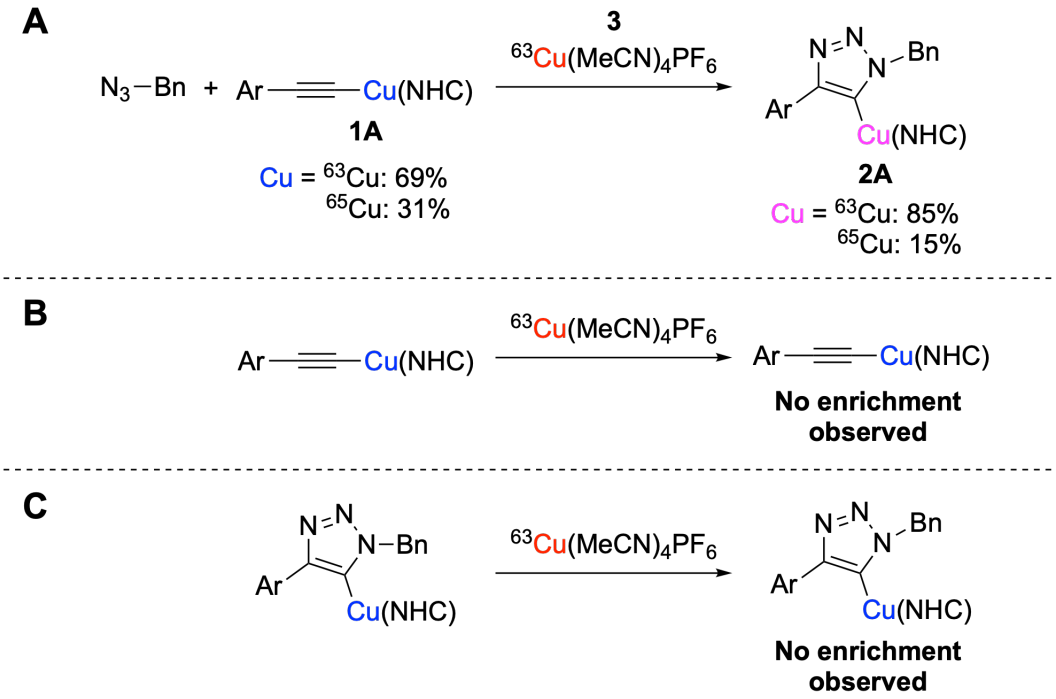

Figure 2.2: Presented here is a summary of the isotopic labeling experimental results by the Fokin lab. Reaction **A** shows that when preformed copper acetylide (**1A**) in natural isotopic distribution is reactions with isotopically pure copper catalyst the final copper substituted intermediate (**2A**) exhibits a 50% isotopic enrichment. Reaction **B** was preformed to show that **1A** does not exchange coppers with the catalyst in solution, and reaction **C** is to show exchange does not occur with **2A** as well.

heterocyclic carbene (NHC) ligands, and it was noted that the presence of NHC ligands may lead to different chemistry.

Finn and coworkers thoroughly investigated the rates of the CuAAC reaction under a variety of reaction conditions. [103] A series of kinetics experiments indicated that with saturating amounts of catalytic copper the reaction rate is second order in metal concentration. Ahliquist and Fokin computationally supported the experimentally observed rate law. [104] DFT studies suggested a second copper center facilitates formation of an intermediate in the rate-determining step that stabilizes the metallacycle intermediate. That work explored a variety of bonding modes to explain the increased reactivity when a second copper is introduced.

More recently, Fokin and co-workers isolated and characterized copper(I)-acetylide **1** and -

triazolide **2**. [105] Using these intermediates they monitored catalyzed and non-catalyzed systems with an azide and preformed copper-acetylide via real-time heat-flow reaction calorimetry. The results show the non-catalyzed reaction does not produce triazole product, while the catalyzed reaction completed within 20 minutes. Interestingly, the isolated copper-triazolide product exclusively features an NHC ligand, even though only one of the coppers of **1** is bound to NHC. They hypothesized the two coppers act independently of each other, with one copper bound in a weak π-complex and the other σ-bound to the acetlyide (**6**). A series of isotopic crossover studies supported this hypothesis (Scheme **??**). Reaction **A** shows the reaction of azide with preformed copper acetylide with both naturally occurring isotopic distributions and isotopically pure copper catalyst. To their surprise isotopic enrichment of the copper-triazolide was observed. These results show that enrichment must occur via the acetylide intermediate, the copper-triazolide intermediate, or somewhere within the cycloaddition steps. Further experiments (Reaction **B** and **C**, Scheme **??**) disproved the ability of the coppers to exchange in the acetylide or the triazolide intermediates, suggesting enrichment must occur within the cycloaddition steps of the CuAAC reaction. Evaluated holistically, results of those studies lead to two key conclusions: (1) the reaction mechanism must include a structure featuring two geometrically equivalent coppers with an equal likelihood of binding to NHC ligands; and (2) the NHC ligand appears to engage in rapid ligand exchange between the two copper centers. Accounting for these two points, Fokin proposed an intermediate featuring an equilibrium between **4a** and **4b** shown in Scheme **??**.

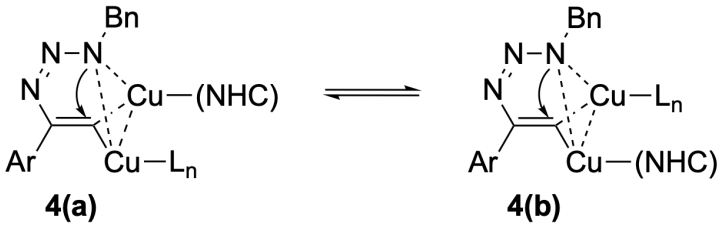

Figure 2.3: Proposed intermediate configurations developed by the Fokin group. These structures were developed to explain the experimental results where the final copper containing intermediate exhibits isotopic enrichment and is always bound to an NHC.

Fokin and co-workers proposed the mechanism shown in Scheme **??**. Their proposed mecha-

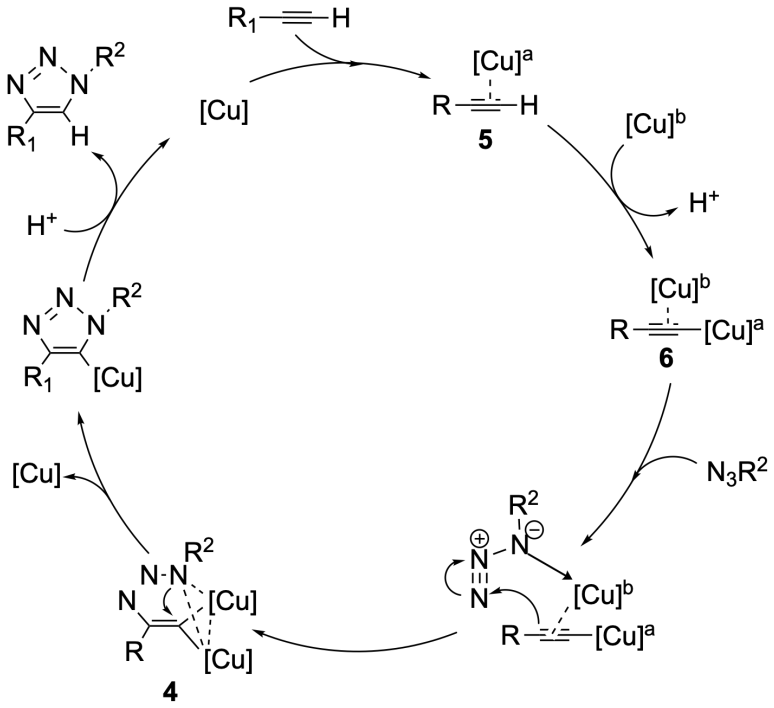

Figure 2.4: Fokin's proposed catalytic mechanism for the CuAAC reaction with two copper atoms.

nism starts with π-bound copper-acetylide **5**. The catalytic copper then forms a η^2 π-bond complex with the triple bond of the acetylide and the initial copper σ-binds to the end of the acetylide. The azide then adds to **6** to form intermediate **4** where the NHC/NCMe ligand-exchange was proposed. This metallacycle then leads to the copper-triazolide to form the desired triazole product. Notably, the mechanism requires the involvement of **4** which features a twisted ethylene.

More recently, T*üzü*n and co-workers reported a computational study primarily focused on a presumed ligand exchange in Scheme **??**. That work proposes a planar 6-member metallacycle facilitating NHC ligand exchange between the two copper centers (Scheme **??**). The ability of the NHC transfer would provide an apparent equal likelihood for the NHC ligand to be coordinated to either copper centers in the final copper-triazolide.

Initially, motivated by questions regarding the electronic structure of intermediate **4** (Scheme **??**) this work presents a density functional theory (DFT) investigation of the complete CuAAC mechanism. We investigated the proposed ligand exchange event and the kinetic competency of

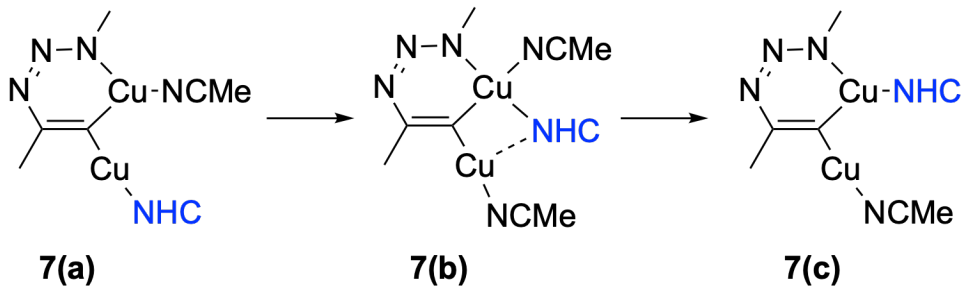

Figure 2.5: Proposed ligand exchange pathway developed by the T*üzü*n group to explain the enrichment observed in Fokin's isotopic labeling experiment. Shown here is a proposed ligand transfer event where the NHC has the ability to transfer from the external copper of the metallacycle to the ring bound copper.

intermediates **8(a)-8(c)** (Scheme **??**), especially in consideration of the well known binding strength of NHC ligands. [106, 107] In this report, we establish the presence of reaction intermediates that clarifies the isotopic enrichment and the ligand bonding observations in the copper-triazolide.

2.2 Methods

All calculations were carried out using a local development version of the Gaussian suite of electronic structure programs. [108] The B3PW91 functional and 6-311G(d) basis set were employed throughout. [109–112] Dispersion was treated using Grimme's empirical D3 correction. [113] Calculations were completed using an acetonitrile solvent with the SMD continuum model. [114] Geometry optimizations were carried out using standard methods and vibrational frequencies were calculated to ensure that optimized minimum energy structures and transitions structures (TSs) correspond to proper stationary points on the potential energy surface. [115] Optimized TSs were further characterized by subsequent intrinsic reaction coordinate (IRC) calculations to ensure located TSs connect with correct reactants and products on the potential energy surface. [116, 117]

As mentioned, the substrate scope and versatility of the CuAAC reaction are quite broad. Additionally, reports of the prototypical CuAAC reaction have involved a diverse set of ligands. To focus our mechanistic investigation while also considering ligand and substituent combinations

with representative steric bulk and electronic structure of those typically employed experimentally, we report results for species that include a benzyl substituted azide and a phenyl substituted alkyne. Further, this work considers copper centers bound to acetonitrile and methyl substituted NHC ligands, which we denote as Cu_{NCMe} and Cu_{NHC} respectively.

2.3 Results

Our investigation of the CuAAC mechanism focused on the copper-catalyzed reaction of benzyl azide with phenylacetylide. The results of the three key mechanistic phases are described in turn: (1) catalyst formation and substrate binding; (2) oxidative cyclization resulting in metallacycle intermediate formation; and (3) product formation and catalyst regeneration.

2.3.1 Catalyst Formation and Substrate Binding

The initial steps of the CuAAC mechanism involve catalyst formation and binding of the azide substrate (Scheme **??**). The Cu_{NHC}-acetylide (**1**) features a linear C-C-Cu_{NHC} angle with a C−C bond length of 1.22 Å and a C−Cu_{NHC} bond length of 1.84 Å. Compound **1** then binds with a second copper center (acetonitrile substituted) to form either bis-copper acetylide structures, **6A** or **6B**.

Compound **6A** features Cu_{NCMe} in an η^1 bond with a length of 1.84 Å, and Cu_{NHC} in an η^2 bond with the acetylide π bond (2.00 Å and 2.03 Å) The formation of **6A** is favorable by -28.37 kcal/mol. The η^2 π-bound copper center serves as the *catalytic* metal center in later steps of the mechanism and is the redox source that drives the catalytic triazole formation (*vide infra*). The benzyl substituted azide substrate then binds with the η^2 Cu_{NHC} in **6** to form intermediate **8**, which has a reaction enthalpy of -22.95 kcal/mol. The two copper centers are bound to the terminal carbon of the acetylide with bond lengths of 1.88 Å and 1.94 Å, and Cu_{NHC} is bound to the azide with a Cu−N bond length of 2.15 Å.

Compound **6B** has a favorable enthalpy of formation of -25.78 kcal/mol and features Cu_{NHC}

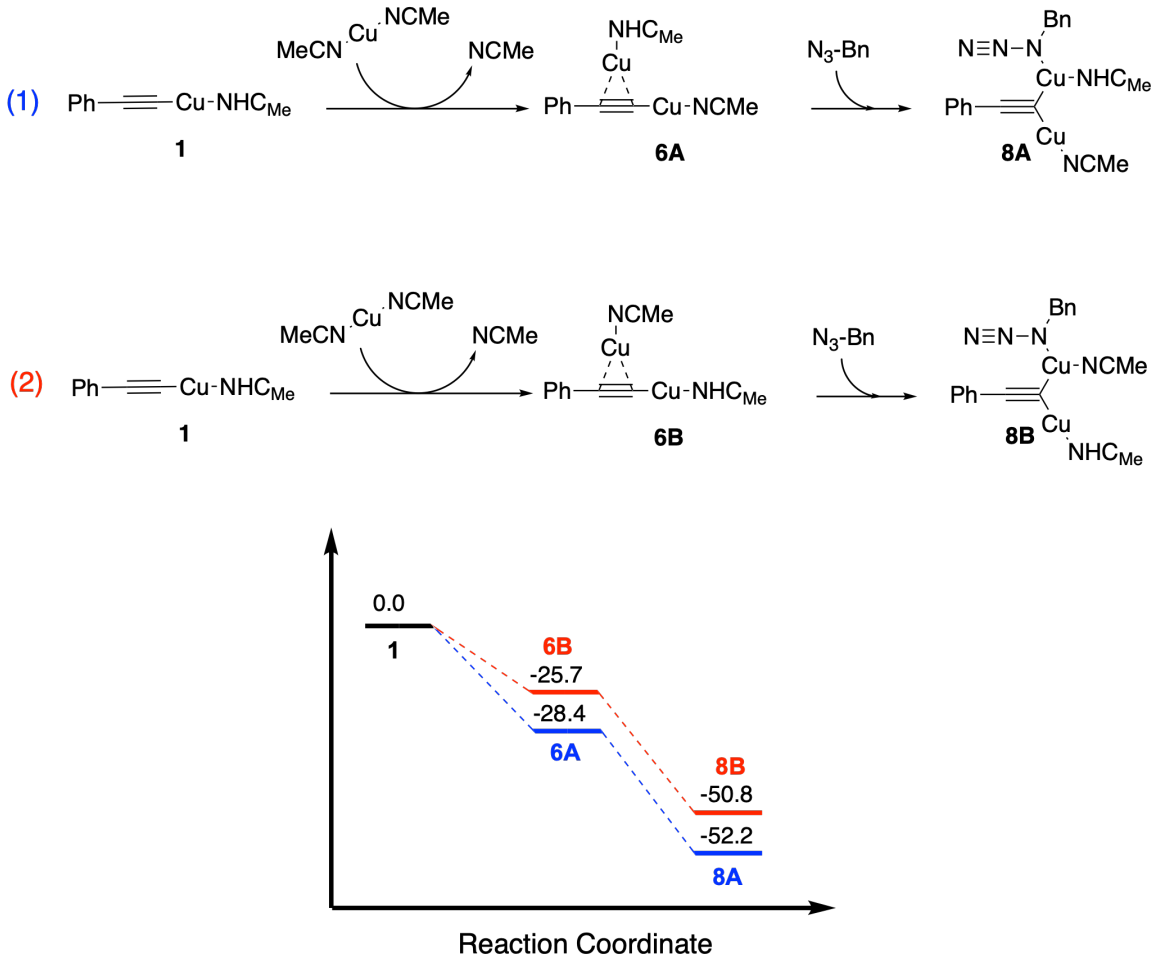

Figure 2.6: The first two steps of the CuAAC mechanism proposed in this work. The initial step is the catalyst formation, where the copper-acetylide binds with the copper catalysts to form **6(A/B)**. This intermediate then binds with the azide to form intermediate **8(A/B)**.

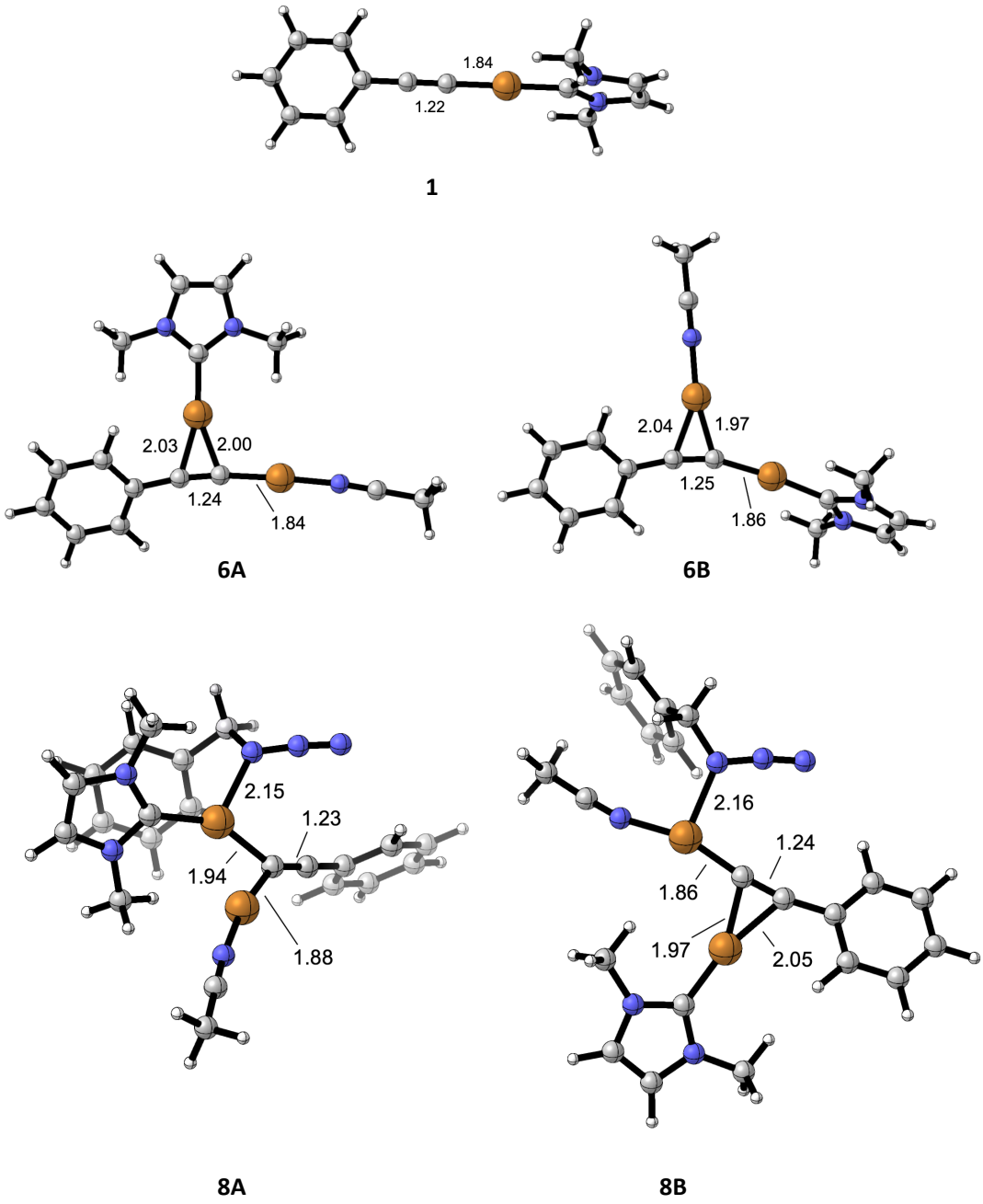

Figure 2.7: Optimized minimum geometries and key bond lengths of the intermediates involved in the catalyst formation and substrate binding steps of the CuAAC mechanism.

in an η^1 bond with a length of 1.86 Å, and Cu_{NCMe} in an η^2 bond with the acetylide (2.04 Å and 1.97 Å, Cu-C Distances). Similar to structure **6A**, the azide binds with Cu_{NCMe} to form **8B**. This reaction is somewhat more favorable than the **6A** → **8A** reaction, with a enthalpy of formation of -32.10 kcal/mol.

2.3.2 Metallacycle Formation and Ring Reduction

The next portion of the mechanism involves 6-member metallacycle formation and subsequent rearrangement to bis-copper 5-member ring **9** (Scheme **??**). Ring closure of intermediates **8A** and **8B** lead to the formation of planar metallacycle **7A** and **7B**, which then reduces to **9**.

The ring formation step, **7A** → **8A** features a NHC_{Me} substituted copper in the metallacycle. As expected, this step results in an increase in the C−C bond (from 1.23 Å to 1.31 Å) as the bond order decreases from 3 to 2. The metallacycle ring C-Cu_{NHC} bond length is 1.80 Å, while the external C-Cu_{NCMe} is slightly longer at 1.85 Å. The enthalpy of formation of this reaction is 5.84 kcal/mol, with a reaction barrier due to **TS 8-7A** of 5.6 kcal/mol. The metallacycle **7** then converts to a planer five-member ring **9** shown in Figure 2.9. This intermediate features a C-C length of 1.41 Å, which lies about halfway between the standard single and double bond lengths. This is due to the three-center two-electron (3C2e) nature of the Cu_{NHC}-C-Cu_{NCMe} bond. Conversion to the five member ring is highly favorable with a ΔH of formation of -59.55 kcal/mol.

The closure of the C-N bond in **8B** to form **7B** features an optimized geometry similar to **7A**, with the only difference being the substitution of the metallacycle copper. The enthalpy of formation for this reaction step is noticeably higher at 13.88 kcal/mol with a similar barrier of 6.7 kcal/mol. This metallacycle reduces to the bis-copper five-member triazolide (**9**), with a highly favorable ΔH of formation of -60.93 kcal/mol.

2.3.3 Catalyst Regeneration and Product Formation

The remaining portion of the mechanism involves the the formation of the triazolide intermediate **2A** or **2B** and the final triazole product **10** shown in Scheme **??**. The Cu_{NCMe} from **9** leaves the

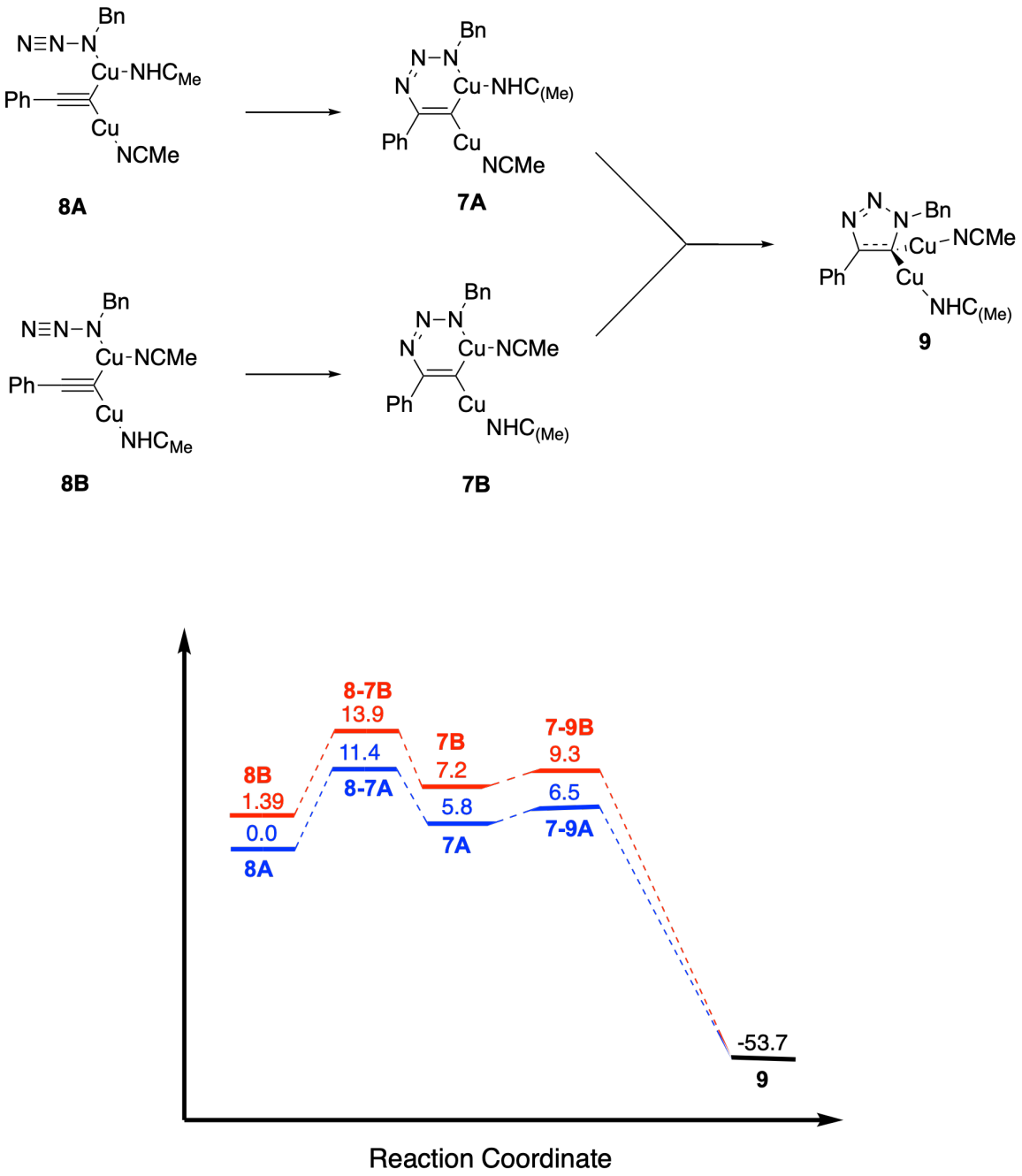

Figure 2.8: Mechanistic steps for the metallacycle formation and ring reduction. Shown in the figure is the formation of the metallacycle and the reduction of the ring to the bis-copper triazolide intermediate.

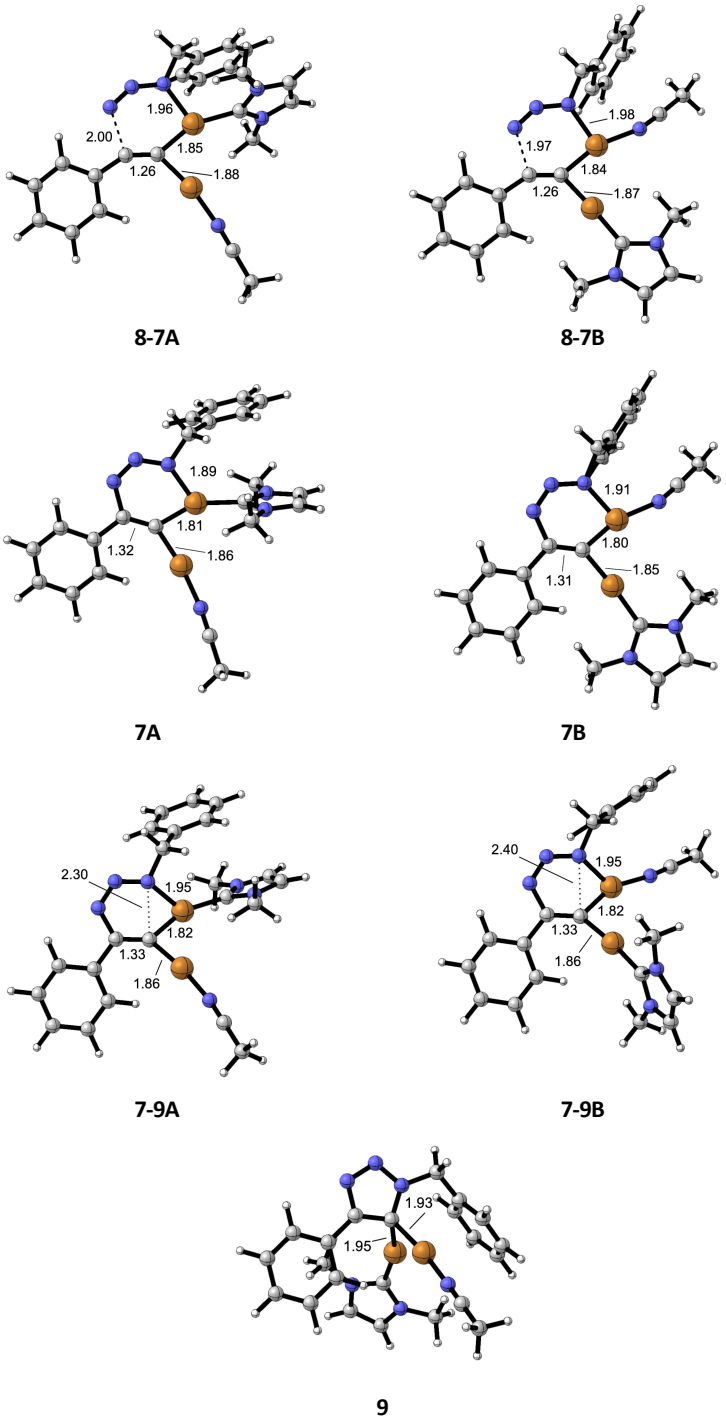

Figure 2.9: Optimized minimum geometries and key bond lengths of the intermediates involved in the metallacycle formation and ring reduction steps of the mechanism.

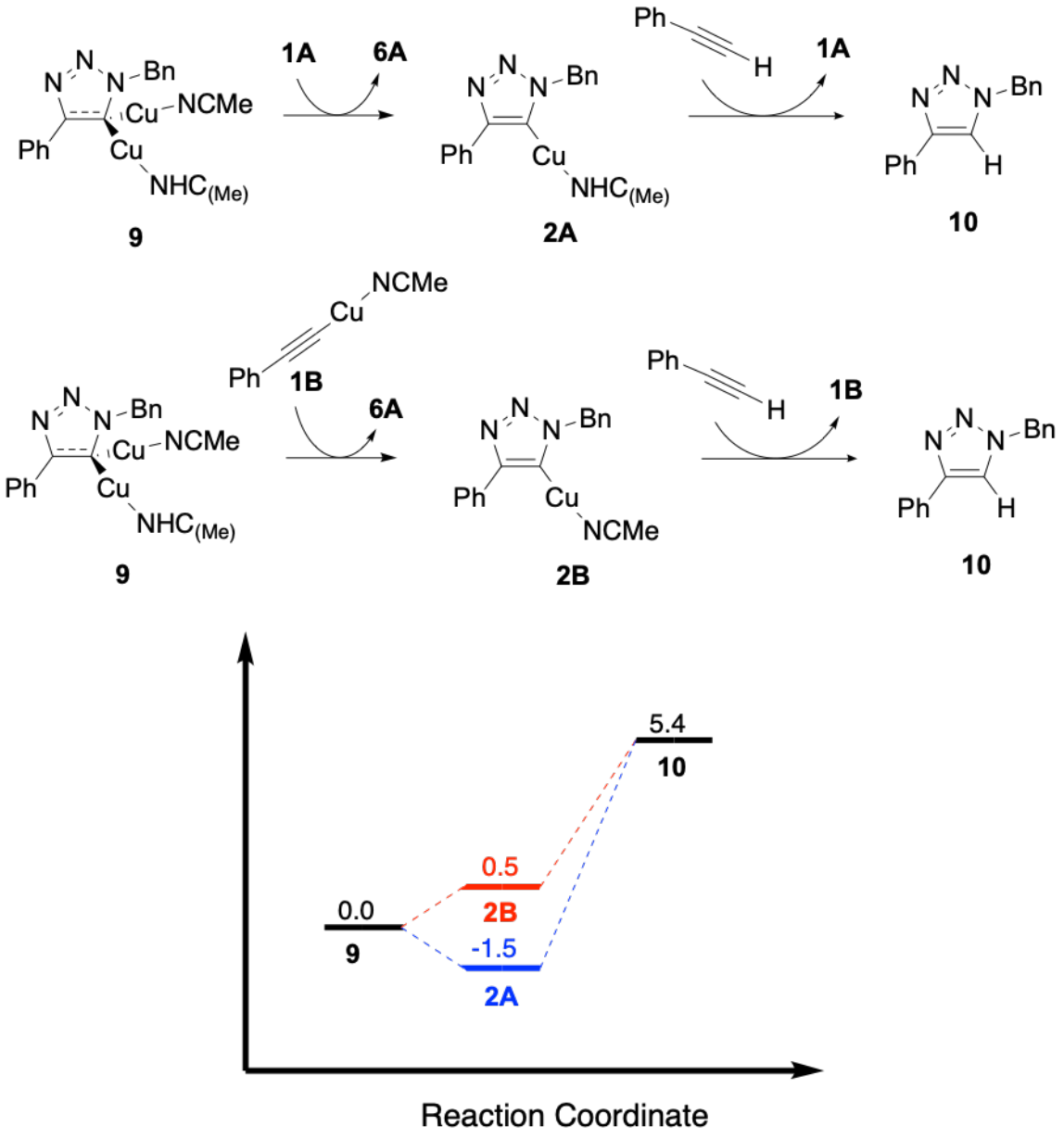

Figure 2.10: Optimized minimum geometries and key bond lengths of the intermediates involved in the catalyst regeneration and product formation steps of the mechanism.

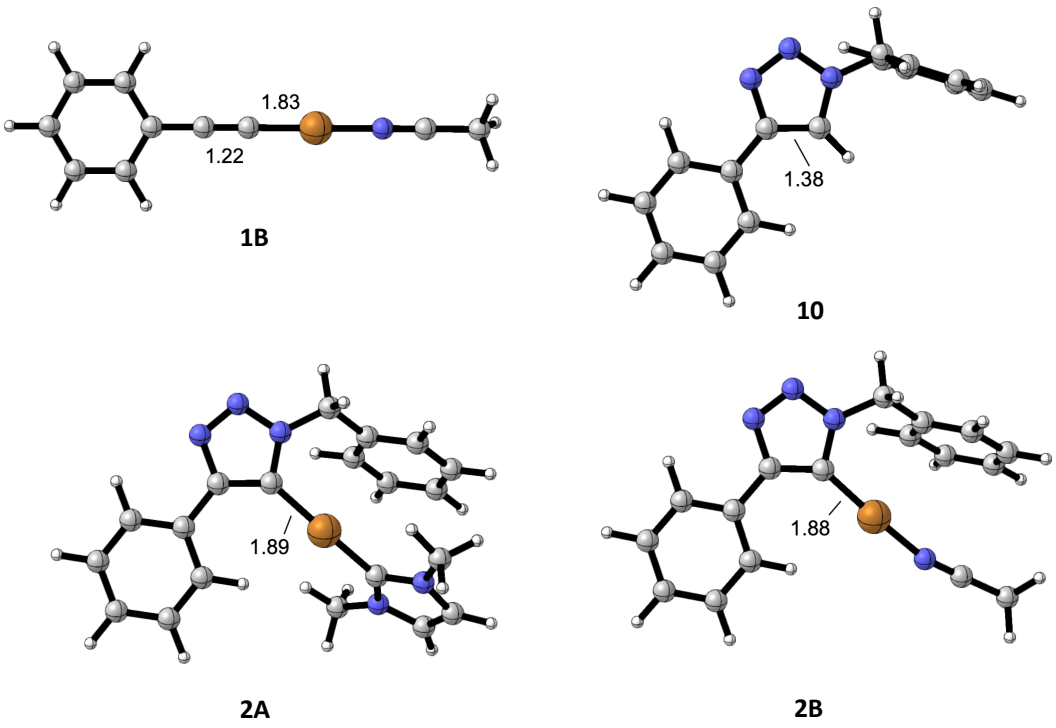

Figure 2.11: Optimized minimum geometries and key bond lengths of the intermediates involved in the formation of the copper-triazolide and the final triazole product.

ring to bind with the Cu_{NHC}-acetylide to reform **6A**. The formation of the triazolide (**2**) is favorable with a ΔH of -5.04 kcal/mol and the bond lengths remain essentially unchanged from the previous intermediate. The Cu_{NHC} in **2** is then exchanged with the hydrogen of an acetylide forming the final product and reforming **1**.

2.3.4 Ligand Coordination

As discussed above, previously reported experimental results show that the final triazole containing intermediate in this reaction mechanism is always be bound to Cu_{NHC} (Scheme **??**). To investigate the experimental observation that intermediate **2** is always ligated with NHC, we considered a set of calculations contemplating a scenario whereby free ligands in solution might coordinate to the two copper centers. These calculations began by adding varying numbers of NHC and NCMe

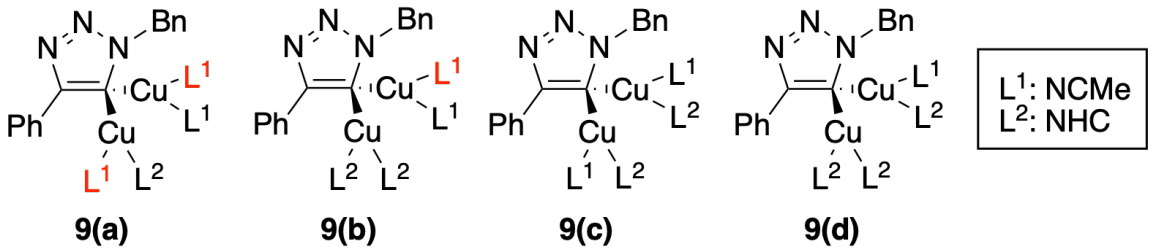

Figure 2.12: Possible ligand arrangements of intermediate **9** when additional NCMe and NHC are added to the coppers. Optimization attempts on **9(a)** and **9(b)** were unsuccessful with one or more of the ligands no longer directly bound (shown in red). Optimized geometries of the remaining intermediates **9(c)** and **9(d)** were found, but it was found that the ΔH of formation for **9(d)** was approximately 14 kcal/mol more favorable.

to compound **9** to yield **9a**-**9d**, creating 4 possible intermediates shown in Scheme **??**. We located and verified potential energy surface minima corresponding to **9c** and **9d**. However, no such energy minima were found for **9a** or **9b**. A comparison of heats of formation for **9c** and **9d** are −12.37 kcal/mol and 1.83 kcal/mol respectively. Thus, intermediate **9c** is the only valid multi-ligand intermediate. This intermediate features two equivalent coppers equally likely to be bound to an NHC and dissociate to yield the final intermediate **2**.

Following that work, Tüzün and co-workers proposed an alternate explanation for the experimental evidence. They show evidence that the NHC has the ability to transfer from one of the coppers in the metallacycle intermediate to the other. (figure 2.5) The group argued this occurred because of the weak nature of the bond the NCMe has with the copper and the inability to find a valid transition structure to **7** when NHC was bound to the copper in the metallacycle ring. Throughout our investigation we were not able to observe this transfer of ligand, instead we investigated the ability of each copper in **9** to bind to an additional ligand. To do this we started with intermediate **9** and added varying amount of NHC and NCMe to form a-d shown in figure 2.12. We were unable to obtain optimized geometries of intermediates **9a** and **9b**, but found valid minimum structures for both **9c** and **9d**. A comparison of ΔH of formation for **9c** and **9d** are -12.37 kcal/mol and 1.83 kcal/mol respectively. With these results we can conclude that intermediate **9c** is the only valid multi-ligand intermediate. This intermediate features two equivalent coppers equally likely to be

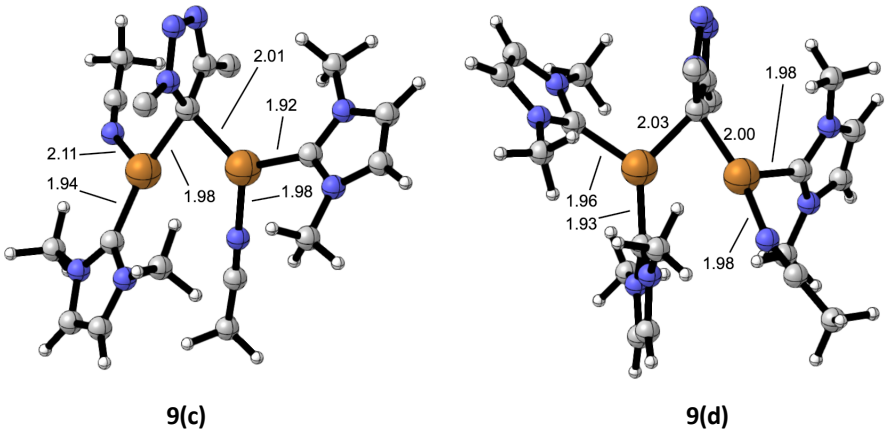

Figure 2.13: Optimized minimum geometries and key bond lengths of intermediate **9** with each copper bound to two ligands.

bound to an NHC and leave the structure and for the final intermediate **2**. We believe we have completed a thorough investigation into the experimental evidence and developed a clear explanation for the results presented in the literature.

2.4 Conclusion & Overall Mechanism

In-depth investigations into the reaction mechanism of the CuAAC reaction has led to Figure 2.14. This mechanism begins with a substituted copper replacing the terminal hydrogen of the substituted alkyne to form copper acetylide (**1**). The copper acetylide then binds with a second copper catalyst forming a dicopper acetylide (**6**). The catalytic copper(I) oxidatively adds to the benzyl substituted nitrogen of the azide to form **8**. The terminal nitrogen of the azide and the singly substituted carbon bond through oxidative cyclization to form a planar 6-member metallacycle (**7**) with a copper(III) present in the ring. The metallacycle then reduce to a five membered ring featuring a 3-center 2-electron bond between the carbon and two coppers. This intermediate then loses one copper to the copper acetylide to reform **1**, and the final quenched product, a triazolide, **2** is formed. This copper in this intermediate is then exchanged for the hydrogen of the acetylide to reform **1** and

the desired triazole product.

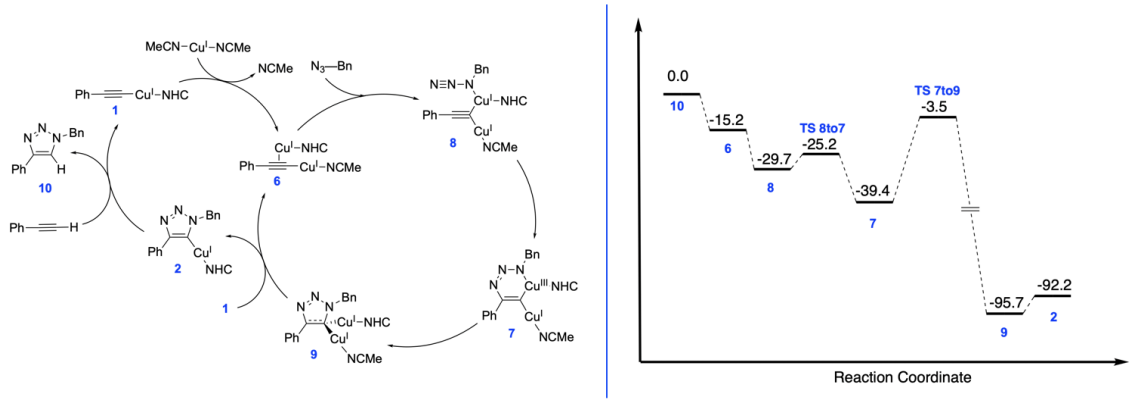

Figure 2.14: The overall proposed mechanistic pathway and energy profile for the copper(I) catalyzed azide alkyne cycloaddition.

Chapter 3

Computational Investigations of Silver Catalyzed Fluorination: A Halogen Bonding Investigation

In this chapter we computationally explore nitrogen–fluorine halogen bonding in Ag(I)–initiated radical C–H fluorinations. Simple pyridines form $[N–F–N]^+$ halogen bonds with Selectfluor to facilitate single electron reduction by catalytic Ag(I). Pyridine electronics affect the extent of halogen bonding, leading to significant differences in selectivity between mono and difluorinated products. Electronic structure calculations show that halogen bonding to various pyridines alters the single–electron reduction potential of Selectfluor, which is consistent with experimental electrochemical analysis. Work presented in this chapter was done in collaboration with Professor Ryan Baxter. All experimental work was performed by the Baxter Lab, and a summary of their experiments and results can be found in the experimental summary section of this chapter. Full details are provided in a joint paper published by our labs in citation [118].

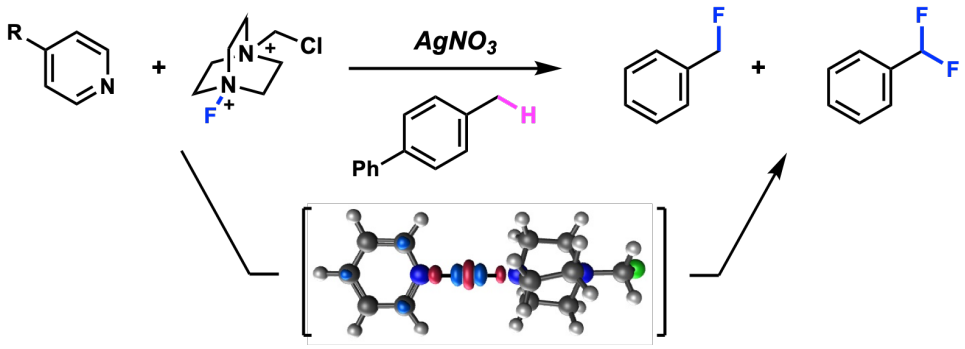

pyridine identity dictates product distribution

3.1 Background & Motivation

Due to their wide applicability, understanding weak molecular interactions is of foundational interest for a wide community of chemists. Noncovalent interactions such as van der Waals, π–π stacking and hydrogen bonding are all capable of altering the electron density of molecules leading to a chemical change. [119–125] Over the past several decades, great advances in the development of organocatalysts have been made using the enhanced reactivity of hydrogen bonding. [126–129] Unfortunately, the capabilities of hydrogen bonding are limited to the interactions of a Lewis basic acceptor and exclusively a hydrogen donor. [130]Halogen bonding has gained attention as a potential replacement for hydrogen bonding. [131–140] Expanding this chemistry, one could utilize the interactions of a halogen and a Lewis basic atom to create a range of chemical and physical properties depending on the size and electronegativity of the halogen used.

3.1.1 Halogen Bonding

Halogen bonding is a noncovalent interaction that has been widely used in many fields such as material science, drug design and catalysis. The first reports of halogen-bound complexes can be dated to nearly two centuries ago, yet it was in 2013 that the International Union of Pure and Applied Chemistry (IUPAC) defined intermolecular interactions involving a halogen as halogen bonds. According to IUPAC, a halogen bond "*occurs when there is evidence of a net attractive interaction between an electrophilic region associated with a halogen atom in a molecular entity and a nucleophilic region in another, or the same, molecular entity*". The strength of a halogen bond is proportional to the polarizability of the halogen bond donor, meaning that fluorine forms the weakest bond while iodine forms the strongest bond. Fluorine halogen bonds are the least likely to be formed and are usually only found when bound to strong electron withdrawing groups.

Some basic features of halogen bond interactions remain unknown and are still debated regularly amongst computational chemists. Politzer's σ–hole concept, which is defined as a noncovalent interaction between a covalently bonded atom of Groups IV–VII and a negative site creating a region

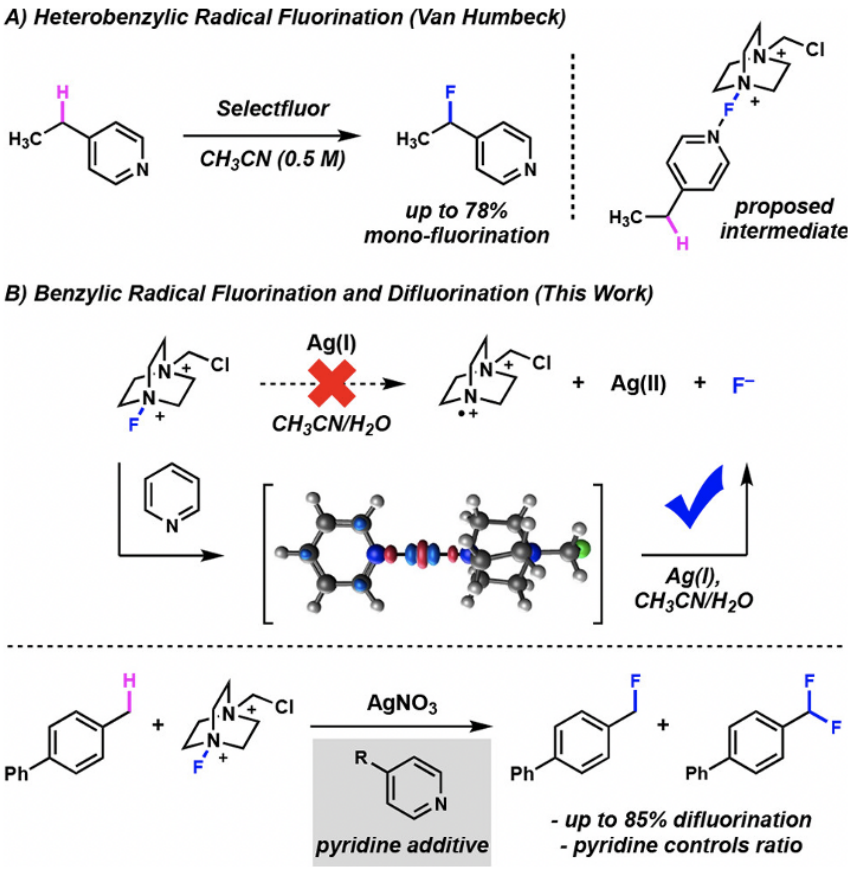

Figure 3.1: (A) Previously published fluorination chemistry with a proposed halogen-bonded intermediate. [141] (B) Proposed pathway for benzylic radical fluorination via a halogen bound intermediate.

of positive electrostatic potential, is commonly used to explain the behavior of halogens in a halogen bond. The current debate among chemists is inspired by a series of halogen bonding complexes that cannot be explained by the σ–hole basis. Consensus on the appropriate theoretical approaches that should be used on systems like these hasn't been achieved, but combined theoretical and experimental evaluations of these halogen bonded species has led to advances in the understanding and applications of their interactions.

3.1.2 Fluorine Chemistry

The use of fluorinated compounds in medicinal chemistry is rapidly becoming an important area of research. Fluorine has the ability to influence conformation, pKa, intrinsic potency, membrane permeability, metabolic pathways, and pharmacokinetic properties of many structures. Fluorine is also used for in–vivo imaging technology, which is often a limiting factor in drug development. Unfortunately traditional fluorinating methodologies require the use of highly toxic chemicals and complicated reaction conditions. As knowledge on fluorine chemistry methodology is gained, new insights and possible reaction pathways are discovered. This avenue of research allows for the investigation of not only the unique properties of fluorine, but information on the entire halogen group. Due to the generally unfavorable properties F_2 gas exhibits, most fluorination chemistry relies on the development of novel electrophilic and nucleophilic fluorinating agents. Interests in fluorinating unactivated C–H bonds are useful for drug discovery because they can be implemented in later steps of the synthesis and be directly attached to their desired products.

Previous work in the Baxter Laboratory focused on radical fluorination promoted by unprotected amino acids. [142] From that work it was concluded that the amino acid acts as a ligand on the Ag(I) catalyst and lowers the oxidation potential to produce Ag(II) under mild conditions. The binding of Ag(I) through an electron rich nitrogen was proven to be critical to promote oxidation. That conclusion was supported by a series of reactions showing that the N–protected amino acids were unable to produce any desired product. Following that work, the Baxter Group established that pyridine was a suitable ligand for Ag(I), enabling it to oxidize to Ag(II) and facilitating C–H

fluorination from previously ineffective N–protected amino acid reactions.

Recently, halogen bonding between the fluorine of Selectfluor and electron–rich pyridines has been implicated in generating complexes that participate in single–electron transfer for heterobenzylic radical fluorinations as shown in Figure 3.1(A). This chapter uses information gathered from experimental and theoretical work, and suggests that a variety of electronically diverse pyridines interact with Selectfluor and affect the efficiency of benzylic radical fluorinations as shown in Figure 3.1(B).

3.2 Results & Discussion

3.2.1 Determination of Reaction Protocol

A thorough investigation into the ability of pyridine to act as a suitable ligand to the Ag(I) to enable oxidation was preformed by the Baxter Lab to determine the reaction protocol. Table 3.1 shows a series of reactions preformed to explore the role of each reagent in the proposed pyridine–mediated fluorination. Control reactions with 4–methylbiphenyl (**1**) showed that Ag(I), Selectfluor and pyridine are required for fluorination, but an amino acid additive, denoted as N–Boc–GLY, was not (Table 3.1, entry 4). Reactions in the presence of (2,2,6,6–tetramethylpiperidin–1–yl)oxyl (TEMPO) produced radical trapped adducts and inhibited fluorination (Table 3.1, entry 5). Replacing Selectfluor with an alternative fluorine source (N–fluoropyridinium) lead to no fluorinated products suggesting that fluorine transfer from Selectfluor to pyridine is not the source of reactivity (Table 3.1, entry 6). Table 3.1 entries 2 and 3 also show that the Ag(I) and pyridine are both required to obtain any fluorinated product.

Overall, it was determined that the amino acid additive was not required to produce the desired fluorinated product. Additionally, it was determined that the Ag(II) catalyst, Selectfluor and pyridine are required, and that within this reaction mechanism there is a radical intermediate.

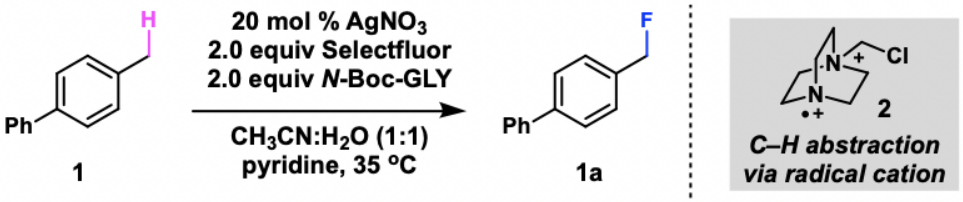

entry	deviation from standard conditions	Yield(%)
1	none	88
2	no $AgNO_3$	00
3	no pyridine	00
4	no *N*-Boc-GLY	51
5	no *N*-Boc-GLY, TEMPO added	*trace*
6	no *N*-Boc-GLY, *N*-fluoropyridinium	00

Table 3.1: A series of reactions experimentally tested to determine an optimized reaction protocol.

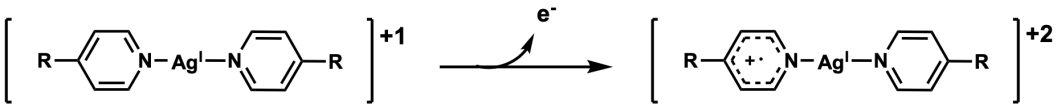

R Group	Experimental E° (V)	Computational E° (V)
OCH_3	1.24	2.04
H	1.31	2.08
CO_2Et	1.54	2.20
CF_3	1.60	2.27

Table 3.2: Experimental and theoretical redox potentials for a bi-pyrindine silver(I) complex.

3.2.2 Silver–Pyridine Oxidation Potentials

Knowing that pyridine is required in the reaction protocol to produced the desired fluorinated product, a series of substituted pyridines were explored to determine how their variations affected the overall reaction. The initial hypothesis was that the pyridines served to lower the oxidation potential of Ag(I), facilitating the electron transfer. This hypothesis was studied via cyclic voltammetry and computational techniques is that electron–rich pyridines would produce Ag(I) species with the lowest oxidation potentials. The first step to computationally calculating the redox potentials of Ag(I)–pyridine complexes was determining the number of pyridines that Ag(I) would prefer to bind with. It was concluded that there are two possible complex options, a mono–pyridine and bis–pyridine substituted silver, where the calculated redox potentials would be compared to the experimental values to determine the structure present in the reaction. A series of computational calculations were run with both possible silver complexes to calculate the redox potentials. These calculations were preformed using the B3PW91/6–311G(d) model chemistry in an implicit acetonitrile solvent modeled using the polarizable continuum model with unrestricted DFT. [35, 143, 144] Standard methods were used for geometry optimizations and all optimized structures were confirmed to be potential energy surface minima by analytical second derivatives calculations and vibrational frequency analyses. Redox potentials were calculated using this procedure published by Baik and Friesner. In this method the change in Gibbs free energy with a solvation correction is divided by n (the number of electrons being transferred) and Faradays constant. The correction factor for the standard hydrogen electrode is then subtracted, and the calculated redox potential is found.

A comparison of the experimental and theoretical redox potential eliminated the mono–pyridine silver complex due to a large value difference (~11 V) and a non-conforming overall trend. Results of this investigation with the bis-pyridine silver complexes generally agreed with experiment within error and can be found in Table 3.2. These results follow the initial hypothesis that electron–rich pyridines produce Ag(I) species with the lowest oxidation potentials.

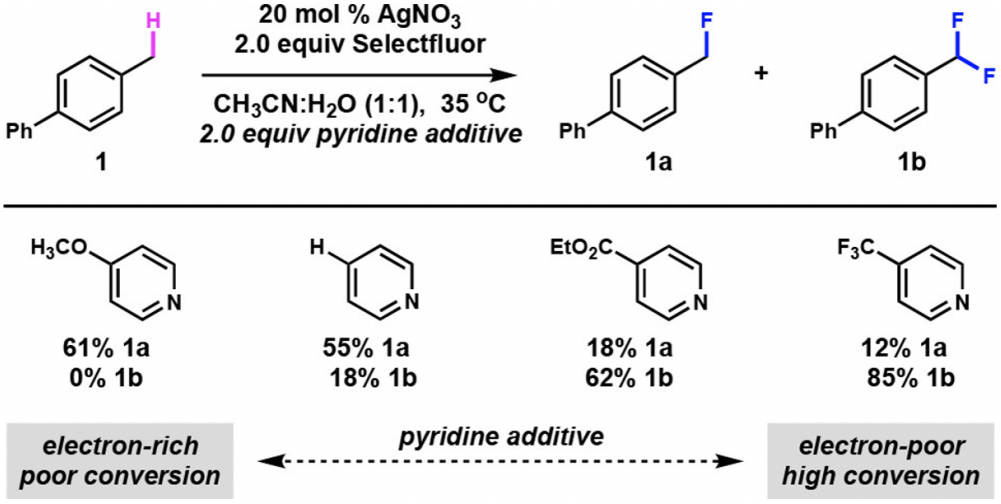

Figure 3.2: The experimental yields of a range of additives, testing how the pyridine substitution effects the overall reaction.

3.2.3 Pyridine–Dependent Product Distribution

Using the experimental and theoretical redox potential results, it was hypothesized that the electron-rich pyridines should preform most effectively in the production of the desired fluorinated product. To test this, the Baxter Lab ran the fluorination protocol shown in Table 3.1 with the same range of pyridines studied in Table 3.2. Surprisingly, the reactions with the highest conversion correlated with the electron poor pyridines, showing results opposite to what was expected. (Figure 3.2) In situ ReactIR reactions preformed by the Baxter Lab suggested that pyridines interact directly with the $[N–F]^+$ bond of Selectfluor, leading to a possible explanation for the counter intuitive results being a halogen bonded species.

3.2.4 Selectfluor–Pyridine Complexes

A combination of theoretical and spectroscopic work by Erdélyi has shown that pyridines have the ability to act as halogen bond acceptors, and that the extent of halogen bonding is directly affected by the electronics of the pyridine. [145–147]In situ ReactIR reactions preformed by the Baxter Lab suggested that pyridines interact directly with the $[N–F]^+$ bond of Selectfluor, leading to

a possible explanation for the counter intuitive results being a halogen bonded species. Initially the Baxter Lab looked into the [N–^{19}F]$^{+}$ ^{15}N NMR shift in the presence of differing pyridine additives, but negligible shifts were observed. [143]However, there were significant changes in the chemical shift of the pyridine nitrogen. In all cases examined, the pyridine ^{15}N signals shifted to more negative values in the presence of Selectfluor, consistent with the generation of a Selectfluor–pyridine complex.

The formation and dissolution of this halogen bonded intermediate was computationally investigated and preliminary results suggested density functional theory (DFT) model chemistries, including those with empirical dispersion corrections, were unable to treat the physics of the halogen bond. Such results are consistent with two extensive benchmark reports by Martin and by Wong, which indicated that only a limited set of approximate density functionals are capable of predicting halogen bonding strengths. Therefore, we turned to correlated wave function methods. Geometries of candidate halogen–bound species were optimized with the MP2/6–311+G(d) level of theory and single point energy corrections were evaluated with the CCSD(T)/6–311+G(d) model chemistry. Our calculations identified pyridine–Selectfluor complexes featuring the anticipated [N–F–N]$^{+}$ bonding motif (Table 3.3, Eq. 1).The halogen–bound species were slightly higher in energy (1 – 4 kcal/mol) than the unbound species, though subsequent reduction to form diazabicyclo radical cation 2 is quite favorable (Table 3.3, Eq. 2).

Computational results suggested that electron–rich pyridines were more effective halogen bond acceptors than electron–deficient pyridines. As shown in Table 3.3, the energetics of [N–F–N]+ bond reduction via single–electron transfer exhibit a clear trend depending on pyridine substitution. Interestingly, all structures exhibit similar bond lengths for both N–F bonds (1.84 Å) in the complex and a linear N–F–N bond angle. Notably, reduction of the [N–F–N]$^{+}$ halogen bound complex is most energetically favorable when possessing an electron withdrawing group in the 4–position. Again, these data correlate directly with the experimental reactivity trends observed in Figure 3.1, whereby electron–poor pyridines are the most efficient at promoting radical fluorination. Studies exploring alternative bonding interactions, including halogen bonding to the chlorine of Selectfluor,

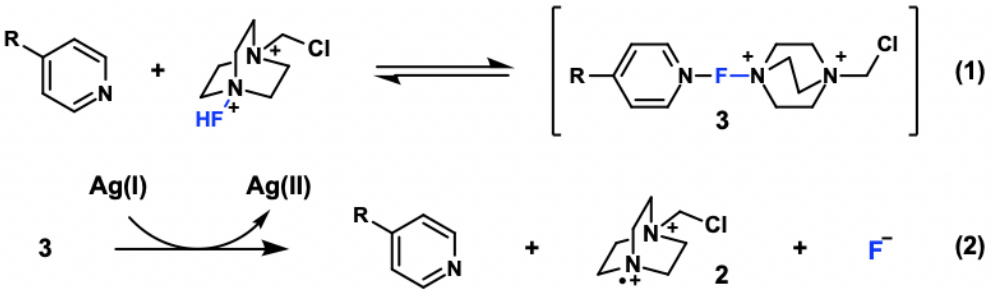

R Group	ΔH1 (kcal/mol)	ΔH2 (kcal/mol)
OCH_3	0.34	-31.42
H	0.74	-31.82
CO_2Et	3.63	-33.66
CF_3	2.57	-34.71

Table 3.3: The ΔH of formation and dissolution for the pyridine-selectfluor halogen bound complex.

showed the only suitable geometry is as shown in structure **3**. In addition, because experimental conditions include water as a cosolvent the possibility of a mixed hydrogen/halogen bonding network was also explored computationally. The inclusion of discrete water molecules into complex **3** did not converge to physically reasonable structures, suggesting the NMR results reported by the Baxter Lab are the result of direct interaction between the pyridine nitrogen and the fluorine of the Selectfluor. Exploring the extent to which post–SCF correlation affects the electron density to give rise to the $[N–F–N]^+$ weak interaction, we evaluated the difference between MP2 and reference Hartree–Fock electron densities. Figure 3.1(B) shows such a plot for **3**. Electron correlation yields symmetric redistribution of electron density in the two N–F bonding regions, which is consistent with our analysis that post–SCF treatment is required to properly account for the $[N–F–N]^+$ weak interactions. To further explore the effects of the pyridine–Selectfluor interactions in the context of radical initiation, the Baxter Lab examined the electrochemical reduction of Selectfluor under synthetic conditions. That work shows that Selectfluor produces an irreversible single-electron reduction of approximately −1.18V. When exposed to the pyridine additives this value is reduced to

lower potentials than Selectfluor alone, which is consistent with ΔH2 in Table 3.3.

3.2.5 Overall Mechanism

Using the knowledge gained from the combination of experimental and results, the following mechanism is proposed for radical C–H fluorination with Selectfluor via Ag(I)–pyridine initiators. (Figure 3.3). Analytical electrochemistry from the Baxter Lab supported by our computational results demonstrate that Ag(I)/pyridine complexes are better reductants than Ag(I) alone, suggesting a pre-equilibrium to bis-pyridine Ag(I) complexes. Single-electron transfer to a halogen-bound pyridine-Selectfluor complex **3** would produce Ag(II)-$[pyr]_2$, pyridine, fluoride anion, and diazabicyclo radical cation **2**. CH abstraction of **1** produces nucleophilic radical **4** that quenches with an additional equivalent of Selectfluor to regenerate **2**, propagating the radical reaction. One contributing factor to the marked difference in efficiency shown in Figure 3.2 is unproductive consumption of Selectfluor from electron rich pyridines. However, it cannot be the only factor affecting reaction efficiency, as the trend correlating pyridine electronics to efficiency holds for pyridines that do not affect the concentration of Selectfluor in an unproductive manner.

3.3 Summary

In conclusion, we have demonstrated experimental and theoretical evidence supporting the presence of halogen bonding in pyridine-mediated radical fluorinations. Analytical electrochemistry shows that pyridine additives affect the single-electron reduction of Selectfluor, consistently producing species that are more easily reduced. A comprehensive mechanistic picture of radical fluorination likely involves equilibration of pyridine with both Ag(I) and Selectfluor, leading to a complicated kinetic scenario that we are currently studying via in situ reaction monitoring and computational modeling. The work presented in this chapter is a stepping stone into a wide range of new chemistries. There are a variety of halogens that could be substituted into this work, and the possibility of the mono- and di-fluorinations for a variety of staring materials.

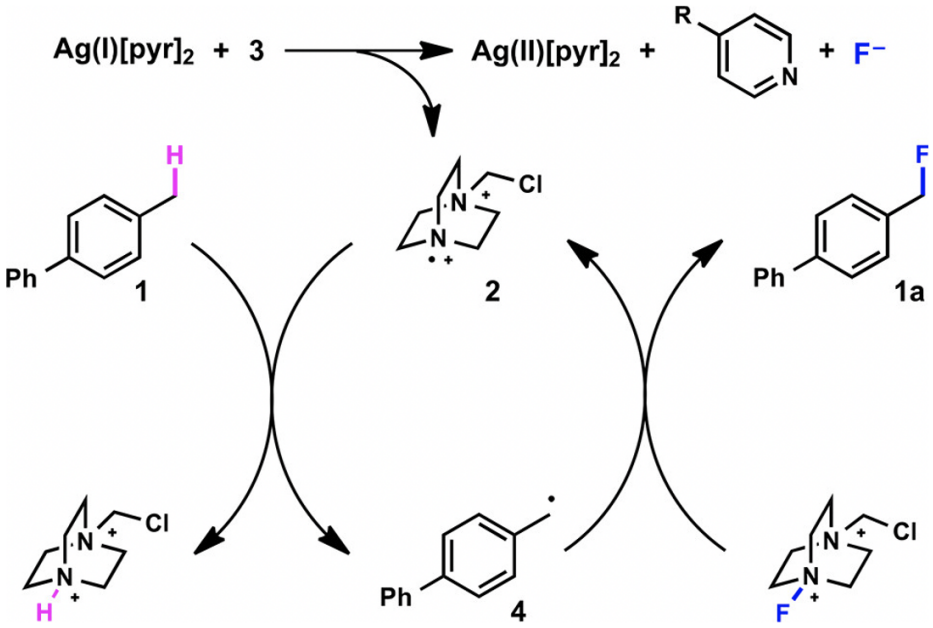

Figure 3.3: The proposed mechanistic pathway of the silver catalyzed fluorination of 4-methylbiphenyl with selectfluor as the fluorine source.

Chapter 4

A Novel Approach for Asymmetric Bromination: A Computational Evaluation

In this chapter we investigate a new method for aromatic bromination using lactic acid derivatives as halogen-bond acceptors with N–bromosuccinimide (NBS). Surprisingly, these derivatives poses different bromination efficiency, presumably via Lewis acid/base halogen-bonding interactions. Our results demonstrate that these Lewis basic additives interact with NBS to increase the electropositive character of bromine prior to electrophilic transfer. Experimental rate comparisons of aromatic brominations demonstrate the reactivity enhancement available via halogen-bonding. Combined computational and experimental efforts led to the selection of mandelic acid as the optimum additive to enhance the reactivity of aromatic bromination. Work presented in this chapter was done in collaboration with Professor Ryan Baxter. All experimental work was performed by the Baxter Lab, and a summary of their experiments and results can be found in the experimental summary section of this chapter.

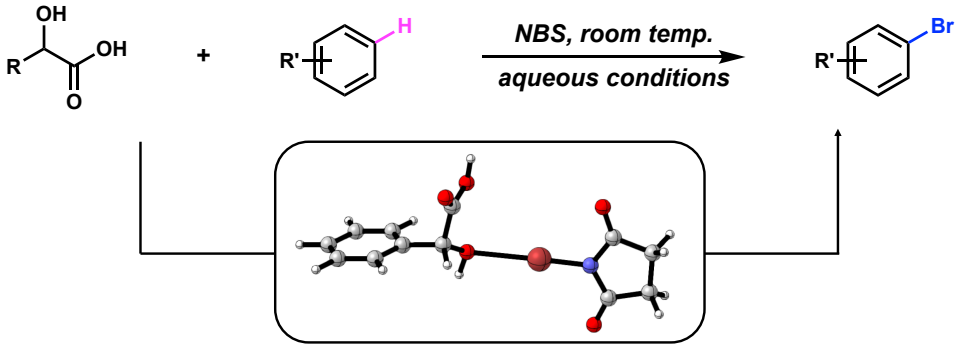

4.1 Introduction & Motivation

A major challenge in synthetic chemistry is the activation of chemically inert C-H bonds. An important factor in the development of new synthetic pathways is to obey to a green chemistry standard. This includes the prevention of waste, the use of less hazardous chemicals, safer solvents, and reusable catalysts. This work focuses on expanding the existing understanding of halogen bonding as discussed in Chapter 3 and broadening its synthetic scope. Halogenated arenes are used in a wide variety of chemistry's, such as metal catalyzed cross coupling reactions, the development of pesticides and pharmaceuticals, and natural product synthesis. This CH bond can be altered in a variety of ways, but one very common method is transition metal catalyst.

The first evidence of bromination was published in 1916 where nitric acid oxidizes molecular bromine facilitating it's addition, while being reduced to a gas. The toxicity of atomic bromine makes it very dangerous to work with. Atomic bromine is corrosive and evaporates easily at standard temperature, and is harmful to all body tissues by causing burns and damaging the respiratory tract by inhalation. It also requires special attention for storage and transportation with a low atomic efficiency. All of this inspired the creation of a less toxic, more stable liquid bromine source. In the 1940's Ziegler and coworkers developed N-bromosuccinimide (NBS) and used it mainly for the bromination of alkenes. In the years that followed NBS was used for electrophilic aromatic substitution of highly activated arenes. This chapter uses information gathered from experimental and theoretical work, and suggests evidence of halogen bonding using lactic acid derivatives to promote electrophilic aromatic bromination.

4.2 Experimental Foundations

Using previous knowledge on benzylic fluorination via halogen bonding, the Baxter Lab began exploring the possibility of halogenation with a variety of halogens. This study was inspired by the reaction conditions of their published fluorination chemistry. Initially the lab tested alternative halogenations by creating Selectfluor analogs and using a variety of halogenated salts. (Figure 4.1)

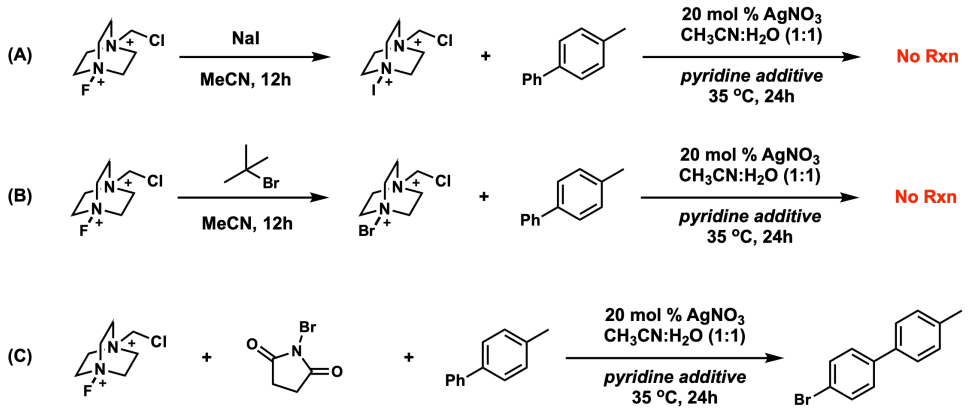

Figure 4.1: Reactions testing the use of selectfluor analogs to promote halogenation. Reaction (A) replaces the fluorine of the selectfluor with iodine and then attempts to promote halogenation of methyl-biphenyl with no success. Reaction (B) replaces the fluorine of the selectfluor with bromine and then attempts to promote halogenation of methyl-biphenyl with no success. Reaction (C) combines selectfluor and NBS to halogenate methyl-biphenyl which leads to a brominated methyl-biphenyl ring.

Unfortunately, reactions A and B in Figure 4.1 did not promote halogenation. This is because the silver of the catalyst binds with the halogenated salts and precipitates out of the reaction. In an effort to promote halogenation, the Baxter Lab then replaced the halogenated salts with NBS as shown in reaction C. This reaction promoted bromination in the para-position of the 4-methylbiphenyl starting material. Following this result, the lab then constructed a series of control reactions to determine the optimal reaction conditions. Using the information presented in Table 4.1, it is shown that the overall reaction proceeds with a 69% yield. Entries 2 and 3 show that the silver catalyst and selectfluor are not required to create the brominated product. Entry 4 shows that the the reaction can proceed without the pyridine additive, but will experiences a large decrease in yield. These results suggests that a possible halogen bonded intermediate is present similar to the fluorination chemistry discussed in Chapter 3. Reactions using a set of mono-substituted pyridine additives that vary in electronics determined that electron rich pyridines lead to lower yields because they consume the NBS (Entry 5-8).The Baxter Lab the looked into the use of a variety of green solvent conditions, which revealed a surprisingly efficient yield when ethyl acetate was used. (Entry 9)

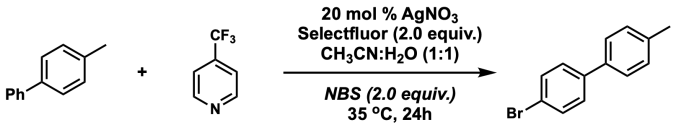

Entry	Deviation from Standard Conditions	Yield(%)
1	none	69
2	No $AgNO_3$	79
3	No $AgNO_3$, No Selectfluor	78
4	No $AgNO_3$, No Selectfluor, No Pyridine	60
5	4-(trifluor)methylpyridine Replacement, no $AgNO_3$ or Selectfluor	78
6	Pyridine Replacement, no $AgNO_3$ or Selectfluor	trace
7	4-Cyanopyridine Replacement, no $AgNO_3$ or Selectfluor	68
8	4-Methoxypyridine Replacement, no $AgNO_3$ or Selectfluor	0
9	Ethyl lactate Solvent, no $AgNO_3$, Selectfluor or Pyridine	77

Table 4.1: A series of control reactions completed to determine the necessary reaction conditions. From this it was determined that the silver catalyst and selectfluor are not necessary to promote bromination. The presence of pyridine greatly increases the overall yield and that electron rich pyridines consume the NBS and lead to lower yields.

4.3 Results & Discussion

The experimental result showing a high yield when using ethyl lactate as a reaction additive inspired a new avenue of interest. According to recent review, when ethyl acetate is subjected to water it undergoes hydrolysis to produce lactic acid and ethanol. It was then hypothesized that the hydrolysis of lactic acid was a key component of the overall reaction. To investigate this a series of lactic acid derivatives were studied to determine which structural features were important for reactivity.

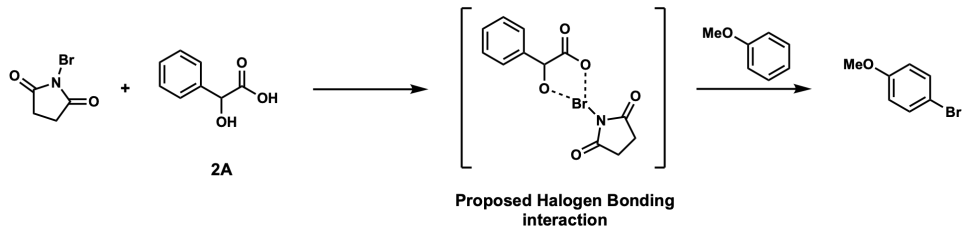

Figure 4.2: The predicted halogen bonding network formed when NBS binds with mandelic acid (2A).

4.3.1 Modeling the Binding of Additives and NBS

A series of lactic acid derivatives (2A-2F) were studied to investigate their binding abilities with NBS. Initial hypotheses were that the additives and NBS would bind in a way that would create a halogen-bonding network shown in Figure 4.2 where NBS binds with mandelic acid (2A). It was proposed that the NBS would act as an electrophilic bromine source and form a halogen bonding network similar to that published in the fluorination chemistry with the mandelic acid. To our surprise, we were unable to find an optimized geometry with a network of halogen bonding and instead found two/three separate intermediates with the NBS binding to all possible oxygen or nitrogen positions at an extended bond length. Each complex structure features bond lengths longer than the ideal Br-O covalent bond length of 1.77Å but within the sum of the Van der Waals radii of 3.37Å. A complete analysis of each of the intermediate can be found in Section 4.3.2, but first a discussion on how to properly model the extended interaction must be established.

At this bond length, there is a region between the bromine and additive oxygen (or nitrogen) where an artificial lack of basis functions exists. This error could be thought of as a type of basis set superposition error, but instead of the basis-sets of atoms basis functions overlapping and artificially giving extra room for the electrons the opposite is happening. To determine if this error is occurring in our calculations we looked at the total charges of the mandelic acid and the total charge of the NBS. If the charge that lies between the O-Br bond is being modeled properly the charges of each fragment will be equal, and if it is not we will see a charge difference between the fragments. As we expected, we see a charge difference between the fragments so additional benchmarking was completed to properly model this interaction.

4.3.1.1 Addition of Ghost Atoms to Extended Bond

Initial efforts to address the extended bond lengths included the addition of ghost atoms between the bromine and the oxygen/nitrogen of the additive. These efforts involved an initial benchmarking study to determine the optimal number of ghost atoms needed to fill the bond and the basis function that will be on those atoms. Three sets of calculations were studied using a mandelic acid

and NBS complex (3A):

1. One hydrogen ghost atom located at the centroid of the bond between the bromine and the oxygen of the hydroxide in the alpha position with respect to the ring. (3A-1Ghost)

2. Two hydrogen ghost atom located at equal distances from each other and from the Br/O. (3A-2Ghost)

3. Three hydrogen ghost atoms, one located at the centroid of the bond and the other located in the middle of the centroid and the connecting atom. (3A-3Ghost)

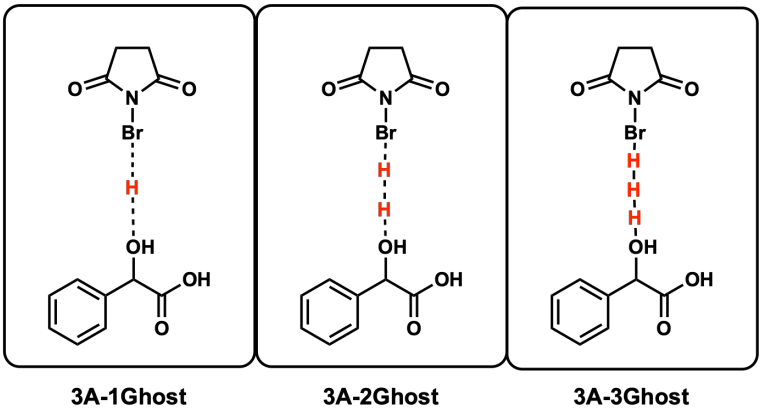

Figure 4.3: Possible placement of one, two and three hydrogen ghost atoms between the oxygen of mandelic acid and the bromine of NBS. 3A-1Ghost contains one ghost atom at the centroid of the O-Br bond. 3A-2Ghost contains two ghost atoms equal distance from the oxygen/bromine and each other. 3A-3Ghost contains three ghost atoms with one at the centroid and the others at the halfway point between the centroid and connecting atom.

Each of these sets of calculations were run with a set of basis functions with varying amounts of s, p and d orbitals on the ghosted hydrogen atoms. (Table 4.2) The results from this bechmarking study showed that there is still unequal sharing of the electron when one and two ghost atoms are placed between the bond, but there is an optimal amount of basis functions added when three ghost atoms are added between the bond. The exploration of the varying size of basis sets provided results all similar to each other, leading us to choose the same basis set we are using on the remainder of the structure (6-311G(d)).

Basis Sets	# of s functions	# of p functions	# of d functions
6-311G(d)	3	0	0
6-311G	3	0	0
6-311++G	4	0	0
6-311G(d,p)	3	1	0
6-311G**	3	1	0
6-311++G(2d,2p)	4	2	0
6-311G(2df,2pd)	3	2	1
6-311++G(2df,2pd)	4	3	1
6-311G-J	6	0	0
6-21G	2	0	0
6-31++G**-J	5	1	0
6-311++G**	4	1	0
6-31G	2	0	0
6-31G**	2	1	0

Table 4.2: Series of basis sets used in benchmarking of the ghost atom calculations with varying amounts of s, p and d orbitals.

4.3.1.2 Addition of Well-Tempered Basis Functions to Extended Bond

Once the ghost atom benchmarking study was completed, there was a realization that to accurately calculate the energy associated with the formation and dissociation of the complexes, ghost atoms could not be present. The inclusion of these ghost atoms only in some molecules when calculating the change in enthalpy of formation leads to errors in values. This led us into this next investigation where we replaced the ghost atoms present in the complexes extended bond with the addition of well tempered basis functions on the atoms on both sides of the bond. To determine the number of basis functions to add to the bromine, oxygen or nitrogen a series of calculations were run adding additional functions with each job until the energies reach a convergence criteria of 10E-5 Hartree as shown in Table 4.3.

Calculation (Bromine)	s	p	d	Energy Difference from 6-311G(d)
1	1	0	0	0.00040
2	2	0	0	0.00001
3	2	1	0	0.01000
4	2	2	0	0.00010
5	2	3	0	0.00001

Calculation (Oxygen)	sp	d	Energy Difference from 6-311G(d)
1	1	0	0.01000
2	2	0	0.00010
3	3	0	0.00004
4	3	1	0.00100
5	3	2	0.00001

Calculation (Nitrogen)	s	sp	d	Energy Difference from 6-311G(d)
1	1	0	0	0.00022
2	2	0	0	0.00046
3	3	0	0	0.00104
4	4	0	0	0.00001
5	4	1	0	0.00319
6	4	2	0	0.01818
7	4	3	0	0.01950
8	4	4	0	0.00022
9	4	5	0	0.00001
10	4	5	1	0.00018
11	4	5	2	0.00001

Table 4.3: Caption

4.3.2 Geometries of Possible Additive-NBS Complex

A series of geometry optimizations were performed to analyze all possible complex formations. The lactic acid derivatives studied in this work include: mandelic acid (2A), benzoylformic acid (2B), alanine (2C), 2-phenylglycine (2D), lactic acid (2E), benzoic acid(2G) and phenylacetic acid(2H). Geometry optimizations of the NBS-additive complex(3A-H) using the B3PW91/6-311G(d) model chemistry including implicit solvation by methanol were carried out using a local development version of Gaussian.

4.3.2.1 Mandelic Acid Complex

Three possible complex geometries were found when 2A binds with NBS. These three structures feature Br-O bond lengths within 0.12Å of each other, and essentially identical bromine charges.The ΔH of formation for each of these complexes are within 1.61 kcal/mol of each other, with the most favorable being the complex bound at 3A-2.

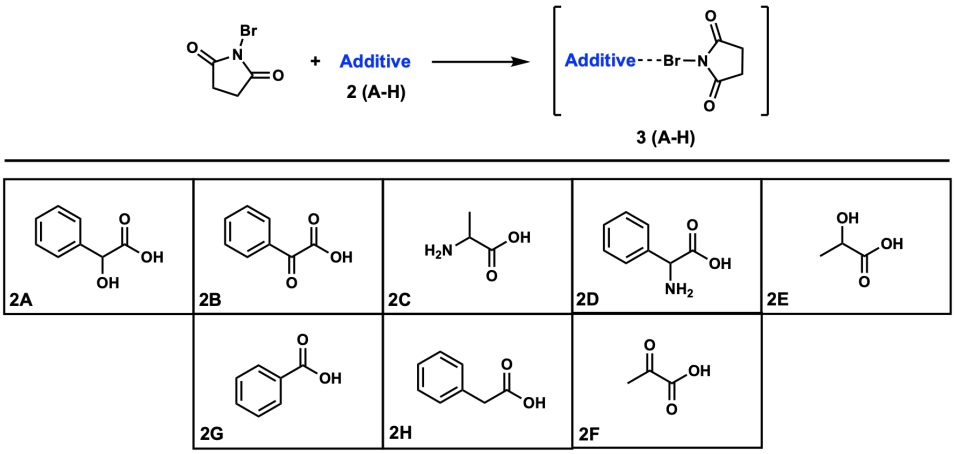

Figure 4.4: The overall reaction computationally studied with a series of additives (2A-2H) and NBS.

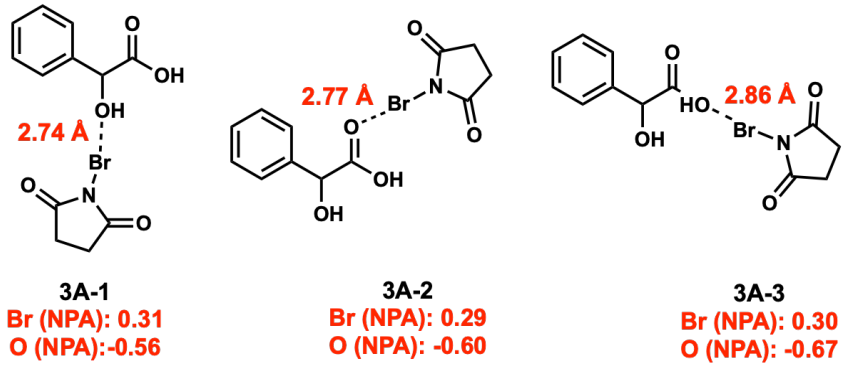

Figure 4.5: The three possible complexes formed when NBS binds with the alpha-oxygen, the carbonyl oxygen and the acid oxygen of mandelic acid.

4.3.2.2 Benzoylformic Acid Complex

Three possible complex geometries were found when 2B binds with NBS. These three structures feature Br-O bond lengths within 0.22Å of each other, and essentially identical bromine charges. The ΔH of formation for each of these complexes are within 1.28 kcal/mol, with the most favorable being the complex bound at 3B-1.

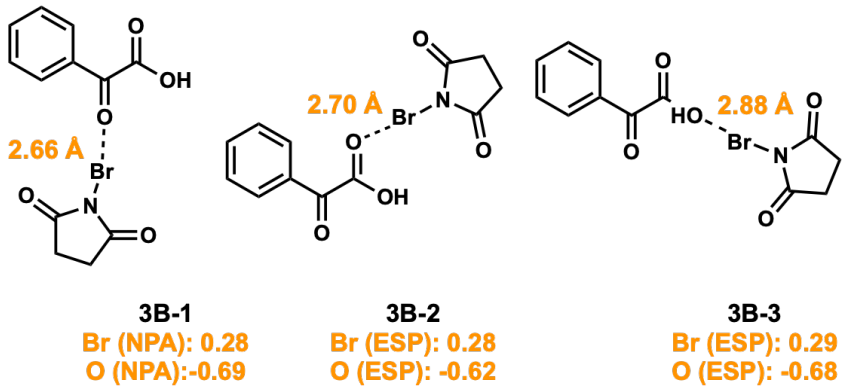

Figure 4.6: The three possible complexes formed when NBS binds with the alpha-oxygen, the carbonyl oxygen and the acidic oxygen of benzoylformic acid.

4.3.2.3 Alanine Complex

Three possible complex geometries were found when 2C binds with NBS. These three structures feature Br-O bond lengths within 0.18Å of each other, with the shortest bond being the N-Br with a length of 2.42Å. The bromine charges for 3C-1 and 3C-1 were the most positive at 0.45/0.41 which are 0.17 higher than the 3C-2. The ΔH of formation for the nitrogen bound complex is most favorable at -2.83 kcal/mol, approximately 4.69(3C-2) and 7.33(3C-3) kcal/mol more favorable than the oxygen bound complex.

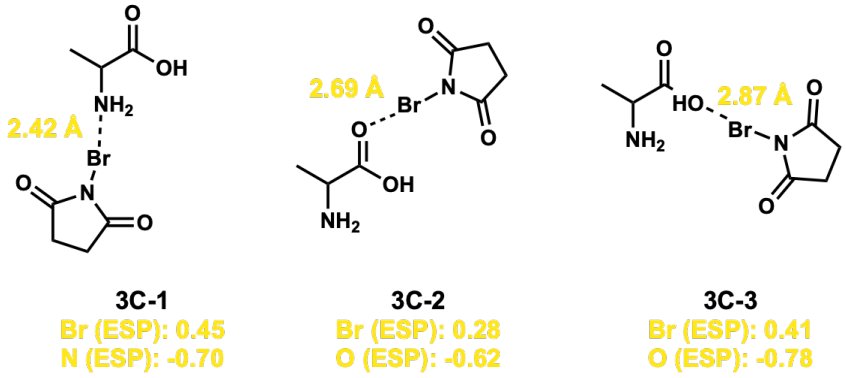

Figure 4.7: The three possible complexes formed when NBS binds with the nitrogen, the carbonyl oxygen and the acidic oxygen of alanine.

4.3.2.4 2-Phenylglycine Complex

Two possible complex geometries were found when 2D binds to NBS (3D-1 and 3D-2). Attempts to find a complex 3D-3 were unsuccessful and converged to the same geometry of 3D-1. These structures feature a Br-O bond length of 2.69Å and Br-N length of 2.45ÅṪhe bromine charges are within 0.06 of each other. The ΔH of formation for the nitrogen bound complex (3D-1) is most favorable at -1.74 kcal/mol, approximately 3.28 kcal/mol lower than the oxygen bound complex (3D-2).

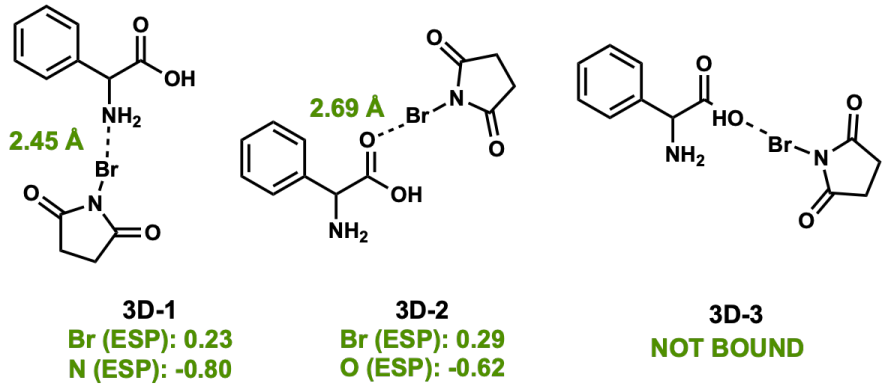

Figure 4.8: The three possible complexes formed when NBS binds with the nitrogen, the carbonyl oxygen and the acidic oxygen of 2-Phenylglycine.

4.3.2.5 Lactic Acid Complex

Two possible complex geometries were found when 3E binds with NBS, and these were 3E-1 and 3E-2. Attempts to find complex 3E-3 were unsuccessful because the NBS dissociates from the acidic position. These structures feature Br-O bond lengths within 0.05Å of each other. The bromine of 3E-1 complex is 0.12 more positive than the 3E-2 complex. The ΔH of formation for the 3E-1 complex is 3.46 kcal/mol more favorable that the 3E-2 complex.

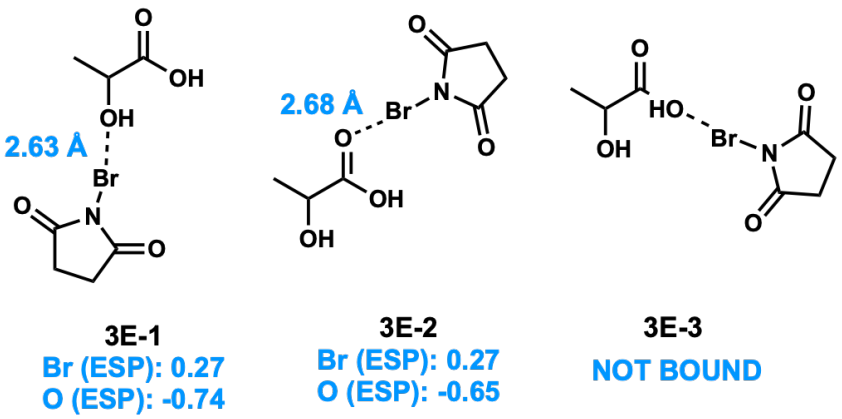

Figure 4.9: The three possible complexes formed when NBS binds with the hydroxide oxygen, the carbonyl oxygen and the acidic oxygen of lactic acid.

4.3.2.6 Benzoic Acid Complex

Two possible complex geometries were found when 2G binds with NBS. These two structures feature Br-O bond lengths of 2.70Å for 3G-1 and a longer length of 2.95Å for 3G-2. The bromine charge differs by 0.12 with the more positive present when NBS binds with 3G-1. The ΔH of formation is more favorable for the 3G-1 structure by 2.80 kcal/mol.

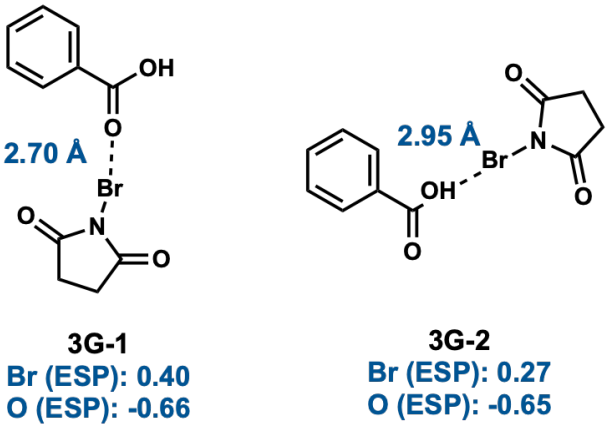

Figure 4.10: The two possible complexes formed when NBS binds with the carbonyl oxygen and the acidic oxygen of benzoic acid.

4.3.2.7 Phenylacetic Acid Complex

Two possible complex geometries were found when 2H binds with NBS. These two structures feature Br-O bond lengths of 2.68 Å for 3H-1 and a longer length of 2.84 Å for 3H-2. The bromine charge differs by 0.09 with the more positive present when NBS binds with 3H-2. The ΔH of formation is more favorable for the 3H-1 structure by 3.46 kcal/mol.

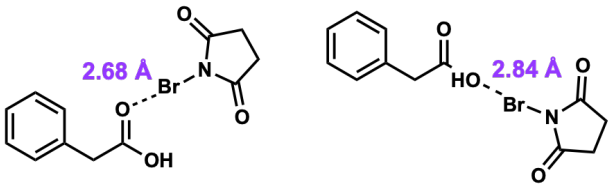

3H-1
Br (ESP): 0.28
O (ESP): -0.63

3H-2
Br (ESP): 0.37
O (ESP): -0.67

Figure 4.11: The two possible complexes formed when NBS binds with the carbonyl oxygen and the acidic oxygen of phenylacetic acid.

Overall, each of the optimized geometries for the complex intermediates featured similar trends. First, the shortest bond length is when NBS binds to the alpha oxygen(nitrogen), and the longest is when the NBS is bound to the oxygen with the acidic proton. Second, all complexes feature bromine with a partial positive charge, with an average of δ+=0.31. With no explicit reasons for the difference in experimental yields presented in the geometric and charge analysis, further studies were preformed.

4.3.3 Formation of Complex and Desired Brominated Product

With the charge and geometric analysis unable to validate the difference in experimental yields observed by the Baxter Lab, we began investigating the Δ's of formation of the complex and of our brominated reagent (Shown in Figure 4.12). The first reaction (ΔH(1)) is looking into the complex formation, while the second reaction is looking at the formation of a brominated methyl-biphenyl reagent (ΔH(2)). The energy values for each of these values can be found in Table 4.4.

From these calculations one can conclude that the formation of the complex (ΔH(1)) can be anywhere from -2.82 to 5.28 kcal/mol. Excluding mandelic acid, the most favorable ΔH(1) of formation is when the NBS binds to the alpha oxygen forming 3(A-H)-1. It should also be noted that the only favorable reactions (less that 0 kcal/mol) are the formation of complexes where the bromine of NBS binds with nitrogen. One may also conclude that in all cases the formation of the brominated methylbiphenyl (ΔH(2)) is favorable by -22.38 to -30.96 kcal/mol, where the opposite trend is observed and the nitrogen bound complexes are the highest energy.

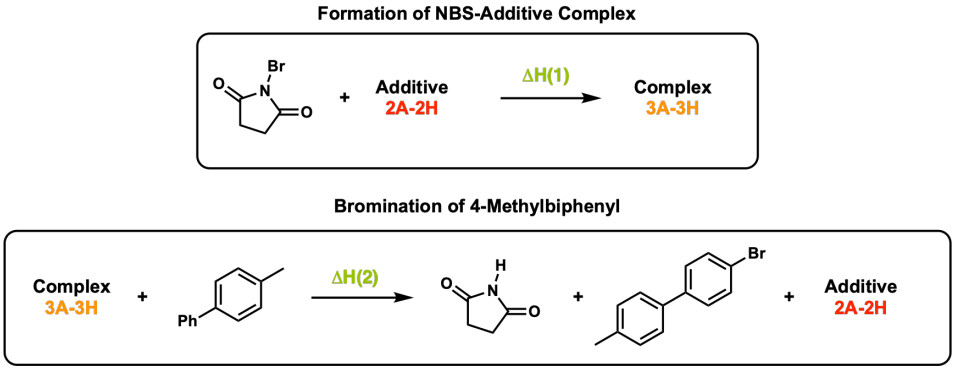

Figure 4.12: (1) The formation of the NBS-additive complex when NBS and the additive in all possible positions. (2) The productions of bromo-methyl-biphenyl, a succinimide ring and the additive when the complex and methyl-biphenyl are mixed.

4.4 Summary and Outlook

Work on this project will be published in a collaborative paper between the Baxter and Hratchian groups. With the geometry, charge and energy analysis preformed a clear explanation as to why each lactic acid derivative exhibits different yields cannot be formed. We hypothesize that investigations into the connecting transition structures and associated barriers could lead to a clear correlation of the experimental and theoretical results.

Additive/Complex	H(1) (kcal/mol)	H(2) (kcal/mol)
2A / 3A-1	3.06	-28.72
2A / 3A-2	1.45	-27.12
2A / 3A-3	1.88	-27.54
2B / 3B-1	1.71	-27.38
2B / 3B-2	2.10	-27.77
2B / 3B-3	2.99	-28.65
2C / 3C-1	-2.82	-22.83
2C / 3C-2	1.86	-27.52
2C / 3C-3	4.50	-30.16
2D / 3D-1	-1.74	-23.93
2D / 3D-2	1.55	-27.21
2E /3E-1	4.37	-30.04
2E /3E-2	5.28	-30.97
2G / 3G-1	1.08	-26.74
2G / 3G-2	4.54	-30.21
2H / 3H-1	1.41	-27.07
2H / 3H-2	4.21	-29.87

Table 4.4: The ΔH of formation for the two reactions shown in Figure 4.12.

Chapter 5

Intermolecular Perturbational Analysis: A Model to Investigate Non-Traditional Bonding

Three-center two-electron bonds play an important role in a rich array of chemistries. Despite a large volume of studies of such systems using molecular orbital theory, a simple-to-use quantitative model is still absent in the computational chemistry toolbox. We have developed such a model based on perturbational molecular orbital theory. This model has been applied to an example system with intentions of application to systems similar to those presented in the previous chapters.

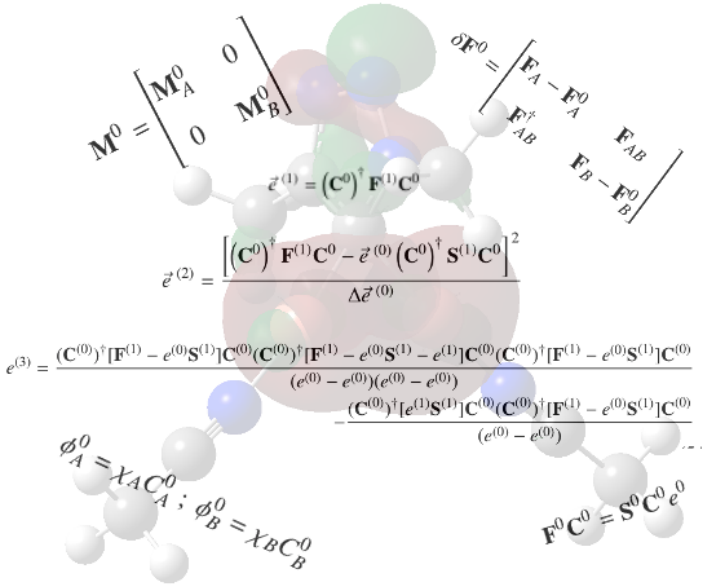

5.1 Introduction

Structure and bonding are fundamental to understanding to explaining physical and chemical properties of molecules and guiding reaction discovery and materials design. A chemical bond is defined as a persistent attraction between atoms, ions or molecules that enables the formation of new chemical compounds. [148] These bonds may be due to an electrostatic force between to atoms of opposite change, such as an ionic bond, or the sharing of electrons in a covalent bond.

Common bonding models employed include VSPER theory and the octet rule, which are usually taught in most general chemistry courses. [149] Quantum chemistry can also be used to describe chemical bonds. Among the more sophisticated models based on quantum chemistry are the linear combinations of atomic orbitals (LCAO) model and molecular orbital theory, ligand field theory, and valence bond theory. [150, 151] Using an electron density determined from a quantum chemistry calculation, one can also apply post hoc bonding models such as the Natural Bond Orbital and atoms-in-molecules schemes. [152]

The energy decomposition analysis (EDA) is a method that was developed to quantitatively analyze chemical bonds. [153] This method bridges the gap between the quantum mechanical descriptions of bonding and more simplified and intuitive interpretations. This analysis decomposes the construction and energy of one-electron molecular orbitals and the total molecular energy into at least three constituent parts: (1) electrostatic, (2) Pauli repulsion and (3) covalent orbital. EDA is generally applied to the formation of molecule (A−B) from two fragments (A and B). The molecule has a total energy (E_{AB}) and wavefunction (Ψ_{AB}), which are formed by the interaction of fragments A^0 and B^0 with corresponding ground states (Ψ_A^0 and Ψ_B^0) and energies (E_A^0 and E_B^0).

Of interest in this chapter is the extension and use of an intramolecular population analysis (IPA) model. As described in other chapters of this dissertation, three-center two-electron bonds are intriguing and seem to appear in a variety of chemical motifs – in intermediates of copper catalyzed reaction mechanisms and in reaction processes facilitated by weak halogen bonds. [154] In this chapter we present an initial effort to develop an IPA based on the perturbational molecular orbital

model of Whangbo, Schlegel, and Wolfe. [155] Once developed, the objective of this new model is to provide a means to distinguish between additive and cooperative effects in three-center two-electron bonds. Such knowledge should provide new insights for molecular design approaches to enhance or hinder such three-center two-electron bonds to impact structure, bonding, and reactivity needs in chemical and materials development.

5.2 Theory and Methods

Standard procedures define the row vector χ as the n atomic orbitals (AOs) and the row vector ϕ_i to be n molecular orbitals (MOs).

$$\chi = (\chi_1\chi_2\cdots\chi_n) \tag{5.1}$$

$$\phi = (\phi_1\phi_2\ldots\phi_n) \tag{5.2}$$

For a closed shell system the Fock equation is written as

$$\mathbf{FC} = \mathbf{SC}e \tag{5.3}$$

where **C** is an n×n coefficient matrix defined by

$$\phi = \chi\mathbf{C} \tag{5.4}$$

The above equations are written for a molecular system AB, which is formed from the mutual perturbations of the MOs of fragments A and B. The row vector for the MOs of the composite system can now be written as

$$\chi = (\chi_1\chi_2\cdots\chi_m\chi_{m+1}\cdots\chi_n) \tag{5.5}$$

where χ_1 to χ_m are the MOs of fragment A and χ_{m+1} to χ_n belong to fragment B. The Fock matrix (**F**) and the overlap matrix (**S**) can be partitioned as

$$\mathbf{F} = \begin{bmatrix} F_A & F_{AB} \\ F_{AB}^{\dagger} & F_B \end{bmatrix} \tag{5.6}$$

$$\mathbf{S} = \begin{bmatrix} S_A & S_{AB} \\ S_{AB}^{\dagger} & S_B \end{bmatrix} \tag{5.7}$$

Each element of the Fock matrix defined above can be written as

$$(\mathbf{F}_A)_{ij} = \langle \chi_i | \hat{F} | \chi_j \rangle \tag{5.8}$$

$$(\mathbf{F}_B)_{ij} = \langle \chi_i | \hat{F} | \chi_j \rangle \tag{5.9}$$

$$(\mathbf{F}_{AB})_{ij} = \langle \chi_i | \hat{F} | \chi_j \rangle \tag{5.10}$$

χ_i and χ_j in Eq. 5.8 both belong to fragment A, χ_i and χ_j in Eq. 5.9 both belong to fragment B, and in Eq. 5.10 χ_i belongs to fragment A and χ_j belongs to fragment B. The same expansions can be applied to the overlap matrix as well. The MOs and Fock equations of fragment **A** and **B** can be written as

$$\phi_A^0 = \chi_A C_A^0 \; ; \; \phi_B^0 = \chi_B C_B^0 \tag{5.11}$$

$$F_A^0 C_A^0 = S_A^0 C_A^0 e_A^0 \; ; \; F_B^0 C_B^0 = S_B^0 C_B^0 e_B^0 \tag{5.12}$$

where the superscript 0 refers to the isolated system.

The MOs of the molecule AB are orthonormal leading to the equation

$$\mathbf{C}^{\dagger}\mathbf{S}\mathbf{C} = \mathbf{1} \tag{5.13}$$

The corresponding expressions for the fragments that make molecule AB are

$$\left(\mathbf{C}_A^0\right)^\dagger \mathbf{S}_A^0 \mathbf{C}_A^0 = \mathbf{1} \tag{5.14}$$

$$\left(\mathbf{C}_B^0\right)^\dagger \mathbf{S}_B^0 \mathbf{C}_B^0 = \mathbf{1} \tag{5.15}$$

With these definitions in place we can now examine the relationship that exists between the MO energies of the molecule and the MO energies of the composite system whose fragment MO are defined in Eq. 5.5. With the implementation of Eq. 5.14 and 5.21 the following generic matrix ($\mathbf{M}^0$) can be defined for the Fock ($\mathbf{F}^0$), coefficient ($\mathbf{C}^0$), overlap ($\mathbf{S}^0$) and energy ($\mathbf{e}^0$):

$$\mathbf{M}^0 = \begin{bmatrix} \mathbf{M}_A^0 & 0 \\ 0 & \mathbf{M}_B^0 \end{bmatrix} \tag{5.16}$$

This simplifies the Eq. 5.3, 5.4 and 5.13 to:

$$\mathbf{F}^0 \mathbf{C}^0 = \mathbf{S}^0 \mathbf{C}^0 e^0 \tag{5.17}$$

$$\phi^0 = \chi \mathbf{C}^0 \tag{5.18}$$

$$\left(\mathbf{C}^0\right)^\dagger \mathbf{S}^0 \mathbf{C}^0 = \mathbf{1} \tag{5.19}$$

Implementing a matrix $\mathbf{T}$ that expresses the MO's of the molecule AB as linear combinations of the individual fragment MOs of A and B allow for the transformation of $\mathbf{C}$ into $\mathbf{C}^0$ such that

$$\mathbf{C} = \mathbf{C}^0 \mathbf{T} \tag{5.20}$$

and T can be expressed as

$$\mathbf{T} = \mathbf{1T} = \left(\mathbf{C}^0\right)^\dagger \mathbf{S}^0 \mathbf{C}^0 \mathbf{T} = \left(\mathbf{C}^0\right)^\dagger \mathbf{S}^0 \mathbf{C}^0 \tag{5.21}$$

The Fock matrix of the molecule, $\mathbf{F}$, can be written as the following expansion,

$$\mathbf{F} = \mathbf{F}^{(0)} + \mathbf{F}^{(1)} = \mathbf{F}^{0} + \delta\mathbf{F}^{0} \tag{5.22}$$

where the molecules Fock matrix ($\mathbf{F}$) is equal to the composite matrix (Eq. 5.16, $\mathbf{F}^0$) plus the matrix $\delta\mathbf{F}^0$ defined as,

$$\delta\mathbf{F}^{0} = \begin{bmatrix} \mathbf{F}_A - \mathbf{F}_A^0 & \mathbf{F}_{AB} \\ \mathbf{F}_{AB}^{\dagger} & \mathbf{F}_B - \mathbf{F}_B^0 \end{bmatrix} \tag{5.23}$$

Additional expansions necessary for the derivation of the first, second and third order fragment mixing components are:

$$e = e^{(0)} + e^{(1)} + e^{(2)} + ... \tag{5.24}$$

$$\mathbf{C} = \mathbf{C}^{(0)} + \mathbf{C}^{(1)} + \mathbf{C}^{(2)} + ... \tag{5.25}$$

$$\mathbf{S} = \mathbf{S}^{(0)} + \mathbf{S}^{(1)} = \mathbf{1} + (\tilde{\mathbf{S}} - \mathbf{1}) \tag{5.26}$$

where $\tilde{\mathbf{S}}$ is the molecules overlap matrix in the fragment MO basis. This is defined as,

$$\tilde{\mathbf{S}} = \left(\mathbf{C}^{0}\right)^{\dagger}\mathbf{S}\mathbf{C}^{0} \tag{5.27}$$

Application of perturbation theory formalism's to Eq. 5.3 using the expansions above lead to the first, second and third order energy corrections.

5.2.1 First Order Energy Correction

The first order energy correction is defined as

$$\vec{e}^{\,(1)} = \left(\mathbf{C}^{0}\right)^{\dagger}\mathbf{F}^{(1)}\mathbf{C}^{0} \tag{5.28}$$

where $\mathbf{F}^{(1)}$ is the zeroth order fock matrix that can be found to equal the difference between the molecular systems Fock matrix($\mathbf{F}$) and the non-interaction composite Fock matrix ($\mathbf{F}^0$). To derive

the first order energy correction one must first expand $\mathbf{FC} = \mathbf{SC}e$ to the appropritate orders and group terms of the same order. After each term is expanded, all of the terms that are first order in total are grouped together leading to:

$$\mathbf{F}^{(0)}\mathbf{C}^{(1)} + \mathbf{F}^{(1)}\mathbf{C}^{(0)} = \mathbf{S}^{(0)}\mathbf{C}^{(0)}\vec{e}^{\,(0)} + \mathbf{S}^{(0)}\mathbf{C}^{(1)}\vec{e}^{\,(0)} + \mathbf{S}^{(1)}\mathbf{C}^{(0)}\vec{e}^{\,(0)} \tag{5.29}$$

Multiplying each side by $\left(\mathbf{C}^{(0)}\right)^{\dagger}$ leads to:

$$\begin{gathered}\left(\mathbf{C}^{(0)}\right)^{\dagger}\mathbf{F}^{(0)}\mathbf{C}^{(0)} + \left(\mathbf{C}^{(0)}\right)^{\dagger}\mathbf{F}^{(1)}\mathbf{C}^{(0)} = \\ \left(\mathbf{C}^{(0)}\right)^{\dagger}\mathbf{S}^{(0)}\mathbf{C}^{(0)}\vec{e}^{\,(1)} + \left(\mathbf{C}^{(0)}\right)^{\dagger}\mathbf{S}^{(0)}\mathbf{C}^{(1)}\vec{e}^{\,(0)} + \left(\mathbf{C}^{(0)}\right)^{\dagger}\mathbf{S}^{(1)}\mathbf{C}^{(0)}\vec{e}^{\,(0)}\end{gathered} \tag{5.30}$$

The following definitions are required to simplify Eq. 5.30:

$$\left(\mathbf{C}^{(0)}\right)^{\dagger}\mathbf{F}^{(0)}\mathbf{C}^{(0)} = \mathbf{C}^{(1)}\mathbf{F}^{(0)}\mathbf{C}^{(0)} = \mathbf{C}^{(1)}\vec{e}^{\,(0)}\mathbf{C}_i^{(0)} = \mathbf{C}^{(1)}\mathbf{C}_i^{(0)}\vec{e}^{\,(0)} = 0 \tag{5.31}$$

$$\left(\mathbf{C}^{(0)}\right)^{\dagger}\mathbf{S}^{(0)}\mathbf{C}^{(0)} = \left(\mathbf{C}^{(0)}\right)^{\dagger}\mathbf{1}\,\mathbf{C}^{(0)} = \left(\mathbf{C}^{(0)}\right)^{\dagger}\mathbf{C}^{(0)} = \mathbf{1} \tag{5.32}$$

$$\left(\mathbf{C}^{(0)}\right)^{\dagger}\mathbf{S}^{(0)}\mathbf{C}^{(1)} = \left(\mathbf{C}^{(0)}\right)^{\dagger}\mathbf{1}\,\mathbf{C}^{(1)} = \left(\mathbf{C}^{(0)}\right)^{\dagger}\mathbf{C}_i^{(1)} = 0 \tag{5.33}$$

$$\left(\mathbf{C}^{(0)}\right)^{\dagger}\mathbf{S}^{(1)}|\mathbf{C}^{(0)} = \left(\mathbf{C}^{(0)}\right)^{\dagger}\tilde{\mathbf{S}} - 1\mathbf{C}^{(0)} = \left(\mathbf{C}^{(0)}\right)^{\dagger}\tilde{\mathbf{S}}\,\mathbf{C}_i^{(0)} - \mathbf{1} = \mathbf{1} - \mathbf{1} = 0 \tag{5.34}$$

Implementing the above definitions into Eq. 5.30 lead to the first order energy correction shown in Eq. 5.28.

5.2.2 Second Order Energy Correction

The second order energy correction is defined as,

$$\vec{e}^{\,(2)} = \frac{\left[\left(\mathbf{C}^{0}\right)^{\dagger}\mathbf{F}^{(1)}\mathbf{C}^{0} - \vec{e}^{\,(0)}\left(\mathbf{C}^{0}\right)^{\dagger}\mathbf{S}^{(1)}\mathbf{C}^{0}\right]^{2}}{\Delta\vec{e}^{\,(0)}} \tag{5.35}$$

where $\mathbf{S}^{(1)}$ is defined as the difference of $\tilde{\mathbf{S}}$ and $\mathbf{1}$ as shown in Eq. 5.26. After each term is expanded and all of the terms that are second order total are grouped together similar to the methods of the first-order derivation, we get

$$\begin{gathered}\mathbf{F}^{(0)}\mathbf{C}^{(2)} + \mathbf{F}^{(1)}\mathbf{C}^{(1)} = \mathbf{S}^{(0)}\mathbf{C}^{(2)}\vec{e}^{\,(0)} + \\ \mathbf{S}^{(0)}\mathbf{C}^{(0)}\vec{e}^{\,(2)} + \mathbf{S}^{(0)}\mathbf{C}^{(1)}\vec{e}^{\,(1)} + \mathbf{S}^{(1)}\mathbf{C}^{(1)}\vec{e}^{\,(0)} + \mathbf{S}^{(1)}\mathbf{C}^{(0)}\vec{e}^{\,(1)}\end{gathered} \tag{5.36}$$

Multiplying each side by $\left(\mathbf{C}^{(0)}\right)^{\dagger}$ leads to:

$$\begin{gathered}\left(\mathbf{C}^{(0)}\right)^{\dagger}\mathbf{F}^{(0)}\mathbf{C}^{(2)} + \left(\mathbf{C}^{(0)}\right)^{\dagger}\mathbf{F}^{(1)}\mathbf{C}^{(1)} = \left(\mathbf{C}^{(0)}\right)^{\dagger}\mathbf{S}^{(0)}\mathbf{C}^{(2)}\vec{e}^{\,(0)} + \\ \left(\mathbf{C}^{(0)}\right)^{\dagger}\mathbf{S}^{(0)}\mathbf{C}^{(0)}\vec{e}^{\,(2)} + \mathbf{S}^{(0)}\mathbf{C}^{(1)}\vec{e}^{\,(1)} + \left(\mathbf{C}^{(0)}\right)^{\dagger}\mathbf{S}^{(1)}\mathbf{C}^{(1)}\vec{e}^{\,(0)} + \left(\mathbf{C}^{(0)}\right)^{\dagger}\mathbf{S}^{(1)}\mathbf{C}^{(0)}\vec{e}^{\,(1)}\end{gathered} \tag{5.37}$$

The following definitions are required to simplify Eq. 5.37:

$$\left(\mathbf{C}^{(0)}\right)^{\dagger}\mathbf{F}^{(0)}\mathbf{C}^{(2)} = \mathbf{C}^{(2)}\mathbf{F}^{(0)}\left(\mathbf{C}^{(0)}\right)^{\dagger} = \left(\mathbf{C}^{(0)}\right)^{\dagger}\mathbf{C}_{i}^{(2)}\vec{e}^{\,(0)} = \mathbf{0} \tag{5.38}$$

$$\left(\mathbf{C}^{(0)}\right)^{\dagger}\mathbf{S}^{(0)}\mathbf{C}^{(2)} = \left(\mathbf{C}^{(0)}\right)^{\dagger}\mathbf{1}\,\mathbf{C}^{(2)} = \left(\mathbf{C}^{(0)}\right)^{\dagger}\mathbf{C}^{(2)} = \mathbf{0} \tag{5.39}$$

$$\left(\mathbf{C}^{(0)}\right)^{\dagger}\mathbf{S}^{(0)}\mathbf{C}^{(0)} = \left(\mathbf{C}^{(0)}\right)^{\dagger}\mathbf{1}\,\mathbf{C}^{(0)} = \left(\mathbf{C}^{(0)}\right)^{\dagger}\mathbf{C}^{(0)} = \mathbf{1} \tag{5.40}$$

$$\left(\mathbf{C}^{(0)}\right)^{\dagger}\mathbf{S}^{(0)}\mathbf{C}^{(1)} = \left(\mathbf{C}^{(0)}\right)^{\dagger}\mathbf{1}\,\mathbf{C}^{(1)} = \left(\mathbf{C}^{(0)}\right)^{\dagger}\mathbf{C}^{(1)} = \mathbf{0} \tag{5.41}$$

$$\left(\mathbf{C}^{(0)}\right)^{\dagger}\mathbf{S}^{(1)}\mathbf{C}^{(0)} = \left(\mathbf{C}^{(0)}\right)^{\dagger}\tilde{(}\mathbf{S}-\mathbf{1})\,\mathbf{C}^{(0)} = \left(\mathbf{C}^{(0)}\right)^{\dagger}\tilde{\mathbf{S}}\,\mathbf{C}^{(0)} - \mathbf{1} = \mathbf{1} - \mathbf{1} = \mathbf{0} \tag{5.42}$$

The implementation of Eq. 5.38 to Eq. 5.42 simplifies Eq. 5.37 to,

$$\left(\mathbf{C}^{(0)}\right)^{\dagger}\mathbf{F}^{(1)}\mathbf{C}^{(1)} = \vec{e}^{\,(2)} + \left(\mathbf{C}^{(0)}\right)^{\dagger}\mathbf{S}^{(1)}\mathbf{C}^{(1)}\vec{e}^{\,(0)} \tag{5.43}$$

Rearrangement of Eq. 5.43 and and expansion leads to:

$$\vec{e}^{\,(2)} = \left[\left(\mathbf{C}^{(0)}\right)^{\dagger}\mathbf{F}^{(1)}\,\vec{e}^{\,(0)}\,\mathbf{S}^{(1)}\,\mathbf{C}^{(0)}\right]\left[\left(\mathbf{C}^{(0)}\right)^{\dagger}\mathbf{C}^{(1)}\right] \tag{5.44}$$

The next step in solving for the second order energy correction is getting all of the terms into the zeroth order. The key to doing this is to find a definition of the second bracketed term in Eq. **??**. To achieve this we start with Eq. 5.29, and multiply each side by $\left(\mathbf{C}^{(0)}\right)^{\dagger}$.

$$\begin{aligned}\left(\mathbf{C}^{(0)}\right)^{\dagger}\mathbf{F}^{(0)}\mathbf{C}^{(1)}+\left(\mathbf{C}^{(0)}\right)^{\dagger}\mathbf{F}^{(1)}\mathbf{C}^{(0)}=\left(\mathbf{C}^{(0)}\right)^{\dagger}\mathbf{S}^{(0)}\mathbf{C}^{(0)}\vec{e}^{\,(1)}+\\ \left(\mathbf{C}^{(0)}\right)^{\dagger}\mathbf{S}^{(0)}\mathbf{C}^{(1)}\vec{e}^{\,(0)}+\left(\mathbf{C}^{(0)}\right)^{\dagger}\mathbf{S}^{(1)}\mathbf{C}^{(0)}\vec{e}^{\,(0)}\end{aligned} \tag{5.45}$$

The following definitions are used to simplify Eq. 5.45:

$$\left(\mathbf{C}^{(0)}\right)^{\dagger}\mathbf{F}^{(0)}\mathbf{C}^{(1)}=\mathbf{C}^{(1)}\mathbf{F}^{(0)}\left(\mathbf{C}^{(0)}\right)^{\dagger}=\left(\mathbf{C}^{(0)}\right)^{\dagger}\mathbf{C}^{(1)}\vec{e}^{\,(0)}=\mathbf{0} \tag{5.46}$$

$$\left(\mathbf{C}^{(0)}\right)^{\dagger}\mathbf{S}^{(0)}\mathbf{C}^{(1)}=\left(\mathbf{C}^{(0)}\right)^{\dagger}\mathbf{1}\,\mathbf{C}^{(1)}=\left(\mathbf{C}^{(0)}\right)^{\dagger}\mathbf{C}^{(1)} \tag{5.47}$$

$$\left(\mathbf{C}^{(0)}\right)^{\dagger}\mathbf{S}^{(0)}\mathbf{C}^{(0)}=\left(\mathbf{C}^{(0)}\right)^{\dagger}\mathbf{1}\,\mathbf{C}^{(0)}=(\mathbf{C}^{(0)})^{\dagger}\mathbf{C}^{(0)}=\mathbf{0} \tag{5.48}$$

Implementing these definitions in Eq. 5.45 and rearranging to solve for $(\mathbf{C}^{(0)})^{\dagger}\mathbf{C}^{(1)}$ leads to:

$$(\mathbf{C}^{(0)})^{\dagger}\mathbf{C}^{(1)}=\frac{\left(\mathbf{C}^{(0)}\right)^{\dagger}\mathbf{F}^{(1)}-\vec{e}^{\,(0)}\mathbf{S}^{(1)}\mathbf{C}^{(0)}}{\vec{e}^{\,(0)}-\vec{e}^{\,(1)}} \tag{5.49}$$

By plugging Eq. 5.49 into Eq. 5.44 leads to the final expression for the second order energy correction.

$$\vec{e}^{\,(2)}=\sum_{j\neq i}\frac{\left(\mathbf{C}^{(0)}\right)^{\dagger}\mathbf{F}^{(1)}-\vec{e}^{\,(0)}\mathbf{S}^{(1)}\mathbf{C}_{j}^{(0)}\left(\mathbf{C}^{(0)}\right)^{\dagger}\mathbf{F}^{(1)}-\vec{e}^{\,(0)}\mathbf{S}^{(1)}\mathbf{C}^{(0)}}{\vec{e}^{\,(0)}-e^{(0)}} \tag{5.50}$$

5.2.3 Third Order Energy Correction

The third order mixing energy expression is defined as,

$$\vec{e}^{\,(3)}=\frac{[\mathbf{A}][\mathbf{B}][\mathbf{A}]}{\left[\Delta\vec{e}^{\,(0)}\right]^{2}}-\frac{[\mathbf{C}][\mathbf{A}]}{\Delta\vec{e}^{\,(0)}} \tag{5.51}$$

where **A**, **B** and **C** are defined as,

$$\mathbf{A} = (\mathbf{C}^0)^\dagger \mathbf{F}^{(1)} \mathbf{C}^0 - \vec{e}^{\,(0)} (\mathbf{C}^0)^\dagger \mathbf{S}^{(1)} \mathbf{C}^0 \tag{5.52}$$

$$\mathbf{B} = (\mathbf{C}^0)^\dagger \mathbf{F}^{(1)} \mathbf{C}^0 - \vec{e}^{\,(0)} (\mathbf{C}^0)^\dagger \mathbf{S}^{(1)} \mathbf{C}^0 - \vec{e}^{\,(1)} (\mathbf{C}^0)^\dagger \mathbf{C}^0 \tag{5.53}$$

$$\mathbf{C} = \vec{e}^{\,(1)} (\mathbf{C}^0)^\dagger \mathbf{S}^{(1)} \mathbf{C}^0. \tag{5.54}$$

To derive this expression, one must take similar steps shown for the first and second energy corrections. After each term is expanded in the Fock equation, all of the terms that are third order are grouped together leading to:

$$\begin{aligned} \mathbf{F}^{(0)}\mathbf{C}^{(3)} + \mathbf{F}^{(1)}\mathbf{C}^{(2)} = \\ \mathbf{S}^{(0)}\mathbf{C}^{(3)}e^{(0)} + \mathbf{S}^{(0)}\mathbf{C}^{(1)}e^{(2)} + \mathbf{S}^{(0)}\mathbf{C}^{(2)}e^{(1)} + \mathbf{S}^{(1)}\mathbf{C}^{(1)}e^{(1)} + \mathbf{S}^{(1)}\mathbf{C}^{(2)}e^{(0)} + \mathbf{S}^{(1)}\mathbf{C}^{(0)}e^{(2)} \end{aligned} \tag{5.55}$$

Multiplying each side by $(\mathbf{C}_i^{(0)})^\dagger$ leads to:

$$\begin{aligned} (\mathbf{C}^{(0)})^\dagger \mathbf{F}^{(0)} \mathbf{C}^{(3)} + (\mathbf{C}^{(0)})^\dagger \mathbf{F}^{(1)} \mathbf{C}^{(2)} = \\ (\mathbf{C}^{(0)})^\dagger \mathbf{S}^{(0)} \mathbf{C}^{(3)} e^{(0)} + (\mathbf{C}^{(0)})^\dagger \mathbf{S}^{(0)} \mathbf{C}^{(1)} e^{(2)} + (\mathbf{C}^{(0)})^\dagger \mathbf{S}^{(0)} \mathbf{C}^{(2)} e^{(1)} + \\ (\mathbf{C}^{(0)})^\dagger \mathbf{S}^{(1)} \mathbf{C}^{(1)} e^{(1)} + (\mathbf{C}^{(0)})^\dagger \mathbf{S}^{(1)} \mathbf{C}^{(2)} e^{(0)} + (\mathbf{C}^{(0)})^\dagger \mathbf{S}^{(1)} \mathbf{C}^{(0)} e^{(2)} \end{aligned} \tag{5.56}$$

The following definitions are necessary to simplify the previous equation.

$$(\mathbf{C}^{(0)})^\dagger \mathbf{F}^{(0)} \mathbf{C}^{(3)} = (\mathbf{C}^{(3)})^\dagger \mathbf{F}^{(0)} \mathbf{C}^{(0)} = (\mathbf{C}^{(3)})^\dagger \mathbf{C}^{(0)} e^{(0)} = \mathbf{0} \tag{5.57}$$

$$(\mathbf{C}^{(0)})^\dagger \mathbf{S}^{(0)} \mathbf{C}^{(3)} = (\mathbf{C}^{(0)})^\dagger \mathbf{1} \mathbf{C}^{(3)} = (\mathbf{C}^{(0)})^\dagger \mathbf{C}^{(3)} = \mathbf{0} \tag{5.58}$$

$$(\mathbf{C}^{(0)})^\dagger \mathbf{S}^{(0)} \mathbf{C}^{(0)} = (\mathbf{C}^{(0)})^\dagger \mathbf{1} \mathbf{C}^{(0)} = (\mathbf{C}^{(0)})^\dagger \mathbf{C}^{(1)} = \mathbf{1} \tag{5.59}$$

$$(\mathbf{C}^{(0)})^\dagger \mathbf{S}^{(0)} \mathbf{C}^{(1)} = (\mathbf{C}^{(0)})^\dagger \mathbf{1} \mathbf{C}^{(1)} = (\mathbf{C}^{(0)})^\dagger \mathbf{C}^{(1)} = \mathbf{0} \tag{5.60}$$

$$(\mathbf{C}^{(0)})^{\dagger}\mathbf{S}^{(0)}\mathbf{C}^{(2)} = (\mathbf{C}^{(0)})^{\dagger}\mathbf{1}\mathbf{C}^{(2)} = (\mathbf{C}^{(0)})^{\dagger}\mathbf{C}^{(2)} = \mathbf{0} \tag{5.61}$$

$$(\mathbf{C}^{(0)})^{\dagger}\mathbf{S}^{(1)}\mathbf{C}^{(0)} = (\mathbf{C}^{(0)})^{\dagger}\tilde{[\mathbf{S}-\mathbf{1}]}\mathbf{C}^{(0)} = (\mathbf{C}^{(0)})^{\dagger}\tilde{\mathbf{S}}\mathbf{C}^{(0)} - \mathbf{1} = \mathbf{1} - \mathbf{1} = 0 \tag{5.62}$$

Implementation and rearrangement of the above definitions into Eq. 5.56 leads us to:

$$e^{(3)} = (\mathbf{C}^{(0)})^{\dagger}\left[\mathbf{F}^{(1)} - e^{(0)}\mathbf{S}^{(1)}\right]\mathbf{C}^{(2)} - (\mathbf{C}^{(0)})^{\dagger}\left[e^{(1)}\mathbf{S}^{(1)}\right]\mathbf{C}_{i}^{(1)} \tag{5.63}$$

Resolving the identity in both terms of Eq. 5.63 leads to:

$$e^{(3)} = (\mathbf{C}^{(0)})^{\dagger}\left[\mathbf{F}^{(1)} - e^{(0)}\mathbf{S}^{(1)}\right]\mathbf{C}^{(0)}\left[\mathbf{C}^{(0)}\mathbf{C}^{(2)}\right] - (\mathbf{C}^{(0)})^{\dagger}\left[e_{i}^{(1)}\mathbf{S}^{(1)}\right]\mathbf{C}^{(0)}\left[\mathbf{C}^{(0)}\mathbf{C}^{(1)}\right] \tag{5.64}$$

The expansion of $(\mathbf{C}^{(0)})^{\dagger}\mathbf{C}^{(1)}$ was derived in the second order expression, and when substituted into Eq. 5.64 the expression becomes:

$$e^{(3)} = (\mathbf{C}^{(0)})^{\dagger}[\mathbf{F}^{(1)} - e^{(0)}\mathbf{S}^{(1)}]\mathbf{C}^{(0)}(\mathbf{C}^{(0)})^{\dagger}\mathbf{C}^{(2)} - \frac{(\mathbf{C}^{(0)})^{\dagger}e^{(1)}\mathbf{S}^{(1)}\mathbf{C}^{(0)}(\mathbf{C}^{(0)})^{\dagger}[\mathbf{F}^{(1)} - e^{(0)}\mathbf{S}^{(1)}]\mathbf{C}^{(0)}}{e^{(0)} - e^{(1)}} \tag{5.65}$$

The next step in solving for the third order energy correction is getting all of the terms into the zeroth order. To do this we start with the Fock equation expanded with all the terms in the second order and multiply each side by $(\mathbf{C}^{(0)})^{\dagger}$.

$$\begin{aligned}(\mathbf{C}^{(0)})^{\dagger}\mathbf{F}^{(0)}\mathbf{C}^{(2)} + (\mathbf{C}^{(0)})^{\dagger}\mathbf{F}^{(1)}\mathbf{C}^{(1)} = (\mathbf{C}^{(0)})^{\dagger}\mathbf{S}^{(0)}\mathbf{C}^{(2)}e^{(0)} + (\mathbf{C}^{(0)})^{\dagger}\mathbf{S}^{(0)}\mathbf{C}^{(0)}e_{i}^{(2)} + \\ (\mathbf{C}^{(0)})^{\dagger}\mathbf{S}^{(0)}\mathbf{C}^{(1)}e^{(1)} + (\mathbf{C}^{(0)})^{\dagger}\mathbf{S}^{(1)}\mathbf{C}^{(1)}e^{(0)} + (\mathbf{C}^{(0)})^{\dagger}\mathbf{S}^{(1)}\mathbf{C}^{(0)}e^{(1)}\end{aligned} \tag{5.66}$$

The following definitions are used to simplify Eq. 5.66:

$$(\mathbf{C}^{(0)})^{\dagger}\mathbf{F}^{(0)}\mathbf{C}^{(2)} = (\mathbf{C}^{(2)})^{\dagger}\mathbf{F}^{(0)}\mathbf{C}^{(0)} = (\mathbf{C}^{(2)})^{\dagger}\mathbf{C}^{(0)}e^{(0)} = (\mathbf{0})e^{(0)} = \mathbf{0} \tag{5.67}$$

$$(\mathbf{C}^{(0)})^{\dagger}\mathbf{S}^{(0)}\mathbf{C}^{(2)} = (\mathbf{C}^{(0)})^{\dagger}\mathbf{C}^{(2)} \tag{5.68}$$

$$(\mathbf{C}^{(0)})^{\dagger}\mathbf{S}^{(0)}\mathbf{C}^{(0)} = (\mathbf{C}^{(0)})^{\dagger}\mathbf{C}^{(0)} = \mathbf{0} \tag{5.69}$$

$$(\mathbf{C}^{(0)})^{\dagger}\mathbf{S}^{(0)}\mathbf{C}^{(1)} = (\mathbf{C}^{(0)})^{\dagger}\mathbf{C}^{(1)} \tag{5.70}$$

$$(\mathbf{C}^{(0)})^{\dagger}\mathbf{S}^{(1)}\mathbf{C}^{(0)} = (\mathbf{C}^{(0)})^{\dagger}[\tilde{\mathbf{S}} - 1]\mathbf{C}^{(0)} = (\mathbf{C}^{(0)})^{\dagger}\tilde{\mathbf{S}}\mathbf{C}^{(0)} - (\mathbf{C}^{(0)})^{\dagger}\mathbf{C}^{(0)} = 0 - 0 = \mathbf{0} \tag{5.71}$$

The substitution and rearrangement of Eq. 5.66 using Eq. 5.67-5.71 leads to,

$$(\mathbf{C}^{(0)})^{\dagger}\mathbf{C}^{(2)} = \frac{(\mathbf{C}^{(0)})^{\dagger}[\mathbf{F}^{(1)} - e^{(0)}\mathbf{S}^{(0)} - e^{(1)}]\mathbf{C}^{(1)}}{e^{(0)} - e^{(0)}} \tag{5.72}$$

A basis expansion and substitution to Eq. 5.72 would lead to,

$$(\mathbf{C}^{(0)})^{\dagger}\mathbf{C}^{(2)} = \frac{(\mathbf{C}^{(0)})^{\dagger}[\mathbf{F}^{(1)} - e^{(0)}\mathbf{S}^{(0)} - e_i^{(1)}]\mathbf{C}^{(0)}(\mathbf{C}^{(0)})^{\dagger}[\mathbf{F}^{(1)} - e^{(0)}\mathbf{S}^{(0)}]\mathbf{C}^{(1)}}{e^{(0)} - e^{(0)}} \tag{5.73}$$

Substituting Eq. 5.73 into Eq. 5.65 leads to,

$$e^{(3)} = \frac{(\mathbf{C}^{(0)})^{\dagger}[\mathbf{F}^{(1)} - e^{(0)}\mathbf{S}^{(1)}]\mathbf{C}^{(0)}(\mathbf{C}^{(0)})^{\dagger}[\mathbf{F}^{(1)} - e^{(0)}\mathbf{S}^{(1)} - e^{(1)}]\mathbf{C}^{(0)}(\mathbf{C}^{(0)})^{\dagger}[\mathbf{F}^{(1)} - e^{(0)}\mathbf{S}^{(1)}]\mathbf{C}^{(0)}}{(e^{(0)} - e^{(0)})(e^{(0)} - e^{(0)})} - \frac{(\mathbf{C}^{(0)})^{\dagger}[e^{(1)}\mathbf{S}^{(1)}]\mathbf{C}^{(0)}(\mathbf{C}^{(0)})^{\dagger}[\mathbf{F}^{(1)} - e^{(0)}\mathbf{S}^{(1)}]\mathbf{C}^{(0)}}{(e^{(0)} - e^{(0)})} \tag{5.74}$$

5.3 Numerical Tests

With the goal of developing an easy to use model to quantitatively analyze multi-center chemical bonding, we have implemented the IPA model described above in an open source code available on GitHub. The program, named IPA, uses Gaussian matrix files prepared by fragment quantum calculations run in Gaussian. [35] The electronic structure calculations were carried out using the B3PW91/3-21G model chemistry. To examine capability of this program, we present results for the prototype three-center two-electron bonding system.

The sample IPA calculation of HFH^- employs two fragments. The first fragment is ${H_2}^{2-}$; and the second fragment is F^+. In this framework, bonding in this system can be described as dihydride donating two electrons into unoccupied F^+ fragment molecular orbitals.

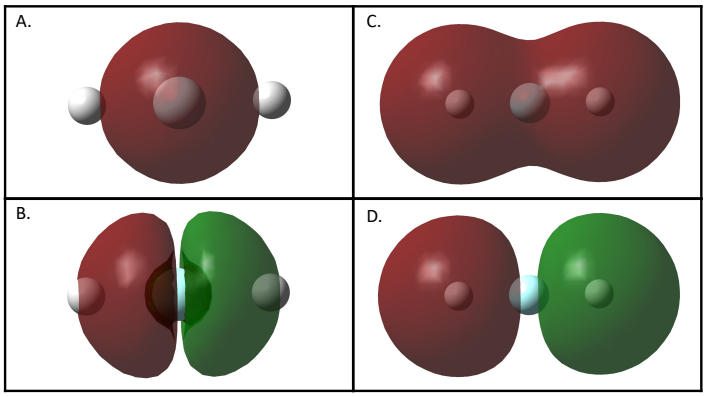

Figure 5.1: Fragment molecular orbitals for H_2^{2-} and F^+ in the HFH^- example complex. Included are contours showing the spatial distribution of the F^+ unoccupied/acceptor fragment molecular orbitals (A and B) and the H_2^{2-} occupied/donor fragment molecular orbitals.

Interestingly, the IPA calculation suggests significant mixing between occupied fragment orbitals, which would lead to four-electron interactions. At second-order, the two most significant of these types of interactions are calculated to be 39.3 kcal/mol and 19.4 kcal/mol. Such interaction energies suggest that the composite MOs involve mixing of multiple fragment MOs.

This point suggests an important observation of the IPA model that will require careful consideration in the future. Namely, alternative fragment orbital choices may be more appropriate to isolate a conceptual description of the electronic interactions of the chosen fragments within a donor/acceptor picture and the selection of a zero-order fragment MO basis is not unique.

In the basis used here, the IPA computation clearly indicated four key fragment molecular orbitals involved in a two-electron donor/acceptor electronic interaction. These fragment MOs are shown in Fig. 5.3. The IPA suggests that the two-electron interaction involves a combination of H_2^{2-} σ and σ^* fragment MOs with s and π^* F^+ fragment MOs. The combined second-order energy correction for these interactions is 41.0 kcal/mol.

5.4 Conclusions and Future Work

In this chapter, an IPA model was developed and we reported initial results from an open source program written to carry out such IPA calculations. The example result shown was for the model three-center two-electron bond system HFH^-. As shown, the model correctly predicts donation of electrons from an ${H_2}^{2-}$ fragment into unoccupied orbitals of the F^+ fragment. As one would expect, the three-center two-electron bond in this case is relatively weak.

Future work will expand this model to compute third-order energy corrections. Such an extension will allow one to evaluate relative degrees of additive and cooperative bonding effects in three-center two-electron bonds. A second future addition will be the generation of wave function corrections. This addition to the program will allow users to visually inspect changes in MO spatial distributions as fragment MOs interact. This feature will also provide a convenient framework for population analyses in fragment and composite molecular bases.

Finally, after completing the above model extensions we will revisit the CuAAC and halogen bonding species described in the previous dissertation chapters. The IPA model will provide a means for quantifying the role of three-center two-electron bonds in stabilizing the intermediate species we identified in those other studies. Such results will aid in future rational design of Cu click catalysts and halogen bonding partners to facilitate selective halogen additions.

Chapter 6

Summary & Outlooks

The combination of chemical curiosity, mathematics, physics and computer science have led to the birth of computational chemistry. The collaborations and connections between these fields allows one the opportunity to model and explore chemical systems and explain unique electronic structures that were once unattainable. The main systems of interest in the work presented in this dissertation include transition metal catalyzed reactions and the intermediates involved in those mechanisms.

It is essential that all research serve a greater purpose. This purpose does not simply stop at job completions or a publication. Novel research findings must be applicable to a variety of other unanswered questions and serve as a stepping stone for future studies. Much of the work presented in this thesis have reached its first stage of completion, but there is much that can be done with the results and what was learned in the process. (Funny enough, this exact idea applies to ever student in graduate school.)

6.1 Future Work

6.1.1 A Computational Exploration of the Copper Catalyzed Azide-Alkyne Cycloaddition

This work computationally investigated the governing mechanism of a copper catalyzed azide-alkyne cycloaddition. From this work a proposed reaction mechanism has been hypothesized. With this work in hand, one can begin working on a similar reaction can be completed using iodoalkyne. [Cite Hein & Chung work] The governing mechanism for this reaction remains unknown, but we believe there could be similarities between these two.

6.1.2 Computational Investigations of Silver Catalyzed Fluorination: A Halogen Bonding Investigation

In collaboration with the Baxter Lab at UC Merced, we investigated the mechanistic intermediates present in the silver(I) initiated radical C-H fluorination reaction. In this work we presented results introducing an unprecedented $[N\text{-}F\text{-}N]^+$ halogen bonding network. Future work for this project includes a thorough analysis of this bond and those similar to it. With this in hand, one could apply the computational knowledge to a variety of other weakly bound intermediates.

6.1.3 A Novel Approach for Asymmetric Bromination: A Computational Evaluation

In collaboration with the Baxter Lab at UC Merced, we investigated a new method for aromatic bromination using lactic acid derivatives as halogen-bond acceptors with NBS. The efficiency of this reaction is altered when the lewis basic additives required for the reaction is changed due to the ability of the intermediates to halogen bond. The knowledge gained from this work could be applied to the wide range of other systems where the extent of halogen-bonding effects the overall reaction yield.

6.1.4 Intermolecular Perturbational Analysis: A Model to Investigate Non-Traditional Bonding

Understanding the interactions between atoms and molecules is foundational to the advancement of chemistry. Despite a large volume of studies done on systems using molecular orbital theory, a simple-to-use quantitative model to investigate multi-body interactions is still absent in the computational chemistry toolbox. In this work derived the necessary equations and completed a preliminary model based on third order perturbational molecular orbital theory to do just that. This work has been applied to a set of example systems, but the future intentions of this code is to apply it to a wide variety of systems including three-center two electron bonds and halogen bonded strtuctures.

Bibliography

[1] A. Cornish-Bowden, Principles of enzyme kinetics, Elsevier, 2014.

[2] E. N. Kotelnikova, A. I. Isakov, L. Y. Kryuchkova, A. A. Zolotarev, S. N. Bocharov, H. Lorenz, Acids with chiral molecules as essential organic compounds of biogenic–abiogenic systems, in: Processes and Phenomena on the Boundary between Biogenic and Abiogenic Nature, Springer, 2020, pp. 695–719.

[3] J. C. Ndukaife, V. M. Shalaev, A. Boltasseva, Plasmonics—turning loss into gain, Science 351 (6271) (2016) 334–335.

[4] Z. Jiang, T. Xiao, V. á. Kuznetsov, P. á. Edwards, Turning carbon dioxide into fuel, Philosophical Transactions of the Royal Society A: Mathematical, Physical and Engineering Sciences 368 (1923) (2010) 3343–3364.

[5] L. Mueck, Quantum software (2017).

[6] J. J. W. Sørensen, M. K. Pedersen, M. Munch, P. Haikka, J. H. Jensen, T. Planke, M. G. Andreasen, M. Gajdacz, K. Mølmer, A. Lieberoth, et al., Exploring the quantum speed limit with computer games, Nature 532 (7598) (2016) 210–213.

[7] A. Robinson, The Last Man who Knew Everything: Thomas Young, the Anonymous Genius who Proved Newton Wrong, and Deciphered the Rosetta Stone, Among Other Surprising Feats, Plume, 2007.

[8] J. Navarro, A History of the Electron: JJ and GP Thomson, Cambridge University Press, 2012.

[9] J. C. Maxwell, Viii. a dynamical theory of the electromagnetic field, Philosophical transactions of the Royal Society of London (155) (1865) 459–512.

[10] D. Baird, R. I. Hughes, A. Nordmann, Heinrich Hertz: Classical physicist, modern philosopher, Vol. 198, Springer Science & Business Media, 2013.

[11] M. Planck, The theory of heat radiation, translated by m, Masius, P. Blackiston's Son & Co, Philadelphia, reprinted by Kessinger (1914).

[12] H. Geiger, The scattering of α-particles by matter, Proceedings of the Royal Society of London. Series A, Containing Papers of a Mathematical and Physical Character 83 (565) (1910) 492–504.

[13] O. Darrigol, Bohr's trilogy of 1913, in: Niels Bohr, 1913-2013, Springer, 2016, pp. 1–11.

[14] R. P. Feynman, QED: The strange theory of light and matter, Princeton University Press, 2006.

[15] C. J. Davisson, L. H. Germer, Reflection of electrons by a crystal of nickel, Proceedings of the National Academy of Sciences of the United States of America 14 (4) (1928) 317.

[16] B. Friedrich, D. Herschbach, Stern and gerlach: How a bad cigar helped reorient atomic physics, Physics Today 56 (12) (2003) 53–59.

[17] K. Camilleri, Heisenberg and the interpretation of quantum mechanics, hiqm (2009).

[18] D. Sen, The uncertainty relations in quantum mechanics, Current Science (2014) 203–218.

[19] T. J. Zielinski, E. Harvey, R. Sweeney, D. M. Hanson, Quantum states of atoms and molecules (2005).

[20] E. Schrödinger, An undulatory theory of the mechanics of atoms and molecules, Physical review 28 (6) (1926) 1049.

[21] M. Born, R. Oppenheimer, Zur quantentheorie der molekeln, Annalen der physik 389 (20) (1927) 457–484.

[22] D. R. Hartree, The wave mechanics of an atom with a non-coulomb central field. part i. theory and methods, in: Mathematical Proceedings of the Cambridge Philosophical Society, Vol. 24, Cambridge University Press, 1928, pp. 89–110.

[23] D. R. Hartree, The wave mechanics of an atom with a non-coulomb central field. part ii. some results and discussion, in: Mathematical Proceedings of the Cambridge Philosophical Society, Vol. 24, Cambridge University Press, 1928, pp. 111–132.

[24] J. C. Slater, The self consistent field and the structure of atoms, Physical Review 32 (3) (1928) 339.

[25] J. C. Slater, Note on hartree's method, Physical Review 35 (2) (1930) 210.

[26] V. Fock, Näherungsmethode zur lösung des quantenmechanischen mehrkörperproblems, Zeitschrift für Physik 61 (1-2) (1930) 126–148.

[27] D. R. Hartree, W. Hartree, Self-consistent field, with exchange, for beryllium, Proceedings of the Royal Society of London. Series A-Mathematical and Physical Sciences 150 (869) (1935) 9–33.

[28] D. R. Hartree, W. Hartree, Self-consistent field, with exchange, for beryllium-ii—the (2 s)(2 p) 3p and 1p excited states, Proceedings of the Royal Society of London. Series A-Mathematical and Physical Sciences 154 (883) (1936) 588–607.

[29] P.-O. Löwdin, Quantum theory of many-particle systems. iii. extension of the hartree-fock scheme to include degenerate systems and correlation effects, Physical review 97 (6) (1955) 1509.

[30] P. Hohenberg, W. Kohn, Inhomogeneous electron gas, Physical review 136 (3B) (1964) B864.

[31] W. Kohn, L. J. Sham, Self-consistent equations including exchange and correlation effects, Physical review 140 (4A) (1965) A1133.

[32] R. G. Parr, Density functional theory of atoms and molecules, in: Horizons of quantum chemistry, Springer, 1980, pp. 5–15.

[33] A. J. Thakkar, A. C. Tanner, V. H. Smith, Inter-relationships between various representations of one-matrices and related densities: A road map and an example, in: Density Matrices and Density Functionals, Springer, 1987, pp. 327–337.

[34] V. L. Lignères, E. A. Carter, An introduction to orbital-free density functional theory, in: Handbook of materials modeling, Springer, 2005, pp. 137–148.

[35] M. J. Frisch, G. W. Trucks, H. B. Schlegel, G. E. Scuseria, M. A. Robb, J. R. Cheeseman, G. Scalmani, V. Barone, B. Mennucci, G. A. Petersson, H. Nakatsuji, M. Caricato, X. Li, H. P. Hratchian, A. F. Izmaylov, J. Bloino, B. Janesko, F. Lipparini, G. Zheng, J. L. Sonnenberg, W. Liang, M. Hada, M. Ehara, K. Toyota, R. Fukuda, J. Hasegawa, M. Ishida, T. Nakajima, Y. Honda, O. Kitao, H. Nakai, T. Vreven, J. A. Montgomery, Jr., J. E. Peralta, F. Ogliaro, M. Bearpark, J. J. Heyd, E. Brothers, K. N. Kudin, V. N. Staroverov, T. Keith, R. Kobayashi, J. Normand, K. Raghavachari, A. Rendell, J. C. Burant, S. S. Iyengar, J. Tomasi, M. Cossi, N. Rega, J. M. Millam, M. Klene, J. E. Knox, J. B. Cross, V. Bakken, C. Adamo, J. Jaramillo, R. Gomperts, R. E. Stratmann, O. Yazyev, A. J. Austin, R. Cammi, C. Pomelli, J. W. Ochterski, R. L. Martin, K. Morokuma, V. G. Zakrzewski, G. A. Voth, P. Salvador, J. J. Dannenberg, S. Dapprich, P. V. Parandekar, N. J. Mayhall, A. D. Daniels, O. Farkas, J. B. Foresman, J. V. Ortiz, J. Cioslowski, D. J. Fox, gaussian Development Version, Revision I.03+, Gaussian, Inc., Wallingford CT, 2014.

[36] J. Kong, C. A. White, A. I. Krylov, D. Sherrill, R. D. Adamson, T. R. Furlani, M. S. Lee, A. M. Lee, S. R. Gwaltney, T. R. Adams, et al., Q-chem 2.0: a high-performance ab initio

electronic structure program package, Journal of Computational Chemistry 21 (16) (2000) 1532–1548.

[37] M. Valiev, E. J. Bylaska, N. Govind, K. Kowalski, T. P. Straatsma, H. J. Van Dam, D. Wang, J. Nieplocha, E. Apra, T. L. Windus, et al., Nwchem: A comprehensive and scalable open-source solution for large scale molecular simulations, Computer Physics Communications 181 (9) (2010) 1477–1489.

[38] T. M. I.S. Ufimtsev, Quantum chemistry on graphical processing units. 3. analytical energy gradients and first principles molecular dynamics, J. Chem. Theory Comput. (2009) 2619.

[39] R. M. P. E. G. H. F. E. J. T. F. B. J. M. L. A. B. J. J. J. M. Turney, A. C. Simmonett, psi4: An open-source ab initio electronic structure program.

[40] T. Chang, H. Gao, Size-dependent elastic properties of a single-walled carbon nanotube via a molecular mechanics model, Journal of the Mechanics and Physics of Solids 51 (6) (2003) 1059–1074.

[41] R. K. Tan, S. C. Harvey, Molecular mechanics model of supercoiled dna, Journal of molecular biology 205 (3) (1989) 573–591.

[42] N. L. Allinger, Y. H. Yuh, J. H. Lii, Molecular mechanics. the mm3 force field for hydrocarbons. 1, Journal of the American Chemical Society 111 (23) (1989) 8551–8566.

[43] D. B. Boyd, K. B. Lipkowitz, Molecular mechanics: The method and its underlying philosophy, Journal of Chemical Education 59 (4) (1982) 269.

[44] J. Moult, Comparison of database potentials and molecular mechanics force fields, Current opinion in structural biology 7 (2) (1997) 194–199.

[45] N. L. Allinger, Molecular structure: understanding steric and electronic effects from molecular mechanics, John Wiley & Sons, 2010.

[46] M. C. Zerner, Semiempirical molecular orbital methods, Reviews in computational chemistry 2 (1991) 313–365.

[47] T. Bredow, K. Jug, Theory and range of modern semiempirical molecular orbital methods, Theoretical Chemistry Accounts 113 (1) (2005) 1–14.

[48] Y. K. Pan, Approximate molecular orbital theory (pople, john a.; beveridge, david l.) (1971).

[49] R. A. Friesner, Ab initio quantum chemistry: Methodology and applications, Proceedings of the National Academy of Sciences 102 (19) (2005) 6648–6653.

[50] C. Draxl, D. Nabok, K. Hannewald, Organic/inorganic hybrid materials: Challenges for ab initio methodology, Accounts of chemical research 47 (11) (2014) 3225–3232.

[51] G. Martin-Head, J. Pople, M. Frisch, Mp2 energy evaluation by direct methods, Chem. Phys. Lett 153 (1988) 503–506.

[52] T. D. Crawford, H. F. Schaefer, An introduction to coupled cluster theory for computational chemists, Reviews in computational chemistry 14 (2000) 33–136.

[53] C. J. Cramer, Essentials of computational chemistry: theories and models, John Wiley & Sons, 2013.

[54] P. J. Knowles, H.-J. Werner, An efficient second-order mc scf method for long configuration expansions, Chemical Physics Letters 115 (3) (1985) 259–267.

[55] H.-J. Werner, W. Meyer, A quadratically convergent multiconfiguration–self-consistent field method with simultaneous optimization of orbitals and ci coefficients, The Journal of Chemical Physics 73 (5) (1980) 2342–2356.

[56] P. Celani, H.-J. Werner, Analytical energy gradients for internally contracted second-order multireference perturbation theory, The Journal of chemical physics 119 (10) (2003) 5044–5057.

[57] P. Celani, H.-J. Werner, Multireference perturbation theory for large restricted and selected active space reference wave functions, The Journal of Chemical Physics 112 (13) (2000) 5546–5557.

[58] K. Shamasundar, G. Knizia, H.-J. Werner, A new internally contracted multi-reference configuration interaction method, The Journal of chemical physics 135 (5) (2011) 054101.

[59] H.-J. Werner, P. J. Knowles, An efficient internally contracted multiconfiguration–reference configuration interaction method, The Journal of chemical physics 89 (9) (1988) 5803–5814.

[60] F. A. Cotton, A millennial overview of transition metal chemistry, Journal of the Chemical Society, Dalton Transactions (13) (2000) 1961–1968.

[61] E. R. Davidson, Computational transition metal chemistry (2000).

[62] L. A. Finney, T. V. O'Halloran, Transition metal speciation in the cell: insights from the chemistry of metal ion receptors, Science 300 (5621) (2003) 931–936.

[63] H. Xu, L. H. Jones, Click chemistry patents and their impact on drug discovery and chemical biology, Pharmaceutical patent analyst 4 (2) (2015) 109–119.

[64] C. Thiele, Tracing fatty acid metabolism by click chemistry, ACS Chemical Biology (9) (2012) 2004–2011.

[65] H. Kolb, K. Sharpless, The growing impact of click chemistry on drug discovery, DRUG DISCOVERY TODAY 8 (24) (2003) 1128–1137. doi:10.1016/S1359-6446(03)02933-7.

[66] J. E. Moses, A. D. Moorhouse, The growing applications of click chemistry, CHEMICAL SOCIETY REVIEWS 36 (8) (2007) 1249–1262. doi:10.1039/b613014n.

[67] J. M. Baskin, J. A. Prescher, S. T. Laughlin, N. J. Agard, P. V. Chang, I. A. Miller, A. Lo, J. A. Codelli, C. R. Bertozzi, Copper-free click chemistry for dynamic in vivo imaging, PRO-

CEEDINGS OF THE NATIONAL ACADEMY OF SCIENCES OF THE UNITED STATES OF AMERICA 104 (43) (2007) 16793–16797. doi:10.1073/pnas.0707090104.

[68] J. Prescher, C. Bertozzi, Chemistry in living systems, NATURE CHEMICAL BIOLOGY 1 (1) (2005) 13–21. doi:10.1038/nchembio0605-13.

[69] G. C. Tron, T. Pirali, R. A. Billington, P. L. Canonico, G. Sorba, A. A. Genazzani, Click chemistry reactions in medicinal chemistry: Applications of the 1,3-dipolar cycloaddition between azides and alkynes, MEDICINAL RESEARCH REVIEWS 28 (2) (2008) 278–308. doi:10.1002/med.20107.

[70] E. J. Yoo, M. Ahlquist, S. H. Kim, I. Bae, V. V. Fokin, K. B. Sharpless, S. Chang, Copper-catalyzed synthesis of n-sulfonyl-1, 2, 3-triazoles: Controlling selectivity, Angewandte Chemie 119 (10) (2007) 1760–1763.

[71] A. Speers, G. Adam, B. Cravatt, Activity-based protein profiling in vivo using a copper(I)-catalyzed azide-alkyne [3+2] cycloaddition, JOURNAL OF THE AMERICAN CHEMICAL SOCIETY 125 (16) (2003) 4686–4687. doi:10.1021/ja034490h.

[72] S. G. Agalave, S. R. Maujan, V. S. Pore, Click Chemistry: 1,2,3-Triazoles as Pharmacophores, CHEMISTRY-AN ASIAN JOURNAL 6 (10, SI) (2011) 2696–2718. doi:10.1002/asia.201100432.

[73] X. Ning, J. Guo, M. A. Wolfert, G.-J. Boons, Visualizing metabolically labeled glycoconjugates of living cells by copper-free and fast huisgen cycloadditions, ANGEWANDTE CHEMIE-INTERNATIONAL EDITION 47 (12) (2008) 2253–2255. doi:10.1002/anie.200705456.

[74] F. Amblard, J. H. Cho, R. F. Schinazi, Cu(I)-Catalyzed Huisgen Azide-Alkyne 1,3-Dipolar Cycloaddition Reaction in Nucleoside, Nucleotide, and Oligonucleotide Chemistry, CHEMICAL REVIEWS 109 (9) (2009) 4207–4220. doi:10.1021/cr9001462.

[75] V. Hong, S. I. Presolski, C. Ma, M. G. Finn, Analysis and Optimization of Copper-Catalyzed Azide-Alkyne Cycloaddition for Bioconjugation, ANGEWANDTE CHEMIE-INTERNATIONAL EDITION 48 (52) (2009) 9879–9883. doi:10.1002/anie.200905087.

[76] A. Speers, B. Cravatt, Profiling enzyme activities in vivo using click chemistry methods, CHEMISTRY & BIOLOGY 11 (4) (2004) 535–546. doi:10.1016/j.chembiol.2004.03.012.

[77] E. M. Sletten, C. R. Bertozzi, From Mechanism to Mouse: A Tale of Two Bioorthogonal Reactions, ACCOUNTS OF CHEMICAL RESEARCH 44 (9, SI) (2011) 666–676. doi:10.1021/ar200148z.

[78] L. Liang, D. Astruc, The copper(I)-catalyzed alkyne-azide cycloaddition (CuAAC) "click" reaction and its applications. An overview, COORDINATION CHEMISTRY REVIEWS 255 (23-24) (2011) 2933–2945. doi:10.1016/j.ccr.2011.06.028.

[79] A. Link, D. Tirrell, Cell surface labeling of Escherichia coli via copper(I)-catalyzed [3+2] cycloaddition, JOURNAL OF THE AMERICAN CHEMICAL SOCIETY 125 (37) (2003) 11164–11165. doi:10.1021/ja036765z.

[80] B. S. Sumerlin, A. P. Vogt, Macromolecular Engineering through Click Chemistry and Other Efficient Transformations, MACROMOLECULES 43 (1) (2010) 1–13. doi:10.1021/ma901447e.

[81] K. Patel, S. Angelos, W. R. Dichtel, A. Coskun, Y.-W. Yang, J. I. Zink, J. F. Stoddart, Enzyme-responsive snap-top covered silica nanocontainers, JOURNAL OF THE AMERICAN CHEMICAL SOCIETY 130 (8) (2008) 2382–2383. doi:10.1021/ja0772086.

[82] Y. L. Angell, K. Burgess, Peptidomimetics via copper-catalyzed azide-alkyne cycloadditions, CHEMICAL SOCIETY REVIEWS 36 (10) (2007) 1674–1689. doi:10.1039/b701444a.

[83] D. Diaz, S. Punna, P. Holzer, A. Mcpherson, K. Sharpless, V. Fokin, M. Finn, Click chemistry in materials synthesis. 1. Adhesive polymers from copper-catalyzed azide-alkyne cycload-

dition, JOURNAL OF POLYMER SCIENCE PART A-POLYMER CHEMISTRY 42 (17) (2004) 4392–4403. doi:10.1002/pola.20330.

[84] J.-F. Lutz, Z. Zarafshani, Efficient construction of therapeutics, bioconjugates, biomaterials and bioactive surfaces using azide-alkyne "click" chemistry, ADVANCED DRUG DELIVERY REVIEWS 60 (9) (2008) 958–970. doi:10.1016/j.addr.2008.02.004.

[85] W. Horne, M. Yadav, C. Stout, M. Ghadiri, Heterocyclic peptide backbone modifications in an alpha-helical coiled coil, JOURNAL OF THE AMERICAN CHEMICAL SOCIETY 126 (47) (2004) 15366–15367. doi:10.1021/ja0450408.

[86] S. Cho, E. Yoo, L. Bae, S. Chang, Copper-catalyzed hydrative amide synthesis with terminal alkyne, sulfonyl azide, and water, JOURNAL OF THE AMERICAN CHEMICAL SOCIETY 127 (46) (2005) 16046–16047. doi:10.1021/ja056399e.

[87] M. Malkoch, K. Schleicher, E. Drockenmuller, C. Hawker, T. Russell, P. Wu, V. Fokin, Structurally diverse dendritic libraries: A highly efficient functionalization approach using Click chemistry, MACROMOLECULES 38 (9) (2005) 3663–3678. doi:10.1021/ma047657f.

[88] C. Y. Jao, A. Salic, Exploring RNA transcription and turnover in vivo by using click chemistry, PROCEEDINGS OF THE NATIONAL ACADEMY OF SCIENCES OF THE UNITED STATES OF AMERICA 105 (41) (2008) 15779–15784. doi:10.1073/pnas.0808480105.

[89] H. Struthers, T. L. Mindt, R. Schibli, Metal chelating systems synthesized using the copper(I) catalyzed azide-alkyne cycloaddition, DALTON TRANSACTIONS 39 (3) (2010) 675–696. doi:10.1039/b912608b.

[90] A. Deiters, T. Cropp, M. Mukherji, J. Chin, J. Anderson, P. Schultz, Adding amino acids with novel reactivity to the genetic code of Saccharomyces cerevisiae, JOURNAL OF THE AMERICAN CHEMICAL SOCIETY 125 (39) (2003) 11782–11783. doi:10.1021/ja0370037.

[91] P. M. E. Gramlich, C. T. Wirges, A. Manetto, T. Carell, Postsynthetic DNA Modification through the Copper-Catalyzed Azide-Alkyne Cycloaddition Reaction, ANGEWANDTE CHEMIE-INTERNATIONAL EDITION 47 (44) (2008) 8350–8358. doi:10.1002/anie.200802077.

[92] N. Stephanopoulos, M. B. Francis, Choosing an effective protein bioconjugation strategy, NATURE CHEMICAL BIOLOGY 7 (12) (2011) 876–884. doi:10.1038/NCHEMBIO.720.

[93] W. Xi, T. F. Scott, C. J. Kloxin, C. N. Bowman, Click Chemistry in Materials Science, ADVANCED FUNCTIONAL MATERIALS 24 (18) (2014) 2572–2590. doi:10.1002/adfm.201302847.

[94] V. O. Rodionov, S. I. Presolski, S. Gardinier, Y.-H. Lim, M. G. Finn, Benzimidazole and related Ligands for Cu-catalyzed azide-alkyne cycloaddition, JOURNAL OF THE AMERICAN CHEMICAL SOCIETY 129 (42) (2007) 12696–12704. doi:10.1021/ja072678l.

[95] P. Cozzi, R. Hilgraf, N. Zimmermann, Acetylenes in catalysis: Enantioselective additions to carbonyl groups and imines and applications beyond, EUROPEAN JOURNAL OF ORGANIC CHEMISTRY 2004 (20) (2004) 4095–4105. doi:10.1002/ejoc.200400246.

[96] J. M. Holub, K. Kirshenbaum, Tricks with clicks: modification of peptidomimetic oligomers via copper-catalyzed azide-alkyne [3+2] cycloaddition, CHEMICAL SOCIETY REVIEWS 39 (4) (2010) 1325–1337. doi:10.1039/b901977b.

[97] Z. Zhou, C. Fahrni, A fluorogenic probe for the copper(I)-catalyzed azide-alkyne ligation reaction: Modulation of the fluorescence emission via (3)(n,pi*)-(1)(pi,pi*) inversion, JOURNAL OF THE AMERICAN CHEMICAL SOCIETY 126 (29) (2004) 8862–8863. doi:10.1021/ja049684r.

[98] J. A. Johnson, M. G. Finn, J. T. Koberstein, N. J. Turro, Construction of linear polymers, dendrimers, networks, and other polymeric architectures by copper-catalyzed azide-alkyne

cycloaddition “Click” chemistry, MACROMOLECULAR RAPID COMMUNICATIONS 29 (12-13) (2008) 1052–1072. doi:10.1002/marc.200800208.

[99] M. Hashemi, A. A. Taherpour, Theoretical kinetic and thermodynamic studies of the strain energies and ring size effects of the 1,3-dipolar cycloaddition reactions on ethinamate medicine analogs, JOURNAL OF MOLECULAR STRUCTURE 1204 (MAR 15 2020). doi:10.1016/j.molstruc.2019.127544.

[100] H. C. Kolb, M. G. Finn, K. B. Sharpless, Click Chemistry: Diverse Chemical Function from a Few Good Reactions, Angew Chem Int Edit 40 (11) (2001) 2004–2021.

[101] V. V. Rostovtsev, L. G. Green, V. V. Fokin, K. B. Sharpless, A Stepwise Huisgen Cycloaddition Process: Copper(I)-Catalyzed Regioselective “Ligation” of Azides and Terminal Alkynes, Angew Chem Int Edit 41 (14) (2002) 2596–2599.

[102] B. F. Straub, μ-acetylide and μ-alkenylidene ligands in “click” triazole syntheses, Chemical Communications (37) (2007) 3868–3870.

[103] V. O. Rodionov, V. V. Fokin, M. G. Finn, Mechamism of the ligand-free cu(i)-catalyzed azide-alkyne cycloaddition reaction, Angew Chem Int Edit 44 (2005) 2211–2215.

[104] M. Ahlquist, V. V. Fokin, Enhanced reactivity of dinuclear copper (i) acetylides in dipolar cycloadditions, Organometallics 26 (18) (2007) 4389–4391.

[105] B. T. Worrel, J. A. Malik, V. V. Fokin, Direct evidence of a dinuclear copper intermediate in cu(i)-catalyzed azide-alkyne cycloadditions, Science 340 (2013) 457–460.

[106] P. L. Arnold, S. Zlatogorsky, N. A. Jones, C. D. Carmichael, S. T. Liddle, A. J. Blake, C. Wilson, Comparisons between yttrium and titanium n-heterocyclic carbene complexes in the search for early transition metal nhc backbonding interactions, Inorganic chemistry 47 (19) (2008) 9042–9049.

[107] A. Comas-Vives, J. N. Harvey, How important is backbonding in metal complexes containing n-heterocyclic carbenes? structural and nbo analysis, European Journal of Inorganic Chemistry 2011 (32) (2011) 5025–5035.

[108] M. Frisch, G. Trucks, H. Schlegel, G. Scuseria, M. Robb, J. Cheeseman, G. Scalmani, V. Barone, B. Mennucci, G. Petersson, et al., Gaussian development version revision J04+ (2011).

[109] A. D. Becke, Density-functional thermochemistry. iv. a new dynamical correlation functional and implications for exact-exchange mixing, The Journal of chemical physics 104 (3) (1996) 1040–1046.

[110] J. P. Perdew, Y. Wang, Accurate and simple analytic representation of the electron-gas correlation energy, Physical Review B 45 (23) (1992) 13244.

[111] R. Krishnan, J. S. Binkley, R. Seeger, J. A. Pople, Self-consistent molecular orbital methods. xx. a basis set for correlated wave functions, The Journal of chemical physics 72 (1) (1980) 650–654.

[112] A. McLean, G. Chandler, Contracted gaussian basis sets for molecular calculations. i. second row atoms, z= 11–18, The Journal of Chemical Physics 72 (10) (1980) 5639–5648.

[113] S. Grimme, Semiempirical gga-type density functional constructed with a long range dispersion correction, Journal of computational chemistry 27 (2006) 1787–1799.

[114] A. V. Marenich, C. J. Cramer, D. G. Truhlar, Universal solvation model based on solute electron density and on a continuum model of the solvent defined by the bulk dielectric constant and atomic surface tensions, Journal of Physical Chemistry B 113 (2009) 6378–6396.

[115] H. P. Hratchian, H. B. Schlegel, Finding minima, transition states, and following reaction pathways on ab initio potential energy surfaces, Elsevier, Amsterdam, 2005, pp. 195–249.

[116] H. P. Hratchian, H. B. Schlegel, Finding minima, transition states, and following reaction pathways on ab initio potential energy surfaces, In Theory and Applications of Computational Chemistry: The First 40 Years (2005) 195–249.

[117] H. P. Hratchian, H. B. Schlegel, Reaction path following using a hessian based predictor-corrector algorithm, Journal of Chemical Physics 120 (2004) 9918–9924.

[118] A. M. Hua, S. L. Bidwell, S. I. Baker, H. P. Hratchian, R. D. Baxter, Experimental and theoretical evidence for nitrogen–fluorine halogen bonding in silver-initiated radical fluorinations, ACS Catalysis 9 (4) (2019) 3322–3326.

[119] V. A. Parsegian, Van der Waals forces: a handbook for biologists, chemists, engineers, and physicists, Cambridge University Press, 2005.

[120] A. J. Neel, M. J. Hilton, M. S. Sigman, F. D. Toste, Exploiting non-covalent π interactions for catalyst design, Nature 543 (7647) (2017) 637–646.

[121] C. A. Hunter, J. K. Sanders, The nature of. pi.-. pi. interactions, Journal of the American Chemical Society 112 (14) (1990) 5525–5534.

[122] A. Frontera, P. Gamez, M. Mascal, T. J. Mooibroek, J. Reedijk, Putting anion–π interactions into perspective, Angewandte Chemie International Edition 50 (41) (2011) 9564–9583.

[123] A. S. Mahadevi, G. N. Sastry, Cation- π interaction: Its role and relevance in chemistry, biology, and material science, Chemical reviews 113 (3) (2013) 2100–2138.

[124] G. A. Jeffrey, G. A. Jeffrey, An introduction to hydrogen bonding, Vol. 12, Oxford university press New York, 1997.

[125] S. J. Grabowski, What is the covalency of hydrogen bonding?, Chemical reviews 111 (4) (2011) 2597–2625.

[126] A. G. Doyle, E. N. Jacobsen, Small-molecule h-bond donors in asymmetric catalysis, Chemical Reviews 107 (12) (2007) 5713–5743.

[127] A. Armstrong, R. A. Boto, P. Dingwall, J. Contreras-Garcia, M. J. Harvey, N. J. Mason, H. S. Rzepa, The houk–list transition states for organocatalytic mechanisms revisited, Chemical Science 5 (5) (2014) 2057–2071.

[128] M. Žabka, R. Šebesta, Experimental and theoretical studies in hydrogen-bonding organocatalysis, Molecules 20 (9) (2015) 15500–15524.

[129] M. N. Grayson, Mechanism and origins of stereoselectivity in the cinchona thiourea-and squaramide-catalyzed asymmetric michael addition of nitroalkanes to enones, The Journal of Organic Chemistry 82 (8) (2017) 4396–4401.

[130] G. R. Desiraju, P. S. Ho, L. Kloo, A. C. Legon, R. Marquardt, P. Metrangolo, P. Politzer, G. Resnati, K. Rissanen, Definition of the halogen bond (iupac recommendations 2013), Pure Appl. Chem 85 (8) (2013) 1711–1713.

[131] P. Nagorny, Z. Sun, New approaches to organocatalysis based on c–h and c–x bonding for electrophilic substrate activation, Beilstein Journal of Organic Chemistry 12 (1) (2016) 2834–2848.

[132] S. Guha, I. Kazi, A. Nandy, G. Sekar, Role of lewis-base-coordinated halogen (i) intermediates in organic synthesis: The journey from unstable intermediates to versatile reagents, European Journal of Organic Chemistry 2017 (37) (2017) 5497–5518.

[133] S. Guha, I. Kazi, A. Nandy, G. Sekar, Role of lewis-base-coordinated halogen (i) intermediates in organic synthesis: The journey from unstable intermediates to versatile reagents, European Journal of Organic Chemistry 2017 (37) (2017) 5497–5518.

[134] R. Ma, L.-N. He, X.-F. Liu, X. Liu, M.-Y. Wang, Dbu as activator for the n-iodosuccinimide

promoted chemical fixation of carbon dioxide with epoxides, Journal of CO2 Utilization 19 (2017) 28–32.

[135] Y. Kobayashi, Y. Nakatsuji, S. Li, S. Tsuzuki, Y. Takemoto, Direct n-glycofunctionalization of amides with glycosyl trichloroacetimidate by thiourea/halogen bond donor co-catalysis, Angewandte Chemie International Edition 57 (14) (2018) 3646–3650.

[136] Y. Lu, H. Nakatsuji, Y. Okumura, L. Yao, K. Ishihara, Enantioselective halo-oxy-and halo-azacyclizations induced by chiral amidophosphate catalysts and halo-lewis acids, Journal of the American Chemical Society 140 (19) (2018) 6039–6043.

[137] R. Brueckner, H. Haller, S. Steinhauer, C. Mueller, S. Riedel, A 2d polychloride network held together by halogen–halogen interactions, Angewandte Chemie International Edition 54 (51) (2015) 15579–15583.

[138] S. Riedel, T. Köchner, X. Wang, L. Andrews, Polyfluoride anions, a matrix-isolation and quantum-chemical investigation, Inorganic chemistry 49 (15) (2010) 7156–7164.

[139] S. Schindler, S. M. Huber, Halogen bonds in organic synthesis and organocatalysis, in: Halogen Bonding II, Springer, 2014, pp. 167–203.

[140] M. Breugst, D. von der Heiden, J. Schmauck, Novel noncovalent interactions in catalysis: a focus on halogen, chalcogen, and anion-π bonding, Synthesis 49 (15) (2017) 3224–3236.

[141] K. E. Danahy, J. C. Cooper, J. F. Van Humbeck, Benzylic fluorination of aza-heterocycles induced by single-electron transfer to selectfluor, Angewandte Chemie International Edition 57 (18) (2018) 5134–5138.

[142] A. M. Hua, D. N. Mai, R. Martinez, R. D. Baxter, Radical c–h fluorination using unprotected amino acids as radical precursors, Organic letters 19 (11) (2017) 2949–2952.

[143] A. Karim, M. Reitti, A.-C. C. Carlsson, J. Gräfenstein, M. Erdélyi, The nature of [n–cl–n]+ and [n–f–n]+ halogen bonds in solution, Chemical Science 5 (8) (2014) 3226–3233.

[144] A. Becke, Density-functional thermochemistry. iii. the role of exact exchange (1993) j, Chem. Phys 98 5648.

[145] P. Metrangolo, G. Resnati, Halogen Bonding I: Impact on Materials Chemistry and Life Sciences, Vol. 358, Springer, 2015.

[146] M. Bedin, A. Karim, M. Reitti, A.-C. C. Carlsson, F. Topić, M. Cetina, F. Pan, V. Havel, F. Al-Ameri, V. Sindelar, et al., Counterion influence on the n–i–n halogen bond, Chemical science 6 (7) (2015) 3746–3756.

[147] A.-C. C. Carlsson, K. Mehmeti, M. Uhrbom, A. Karim, M. Bedin, R. Puttreddy, R. Kleinmaier, A. A. Neverov, B. Nekoueishahraki, J. Gräfenstein, et al., Substituent effects on the [n–i–n]+ halogen bond, Journal of the American Chemical Society 138 (31) (2016) 9853–9863.

[148] D. Cremer, E. Kraka, A description of the chemical bond in terms of local properties of electron density and energy, Croatica Chemica Acta 57 (6) (1984) 1259–1281.

[149] A. R. Barron, Valence shell electron pair repulsion (vsepr) theory, Creative Commons Attribution License (by 3.0), 3rd ed (2009).

[150] D. Bakowies, W. Thiel, Hybrid models for combined quantum mechanical and molecular mechanical approaches, The Journal of Physical Chemistry 100 (25) (1996) 10580–10594.

[151] F. Fantuzzi, M. A. C. Nascimento, Description of polar chemical bonds from the quantum mechanical interference perspective, Journal of chemical theory and computation 10 (6) (2014) 2322–2332.

[152] F. Weinhold, C. Landis, E. Glendening, What is nbo analysis and how is it useful?, International reviews in physical chemistry 35 (3) (2016) 399–440.

[153] M. v. Hopffgarten, G. Frenking, Energy decomposition analysis, Wiley Interdisciplinary Reviews: Computational Molecular Science 2 (1) (2012) 43–62.

[154] R. L. DeKock, W. B. Bosma, The three-center, two-electron chemical bond, Journal of Chemical Education 65 (3) (1988) 194.

[155] M.-H. Whangbo, H. B. Schlegel, S. Wolfe, Molecular orbitals from group orbitals. 3. quantitative perturbational molecular orbital analysis of ab initio scf-mo wave functions, Journal of the American Chemical Society 99 (5) (1977) 1296–1304.